A Comparative Study of Adsorbents Derived from Coal Fly Ash for the Adsorption of Tetracycline from Aqueous Solutions

By

Eric Emmanuel Houghton

A Comparative Study of Adsorbents Derived from Coal Fly Ash for the Adsorption of Tetracycline from Aqueous Solutions

By

Eric Emmanuel Houghton

Submitted in partial fulfilment of the requirements for the degree

Master's Chemical Engineering

Department of Chemical Engineering
Faculty of Engineering, Built Environment and Information Technology

University of Pretoria

2024

A Comparative Study of Adsorbents Derived from Coal Fly Ash for the Adsorption of Tetracycline from Aqueous Solutions

Author: Eric Emmanuel Houghton
Supervisor: Professor Shepherd M. Tichapondwa
Co-Supervisor: Doctor Litha Yapi
Department: Chemical Engineering
University: University of Pretoria
Degree: Masters (Chemical Engineering)

ABSTRACT

Emerging contaminants (ECs) like tetracycline (TC) are generated from various human activities, such as pharmaceutical manufacturing, agricultural runoff, and wastewater discharge. The presence of TC poses severe risks to the environment and public health. Various methods have been proposed for removing TC from water, such as chemical precipitation, membrane filtration, and advanced oxidation processes. However, adsorption has gained prominence as an effective method for removing tetracycline due to its simplicity, cost-effectiveness, and ability to achieve high removal efficiencies. Fly ash is a hazardous byproduct of coal combustion, often discarded in landfills, posing environmental risks. However, it can be repurposed into low-cost adsorbents through various modifications and treatments. Utilizing fly ash-derived adsorbents for tetracycline removal not only helps reduce waste but also provides an eco-friendly and cost-effective alternative to conventional, more expensive adsorbents. This study aimed to develop and evaluate various fly ash (FA)-derived adsorbents for TC removal, leveraging waste materials for environmental sustainability.

Firstly, FA was acid-treated with hydrochloric acid to produce acid-modified FA (AM-FA). Secondly, FA was base-treated with sodium hydroxide to yield base-modified FA (BM-FA). Additionally, Zeolite Na-P1 (ZNa-P1) was synthesized from FA using hydrothermal treatment. These three adsorbents were subjected to adsorption tests to compare their adsorption performance. Furthermore, silica nanoparticles (SiNPs) were derived from FA (FA-SiNPs) and subsequently FA-SiNPs was doped with iron to create Fe-SiNPs. For comparison, silica nanoparticles were also synthesized directly from a pure sodium silicate solution (SSSNPs). All silica nanoparticle-based adsorbents (i.e. FA-SiNPs, Fe- SiNPs, SSSNPs) underwent adsorption tests to compare their adsorption efficiency.

The comparative adsorption test among FA, AM-FA, BM-FA and ZNa-P1 revealed that BM-FA and ZNa-P1 removed 76 % and 90 % of TC, respectively, compared to 35 % with unmodified FA. AM-FA had the lowest performance, removing just 11 % of TC. ZNa-P1's superior performance was linked to its high zeolite purity, with a high cation exchange capacity (CEC) of 6.37 meq/g and a surface area of 35.7 m^2/g. BM-FA, had a larger surface area of 110.8 m^2/g, but exhibited a lower CEC of 3.42 meq/g. The adsorption efficiency of these adsorbents was more closely related to CEC than surface area. Optimal TC removal with ZNa-P1 was achieved at 7.5 g/L dosage and pH 5. The adsorption of TC on ZNa-P1 followed pseudo-second-order kinetics and the Langmuir isotherm model, with a maximum capacity of 46.34 mg/g at 30 °C. Thermodynamic studies with ZNa-P1 indicated that the process was spontaneous and endothermic. The adsorption mechanism of TC on ZNa-P1 involved ion-exchange, hydrogen bonding, and electrostatic attraction.

The comparative adsorption tests among FA-SiNPs, SSSNPs, and Fe-SiNPs revealed that Fe-SiNPs demonstrated superior performance, removing 59 % of tetracycline, compared to 30 % and 20 % removal by FA-SiNPs and SSSNPs, respectively. The enhanced removal efficiency of Fe-SiNPs was attributed to the iron content, which facilitated TC adsorption through chelation. Optimal TC removal using Fe-SiNPs was achieved at a dosage of 5 g/L and within a pH range of $4-5$. The adsorption of TC on Fe-SiNPs followed Elovich kinetics and the Langmuir isotherm model, with a maximum capacity of 32.31 mg/g at 30 °C. Thermodynamic studies with Fe-SiNPs indicated that the adsorption process was spontaneous and exothermic. The adsorption mechanism of TC on Fe-SiNPs was chemisorption involving electrostatic attraction and hydrogen bonding.

This study highlights the potential of FA-derived adsorbents, particularly ZNa-P1 and Fe-SiNPs, as sustainable solutions for removing TC from contaminated water. The findings contribute to advancing waste utilization strategies particularly, adsorption, for environmental remediation.

Keywords: Fly ash, Tetracycline, Emerging Contaminants, Adsorption, Zeolite Na-P1, Silica Nanoparticles

DECLARATION

I, Eric Emmanuel Houghton, hereby declare that all the work provided in this dissertation is to the best of my knowledge original and that neither the whole work nor any part of it has been, or is to be submitted for another degree at this or any other University or tertiary education institution or examining body.

Signature: ..... Date: .....

DEDICATION

This work is dedicated to the Almighty God, my dear friends and family.

ACKNOWLEDGEMENT

First and foremost, I thank the Almighty God for bestowing me with the grace, hope, wisdom and perseverance to complete this research.

I extend my sincere thanks to my supervisor, Shepherd Tichapondwa, and my co-supervisor, Litha Yapi, for their invaluable guidance, insightful feedback, and unwavering encouragement, which have been instrumental in shaping this work.

I am also immensely grateful to the Water Utilisation Department of the University of Pretoria for providing the necessary resources, facilities, and a conducive environment for research. My heartfelt thanks go to Alette Devaga and Elmarie Otto, who offered their time and knowledge generously, assisting me in overcoming challenges during this study.

Thank you to my family and friends for their unending support and motivation. Their encouragement have been a great source of strength and hope for me.

I would also like to acknowledge the financial contributions from National Research Foundation whose support has been pivotal in completing this research.

I am grateful to each and every one of the aforementioned individuals whose collective support and inspiration made this thesis possible.

Table of Contents

ABSTRACT ii

DECLARATION iv

DEDICATION v

ACKNOWLEDGEMENT iii

LIST OF NOMENCLATURE x

CHAPTER 1 – INTRODUCTION 1

CHAPTER 2 – LITERATURE REVIEW 4

2.1 Tetracycline and Environmental Concerns . . . 4
2.1.1 Physio-chemical Properties of Tetracycline . . . 4
2.1.2 Sources of Tetracycline Pollution . . . 5
2.1.3 Toxicity of Tetracycline . . . 5
2.1.4 Tetracycline Removal Strategies . . . 7
2.2 Adsorption Process . . . 8
2.2.1 Adsorption Kinetics . . . 10
2.2.1.1 Adsorption Kinetic Models . . . 11
2.2.2 Adsorption Isotherms . . . 11
2.2.2.1 Langmuir Isotherm . . . 12
2.2.3 Freundlich Isotherm . . . 12
2.2.4 Temkin Isotherm . . . 12
2.2.5 Adsorption Thermodynamics . . . 13
2.2.6 Adsorbent Regeneration . . . 14
2.3 Fly ash and Environmental Concerns . . . 15
2.3.1 Fly ash . . . 15
2.3.2 Physical and Chemical characteristics of Fly Ash . . . 16
2.3.3 Current applications of fly ashes . . . 17
2.3.4 Environmental concerns . . . 19
2.4 Modifications of Fly Ash . . . 20
2.5 Zeolites . . . 20
2.5.1 Zeolite synthesis from Fly Ash . . . 21
2.5.1.1 Hydrothermal Synthesis . . . 22
2.5.1.2 Alkaline-Fusion assisted Hydrothermal Synthesis . . . 22
2.6 Silica Nanoparticles . . . 22

CHAPTER 3 – MATERIALS AND METHOD 25

3.1 Materials and reagents . . . 25
3.2 Adsorbent Synthesis . . . 25
3.2.1 Pretreatment of Fly Ash (FA) . . . 25
3.2.2 Acid Modification of Fly Ash . . . 25
3.2.3 Base Modification of Fly Ash . . . 26
3.2.4 Preparation of Zeolite Na-P1 . . . 26
3.2.5 Synthesis of Silica Nanoparticles . . . 26
3.2.5.1 Silica Nanoparticles derived from Fly Ash (FA-SiNPs) . . . 26
3.2.5.2 Iron impregnation of FA-SiNPs (Fe-SiNPs) . . . 27
3.2.5.3 Silica Nanoparticles derived from Sodium Silicate Solution (SSSNPs) . . . 27
3.3 Characterization Techniques . . . 28
3.3.1 X-ray Diffraction (XRD) . . . 28
3.3.2 X-ray Fluorescence (XRF) . . . 28
3.3.3 Surface Area Analysis (BET) . . . 28
3.3.4 Scanning Electron Microscopy (SEM) . . . 29
3.3.5 Zeta Potential . . . 29
3.3.6 Fourier Transform Infrared Spectroscopy (FTIR) . . . 29
3.3.7 Cation Exchange Capacity (CEC) . . . 29
3.3.7.1 FA and AM-FA CEC Measurement . . . 30
3.3.7.2 BM-FA and ZNa-P1 CEC Measurement . . . 30
3.4 Analytic Analysis . . . 30
3.4.1 UV-VIS Analysis . . . 30
3.5 Adsorption Studies . . . 31
3.5.1 Adsorption studies with modified FA and ZNa-P1 . . . 31
3.5.2 Adsorption studies with silica nanoparticles . . . 32

CHAPTER 4 — RESULTS AND DISCUSSION: MODIFICATIONS AND ZEOLITES 33

4.1 XRD Results . . . 33
4.2 XRF Results . . . 34
4.3 SEM and BET Results . . . 35
4.4 CEC Results . . . 36
4.5 Comparison of AM-FA, BM-FA and ZNa-P1 for Tetracycline adsorption . . . 37
4.6 Tetracycline Adsorption with ZNa-P1 . . . 38
4.6.1 The effect of Dosage . . . 38
4.6.2 The effect of pH . . . 38
4.6.3 Adsorption Kinetics . . . 39
4.6.4 Adsorption Isotherms . . . 41

4.6.5 Adsorption Thermodynamics 43
4.6.6 Adsorption Mechanism 43

CHAPTER 5 – RESULTS AND DISCUSSION: SILICA NANOPARTICLES 45

5.1 XRD Results 45
5.2 XRF Results 45
5.3 SEM and BET Results 46
5.4 Comparison of FA-SiNPs, SSSNPs, and Fe-SiNPs for Tetracycline Adsorption 48
5.5 Tetracycline Adsorption with Fe-SiNPs 49
5.5.1 The effect of Dosage 49
5.5.2 The effect of pH 49
5.5.3 Adsorption Kinetics 50
5.5.4 Adsorption Isotherms 52
5.5.5 Adsorption thermodynamics 54
5.5.6 Adsorption Mechanism 54

CHAPTER 6 – CONCLUSIONS AND RECOMMENDATIONS 56

REFERENCES 57

List of Figures

1 (a) Tetracycline chemical structure and (b) speciation of tetracycline. . 5
2 Pathways of TC pollution: sources, contamination routes, and environmental impact (adapted from Ahmad *et al* (2021)). 7
3 Steps in the adsorption process (adapted from Wang & Guo (2020b)). . 8
4 Factors that affect the adsorption process. 10
5 Fly ash production and utilisation for various countries (Ahmed *et al*, 2016). 16
6 Various applications of fly ash. 18
7 2D illustration of a zeolite structure consisting of silicon and aluminium tetrahedrons. Note the yellow dot (-) represents a negative charge (adapted from Zdretsov & Gerasimov (2024)). 21
8 XRD Patterns for FA, AM-FA, BM-FA, and ZNA-P1. The phases indicated in the XRD patterns: mullite (M), quartz (Q), sillimanite (S), hydroxy-sodalite (HS), and zeolite Na-P1 (P). 33
9 SEM images for (a) FA, (b) AM-FA, (c) BM-FA and (d) ZNa-P1. Note that due to the differences in particle sizes, the magnification for FA and AM-FA is 5000 and BM-FA and ZNa-P1 is 40 000. 35
10 Cation exchange capacity for FA, AM-FA, BM-FA and ZNa-P1. 36
11 The percentage removal, Surface Area (right axis) and CEC (far-right axis) of FA, AM-FA, BM-FA and ZNA-P1 (conditions for removal experiments - pH: 5, Dosage: 5 g/L, contact time: 2 h, C_O: 40 ppm). 37
12 (a) The effect of ZNa-P1 dosage and (b) the effect of pH on TC removal. 38
13 Zeta potential of ZNa-P1 as a function of pH as determined using a Zetasizer. 39
14 Adsorption kinetics of TC on ZNa-P1 fitted with adsorption kinetic models (conditions for kinetic experiments - pH: 5, Dosage: 7.5 g/L, C_O: 60 ppm). 40
15 Adsorption isotherms of tetracycline at 30 °C, 40 °C and 50 °C fitted with the adsorption isotherm models (conditions for isotherm experiments - pH: 5, Dosage: 7.5 g/L, contact time: 4 h). 41
16 FTIR spectra of ZNa-P1 before and after adsorption of TC. Note that the FTIR spectra before adsorption is denoted as ZNa-P1 and the FTIR spectra after adsorption is denoted as ZNa-P1-TC. 44
17 XRD Patterns for FA-SiNPs, SSSNPS, and Fe-SiNPs. 45
18 SEM images for (a & b) FA-SiNPs, (c & d) SSSNPs, and (e & f) Fe-SiNPs. Note that the magnification for (a), (c), (e) is 25 000 and for (b), (d), (f) is 140 000. 47
19 The percentage removal of FA-SiNPs, SSSNPs, and Fe-SiNPs (conditions for removal experiments - pH: 5, Dosage: 5 g/L, contact time: 30 min, C_O: 100 ppm). 48

20 (a) The effect of Fe-SiNPs dosage and (b) the effect of pH on TC removal. 49
21 Zeta potential of Fe-SiNPs as a function of pH determined using a Zetasizer. 50
22 Adsorption kinetics of TC on Fe-SiNPs fitted with adsorption kinetic models (conditions for kinetic experiments - pH: 5, Dosage: 5 g/L, C_O: 70 ppm). 51
23 Adsorption isotherms of TC on Fe-SiNPs at 30 °C, 40 °C and 50 °C fitted with the adsorption isotherm models (conditions for isotherm experiments - pH: 5, Dosage: 5 g/L, contact time: 6 h). 52
24 FTIR spectra of Fe-SiNPs before and after adsorption of TC. Note that the FTIR spectra before adsorption is denoted as Fe-SiNPs and the FTIR spectra after adsorption is denoted as Fe-SiNPs-TC. 55
A.1 Calibration curve for tetracycline at 381 nm. 78

List of Tables

1 Chemical and physical properties of Tetracycline (Ozumchelouei *et al*, 2020; Peng *et al*, 2024). . . . 4
2 Advantages and disadvantages of TC removal strategies. . . . 9
3 Information about adsorption process based on thermodynamic parameters (Doke & Khan, 2013; Molina-Calderón *et al*, 2022). . . . 13
4 Advantages and disadvantages of several regeneration methods (Omorogie *et al*, 2016; Patel, 2021). . . . 15
5 Different fly ash compositions based on the type of coal (Boboc *et al*, 2010). 17
6 ASTM C618 standards for fly ash classes (Suraneni *et al*, 2021). . . . 17
7 Advantages and disadvantages of hydrothermal and alkali-fusion zeolite synthesis methods. . . . 21
8 Summary of results on the adsorption of organic pollutants, particularly tetracycline, using modified FA, zeolites and SiNPs. . . . 24
9 Summary of the ZNa-P1 adsorption experiments conditions and variables studied. . . . 32
10 Summary of the Fe-SiNPs adsorption experiments conditions and variables studied. . . . 32
11 Chemical composition of FA, AM-FA, BM-FA, and ZNa-P1. . . . 34
12 Specific surface area for FA, AM-FA, BM-FA, and ZNa-P1 determined using the BET method. . . . 36
13 Adsorption kinetic model parameters and statistical parameters for the adsorption of TC on ZNa-P1. . . . 40
14 Adsorption isotherm model parameters and statistical parameters for the adsorption of TC on ZNa-P1 at 30 °C, 40 °C, and 50 °C. . . . 42
15 Comparison of maximum adsorption capacities of adsorbents for TC removal 42
16 Thermodynamics parameters for tetracycline adsorption on ZNa-P1. . . . 43
17 Chemical composition of FA-SiNPs, SSSNPs, and Fe-SiNPs. . . . 46
18 Specific surface area for FA-SiNPs, SSSNPs, and Fe-SiNPs using BET method. . . . 47
19 Adsorption kinetic model parameters and statistical parameters for the adsorption of TC on Fe-SiNPs. . . . 51
20 Adsorption isotherm model parameters and statistical parameters for the adsorption of TC on Fe-SiNPs at 30 °C, 40 °C, and 50 °C. . . . 53
21 The maximum adsorption capacity of tetracycline for adsorbents similar to Fe-SiNPs. . . . 54
22 Thermodynamics parameters for tetracycline adsorption on Fe-SiNPs. . . . 54

LIST OF NOMENCLATURE

AM-FA	Acid modified fly ash
ARB	Antibiotic resistant bacteria
ARGs	Antibiotic resistant genes
AZM	Azithromycin
BET	Brunauer-Emmett-Teller
BM-FA	Base modified fly ash
CEC	Cation exchange capacity
CHD	Chlorhexidine digluconate
CIP	Ciprofloxacin
ECs	Emerging contaminants
EE	7-alpha-ethinylestradiol
FA	Fly ash
FA-SiNPs	Fly ash derived silica nanoparticles
Fe-SiNPs	Iron modified fly ash derived silica nanoparticles
FTIR	Fourier transform infrared spectroscopy
PFO	Pseudo first order model
PSO	Pseudo second order model
SEM	Scanning electron microscopy
SSSNPs	Sodium silicate solution derived silica nanoparticles
TC	Tetracycline
UV-VIS	Ultraviolet-visible spectroscopy
WWTPs	Waste water treatment plants
XRD	X-ray diffraction
XRF	X-ray fluorescence
ZNa-P1	Zeolite Na-P1

CHAPTER 1 – INTRODUCTION

Water pollution poses a significant threat to ecosystems and human health. Emerging Contaminants (ECs) are a class of contaminants that have garnered increasing attention due to their persistence in ecosystems and resistance to conventional biological wastewater treatment methods (Fahimi *et al*, 2020; Deletic & Wang, 2019). One prominent emerging contaminant is tetracycline (TC), one of the most widely used antibiotics (Amangelsin *et al*, 2023). TC is not fully metabolized by humans and animals and is excreted in its original form through urine and faeces (Raykova *et al*, 2023). Many wastewater treatment plants (WWTPs) employing biological treatment methods, such as activated sludge processes, are unable to effectively remove TC, leading to its discharge into the environment (Wang & Jian, 2015). The hydrophilic properties and low volatility of TC allow it to remain stable in aquatic environments for a long time (Daghrir & Drogui, 2013). Prolonged exposure to low levels of TC can lead to the emergence of antibiotic-resistant bacteria (ARB) and the proliferation of antibiotic resistance genes (ARGs) in microorganisms (Shao & Wu, 2020). The spread of antibiotic-resistant bacteria (ARB) poses a significant threat to human health by rendering antibiotic treatments ineffective (Ding *et al*, 2023). There are many TC removal methods available including biodegradation, advanced oxidation, adsorption, flocculation, membrane filtration, and ion-exchange. Among these, adsorption is regarded as one of the simplest and most cost-effective treatment methods for TC removal (Yan *et al*, 2024). Although activated carbon is a widely used adsorbent, its high cost limits its broader application in wastewater treatment. Several low-cost alternatives, including manufacturing by-products (e.g., fly ash, red mud), clay minerals, and biological materials (e.g., chitin, chitosan), offer promising solutions (Rathi & Kumar, 2021; Crini *et al*, 2019).

Fly Ash (FA) is a solid waste primarily generated by coal-fired thermal power plants, with an estimated global production of 600 million tonnes annually (Aigbe *et al*, 2021). According to Nawaz (2013), in developed countries about 80 % of fly ash produced is reused however in developing countries like India and South Africa only $10 - 15$ % are reused, largely in cement/concrete manufacturing industries. The valorisation of FA is still of great concern, especially in developing countries. Due to the presence of hazardous components, FA must be disposed of in controlled landfills, which is both costly and time-consuming (Khan *et al*, 2014). As noted, FA can be repurposed as a low-cost adsorbent for removing pollutants from water (Rathi & Kumar, 2021). However, its adsorption capacity is limited by its low surface area and crystalline structure. To address this, researchers have explored various modification techniques to enhance FA's adsorption performance (Hussain *et al*, 2022). Given its high silica and alumina content, FA is also a suitable precursor for synthesizing zeolites, which can serve as effective adsorbents (Aigbe

et al, 2021). The large silica content of fly ash can be extracted for the production of silica nanoparticles (Aphane *et al*, 2020). The application of fly ash (FA) as an adsorbent is well-established, with over 4 594 documents identified using the SCOPUS search engine and the keywords 'Fly ash' and 'adsorption.' However, only 3 articles by Bandura *et al* (2022), Sun *et al* (2022) and Ren *et al* (2024), explored the use of FA for TC adsorption. Notably, none of these studies compared the performance of unmodified FA, modified FA, zeolites, and silica nanoparticles as adsorbents. This gap underscores the novelty of the present study.

This study focused on developing and evaluating fly ash (FA)-derived adsorbents for tetracycline (TC) removal from aqueous solutions. The research involved synthesizing acid-modified FA (AM-FA), base-modified FA (BM-FA), and zeolite Na-P1 (ZNa-P1) through hydrothermal synthesis. These adsorbents were characterized using XRD, XRF, BET, SEM, and cation exchange capacity (CEC) analyses and subjected to adsorption studies, examining dosage, pH, isotherms, kinetics, and thermodynamics, with detailed evaluation for ZNa-P1. Additionally, silica nanoparticles were synthesized from a sodium silicate solution (SSSNPs) and FA (FA-SiNPs), with further iron doping of FA-SiNPs to produce Fe-SiNPs. The synthesized nanoparticles were characterized using XRD, XRF, BET, SEM and tested comparatively, focusing on Fe-SiNPs adsorption efficiency under varying conditions.

This thesis consists of seven chapters:

Chapter 1 Introduction
Provides a concise background and identifies the problem statement. It outlines the aim and objectives of the study and discusses the framework of the thesis.

Chapter 2 Literature review
This chapter discusses the literature and identifies the gaps that this study aims to fill with regard to valorisation of fly ash in wastewater treatment.

Chapter 3 Materials and methods
Builds on the theoretical framework and recent advancements in the valorization of fly ash discussed in chapter 2. It delves into the experimental methods for synthesizing acid-modified and base-modified fly ash, as well as zeolite Na-P1 and silica nanoparticles. Additionally, it outlines the design and execution of the adsorption experiments.

Chapter 4 Results and discussion: modification and zeolites
This chapter presents and discusses the results of the experiments outlined chapter 3. First, the synthesis outcomes of acid-modified fly ash (AM-FA), base-modified fly ash

(BM-FA), and zeolite Na-P1 (ZNa-P1) are analysed using XRD, XRF, SEM, CEC and BET techniques. Finally, the adsorption performance of each adsorbent is assessed.

Chapter 5 Results and discussion: silica nanoparticles
This chapter focuses on the results of FA-SiNPs, Fe-SiNPs, and SSSNPs, providing a parallel investigation into their characteristics and similarly, their application in the adsorption of TC.

Chapter 6 Conclusions and recommendations
The overall findings from the study are presented and suggestions are made for potential future research.

CHAPTER 2 – LITERATURE REVIEW

2.1 Tetracycline and Environmental Concerns

Pharmaceuticals, including antibiotics, analgesics, and anti-inflammatories, are considered major emerging contaminants (ECs) due to their persistence in the environment and their toxicity to living organisms (Samal *et al*, 2022). One of the most commonly used antibiotics in the world is tetracycline (TC) (Amangelsin *et al*, 2023). It is largely used for human therapy, veterinary application and in the agricultural sector, due to its low cost and low toxicity (Abbasnia *et al*, 2022).

2.1.1 Physio-chemical Properties of Tetracycline

Tetracycline chemical structure and speciation are shown in Figure 1. The name "tetracycline" originates from the four (tetra-) hydrocarbon rings (-cycline) in the chemical structure (Ozumchelouei *et al*, 2020). Table 1 presents the chemical and physical properties of tetracycline. The low Henry's constant suggests that TC has a low volatility in water (Pal *et al*, 2017). The low octanol-water partition coefficient (log K_{OW}) and high water solubility illustrates the hydrophilic nature of TC (Conde-Cid *et al*, 2020). TC is amphoteric, existing as a cation at pH values below 3, as a zwitterion between pH 3.3 and 7.7, and as an anion at pH values above 7.7. The amphoteric nature is attributed to the three ionizable functional groups, namely the tricarbonylamide group (pK_{a1}), the phenolic diketone group (pK_{a2}) and the dimethylamino group (pK_{a3}) (Zhao *et al*, 2014). TC can easily undergo photolysis, decomposing into several products. The electron rich functional groups of TC are readily able to form bonds with divalent and trivalent metal ions, such as iron (Fe^{3+}), magnesium (Mg^{2+}), calcium (Ca^{2+}), aluminium (Al^{3+}) (Halling-Sørensen *et al*, 2002). The chelation of TC and metal cations makes TC more stable by neutralising the charge of TC (Pulicharla *et al*, 2017).

Table 1: Chemical and physical properties of Tetracycline (Ozumchelouei *et al*, 2020; Peng *et al*, 2024).

Henry's constant	log K_{OW}	Molar mass (g/mol)	Water Solubility (mg/L)	pK_{a1}	pK_{a2}	pK_{a3}
$3.45 \times 10^{-24} - 3.91 \times 10^{-26}$	−1.37	444.4	231	3.3	7.7	9.7

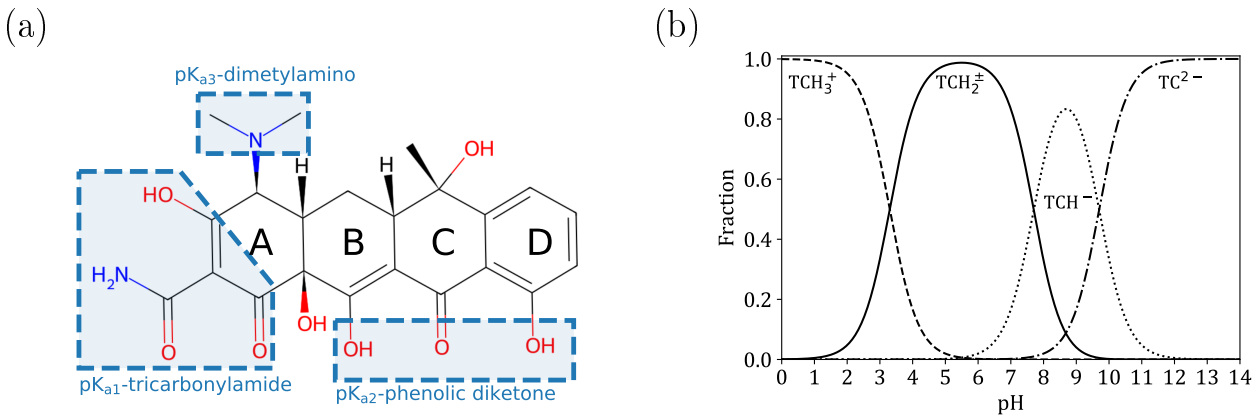

Figure 1: (a) Tetracycline chemical structure and (b) speciation of tetracycline.

2.1.2 Sources of Tetracycline Pollution

TC has been detected in surface water, groundwater, drinking water, wastewater and wastewater sludge, river-sediments and soil (Islam & Gilbride, 2019). The three main reasons for TC-detection in water sources: (1) excessive use of TC as a therapeutic agent or growth enhancer, (2) partial removal of TC in wastewater treatment plants (WWTPs), and (3) run-off and leaching of TC from agricultural fields (Balakrishnan *et al*, 2023).

TC is not fully metabolized by humans and animals, with approximately $50 - 80$ % of it being excreted in its original form through urine and faeces (Chen *et al*, 2022b). Many WWTPs use activated sludge processes that are not fully effective in removing TC, resulting in the discharge of TC into the environment (Liao *et al*, 2021). A portion of TC is removed through adsorption onto the sludge. However, in some cases, this TC-contaminated sludge is repurposed as fertilizer, which can subsequently lead to soil contamination. (Chang *et al*, 2023). Similarly, the inclusion of TC in animal feed results in TC-contaminated manure. When this manure is used as fertilizer, it can contribute to soil contamination (Kasumba *et al*, 2020). Le *et al* (2018) note that the soil contamination can lead to surface water and groundwater contamination via surface run-off and leaching, respectively. Another pathway of TC pollution is through the landfill disposal of unused and expired pharmaceuticals which could leach into groundwater (Chang *et al*, 2023). The unused/expired pharmaceuticals could also be improperly disposal of into wastewater system without any pre-treatment (Saravanan *et al*, 2022).

2.1.3 Toxicity of Tetracycline

The hydrophilic nature, low volatility, and extended half-life of TC contribute to its persistence in aquatic environments (Fang *et al*, 2022; Varadharajan *et al*, 2022). TC

also has a chemically stable structure, characterized by aromatic rings, and exhibits biotoxicity, making it resistant to degradation and biodegradation (Abbasnia *et al*, 2022). The continual introduction of TC and its low degradation rate have led to its accumulation in the environment (Chang *et al*, 2023).

At low concentrations, TC may not affect aquatic species but can result in the accelerated development of antibiotic resistant genes (ARGs) and antibiotic resistant bacteria (ARB) (Cheng *et al*, 2020). One of the risks associated with ARGs and ARB is their potential transmission to animals and humans (Lundström *et al*, 2016). Their antibiotic resistance can render most antibiotic treatments ineffective (Mancuso *et al*, 2021). Amarasiri *et al* (2020) note that infections stemming from ARB have higher mortality and morbidity rates. Humans can contract ARGs and ARB through consumption of food irrigated with reclaimed water (Amarasiri *et al*, 2020). Additionally, conventional disinfection processes, such as chlorination, are often unable to completely eliminate ARB, resulting in their presence in "treated" drinking water (Umar, 2022). It should be noted that ARGs and ARB are also classified as emerging contaminants (Cedeño-Muñoz *et al*, 2024).

Tetracycline can have severe effects on organisms in the aquatic and terrestrial environment (Serwecińska, 2020). According to Liu *et al* (2018a), exposure of zebrafish to TC resulted in yolk sac edema, uninflated swim bladder and growth inhibition depending on the TC dosage. Zebrafish are commonly used as model organisms to study the toxic effects of contaminants on the early development of vertebrates (Lin *et al*, 2023). These toxic effects observed in the zebrafish suggest that exposure to TC could lead to developmental issues in other vertebrates. Similarly, *Daphnia* are used as model organisms to infer the toxic effects of contaminants on aquatic invertebrates (Tkaczyk *et al*, 2021). According to Kim *et al* (2014), exposure to TC had multi-generational effects on the reproduction and physical growth of *D. magna*. The presence of TC in soil has led to a decline the microbial community and inhibition of enzymatic activities of bacterial communities. This, in turn has affected various essential environmental processes, including methanogenesis, biomass production, and organic matter decomposition (Conde-Cid *et al*, 2020). Another concern is the uptake and bioaccumulation of TC in plants, which could impact the ecosystem and humans through the food chain (He *et al*, 2023). According to Balakrishnan *et al* (2023), TC can accumulate in various edible plants, including cucumber, lettuce, and tomato with particularly high TC levels observed in the roots and leaves.

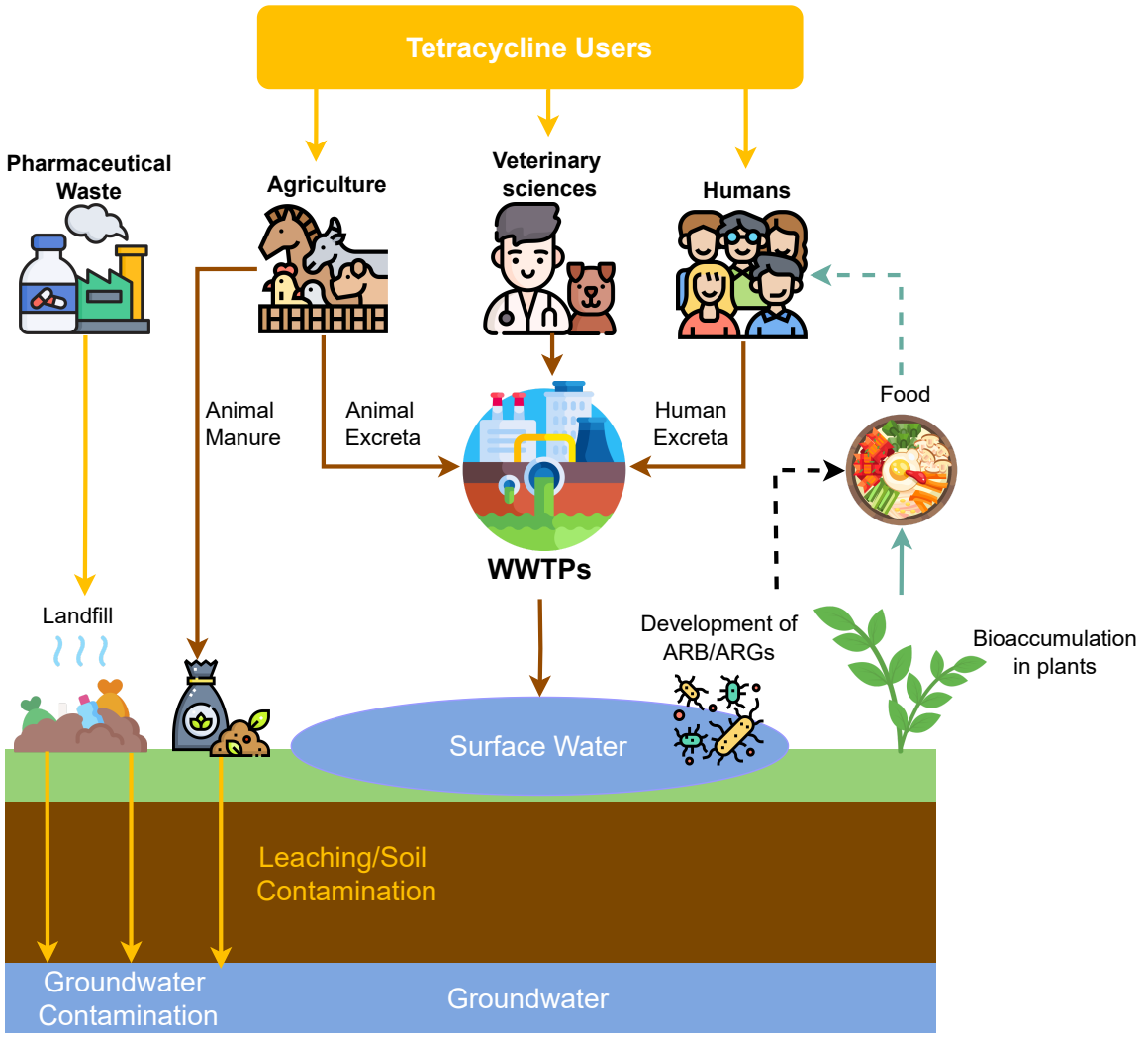

Figure 2: Pathways of TC pollution: sources, contamination routes, and environmental impact (adapted from Ahmad *et al* (2021)).

2.1.4 Tetracycline Removal Strategies

Various treatment methods can be employed for the removal of TC from wastewater, including photocatalysis, ozonation, adsorption, membrane filtration, microbial fuel cells, and phytoremediation (Leichtweis *et al*, 2022). Table 2 gives the advantages and disadvantages of some TC removal strategies.

2.2 Adsorption Process

The process by which a substance, known as an adsorbate, moves from the liquid phase to the surface of a solid, known as the adsorbent, is called adsorption (Abas *et al*, 2013). The adsorption of an adsorbate onto an adsorbent comprises of three steps (Tan & Hameed, 2017):

- Transport of the adsorbate from bulk phase to the external surface of the adsorbent (External diffusion)
- Pore diffusion referring to the transport of the adsorbate from the external surface into the pores of adsorbent (Intraparticle diffusion).
- Adsorption of the adsorbate on the active sites

Figure 3 depicts the adsorption process. The slowest step in the adsorption process is referred to as the rate-controlling or rate-limiting step (Muliwa *et al*, 2023).

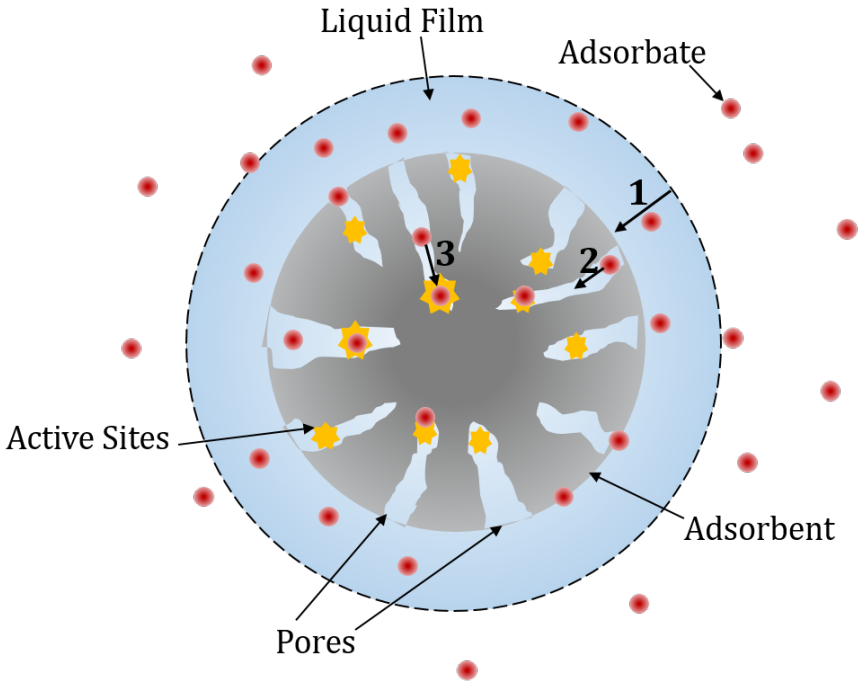

Figure 3: Steps in the adsorption process (adapted from Wang & Guo (2020b)).

Adsorption can be influenced by several factors, including pH, initial concentration of adsorbates, contact time, adsorbent dosage, adsorbent particle size, temperature, and agitation speed (Vasu *et al*, 2023). Figure 4 presents a summary of the factors affecting the adsorption process. The main driving forces for the adsorption process involves van der Waals forces, hydrogen bonding, electrostatic attraction, $\pi - \pi$ interactions and

Table 2: Advantages and disadvantages of TC removal strategies.

Removal Strategy	Advantages	Disadvantages	Reference
Adsorption	High efficiency, simple design Adsorbents can be regenerated Eco-and cost-friendly	High initial cost Sludge production and disposal considerations	(Rizwan *et al*, 2022)
Photocatalysis	High efficiency, eco-friendly Complete mineralisation of pollutants Photocatalyst can be reused	Limited response to visible light Potential toxic by-products	(Litynska *et al*, 2021)
Ozonation	Rapid reaction with high degradation No waste generation Can be improved with catalyst	High cost Possible toxic by-products Mass transfer limited	(Ahmad *et al*, 2021)
Fenton Process	High efficiency, fast reaction time Requires simple equipment No toxic by-products	Requires low pH Sludge generation Instability of Fenton reagent	(Ziembowicz & Kida, 2022)
Phytoremediation	Simple, low-cost No sludge or by-products generated Eco-friendly	Slow process Pollutants accumulate in plants Plants affected by many factors	(Kafle *et al*, 2022) (Leichtweis *et al*, 2022)

other hydrophobic interactions (Sophia & Lima, 2018). There are two forms of adsorption, namely, physical adsorption and chemisorption (Shaikh, 2020: 24). In physical adsorption or physisorption, the main form of attraction is through weak van der Waals forces alongside electrostatic attraction between the adsorbate and absorbent. In chemical adsorption or chemisorption, the main form of attraction is through chemical bonds (i.e. covalent or ionic bonds) between the adsorbate and adsorbent (Van Den Broek & Boeriu, 2020: 433). Physical adsorption is reversible and associated with a small enthalpy whereas chemisorption is irreversible due to the strong chemical bonds and is associated with a high exothermic enthalpy (Somashekara & Mulky, 2023).

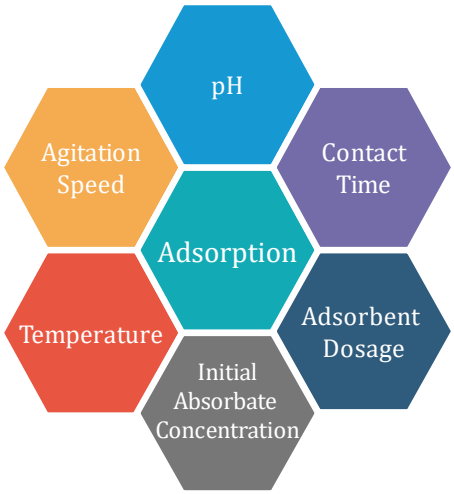

Figure 4: Factors that affect the adsorption process.

2.2.1 Adsorption Kinetics

Adsorption kinetics studies the amount of adsorbate adsorbed or adsorption capacity, q_t, as a function of time. The adsorption capacity at any time, q_t, can be calculated using Equation 1 (Worch, 2021: 141):

$$q_t = \frac{V(C_O - C_t)}{m} \tag{1}$$

where C_O (mg/L) is the initial concentration of adsorbate, C_t (mg/L) is the concentration of adsorbate at any time, t, V (L) is the solution volume, and m (g) is the mass of adsorbent. Adsorption kinetics provides valuable information, such as the adsorption rate and adsorbent performance, and offers insights into the adsorption mechanism and the rate-limiting step (Wang & Guo, 2020b). This knowledge is crucial for developing large-scale adsorption systems and identifying the best operating conditions, including the residence time of the adsorbate and the dimensions of the reactor (Wang *et al*, 2022).

2.2.1.1 Adsorption Kinetic Models

The commonly used pseudo first order and second order models and Elovich model are given by Equations 2, 3 and4 (Shi *et al*, 2021):

$$q_t = q_e \left(1 - e^{-k_1 t}\right) \tag{2}$$

$$q_t = \frac{q_e^2 k_2 t}{1 + q_e k_2 t} \tag{3}$$

$$q_t = \frac{1}{\beta} \ln(1 + \alpha\beta t) \tag{4}$$

where q_t (mg/g) and q_e (mg/g) are the adsorption capacity at at time, t (min), and equilibrium, respectively, k_1 is the pseudo first order rate constant (min^{-1}), and k_2 is the pseudo second order rate constant ($g{\cdot}mg^{-1}{\cdot}min^{-1}$), α is initial adsorption rate ($mg{\cdot}g^{-1}{\cdot}min^{-1}$) and β is the adsorption/desorption constant (g/mg). Wang & Guo (2020b) note that the pseudo first order and second order models and the Elovich models are empirical models and do not have any definite physical meaning regarding the adsorption mechanism. Islam *et al* (2021) also remark that the rate constants from empirical models are dependent on the experimental conditions (i.e. initial concentration, dosage, etc.). Thus, the rate constants may not be applicable for the design of full-scale plant (Islam *et al*, 2021).

The Langmuir kinetic model, shown in Equation 5, has a theoretical basis and can, therefore, be used to determine rate constants that are independent of operating conditions (Lohrentz *et al*, 2023).

$$\frac{dq_t}{dt} = k_{\text{ads}} C_t \left(1 - \frac{q_t}{q_m}\right) - k_{\text{des}} \frac{q_t}{q_m} \tag{5}$$

where q_{max} (mg/g) is the maximum adsorption capacity constant, k_{ads} ($L{\cdot}mg^{-1}{\cdot}min^{-1}$), k_{des} ($mg{\cdot}L^{-1}{\cdot}min^{-1}$) are the adsorption and desorption rate constants for the Langmuir model.

2.2.2 Adsorption Isotherms

An adsorption isotherm refers to the equilibrium relationship between the concentration of the absorbate in solution (C_e) and the amount of adsorbate adsorbed on the adsorbent (q_e) at a constant temperature and pH (Lima *et al*, 2015: 35). The graphical representation of an adsorption isotherm is the adsorption capacity at equilibrium, q_e, expressed as a function of the equilibrium concentration of the adsorbate, C_e, in essence, $q_e = f(C_e)$ (Molina-Calderón *et al*, 2022). Modelling adsorption isotherms helps determine the adsorption mechanism, predict the removal performance of the adsorbent, and estimate the amount of adsorbent required for an adsorption system (Muliwa *et al*, 2023). However, it

should be noted that empirical isotherm models, such as Sips, Freundlich, and Temkin, do not help in determining the adsorption mechanism, as they are not derived from fundamental principles (Wang & Guo, 2020a).

2.2.2.1 Langmuir Isotherm

The Langmuir isotherm is based on the assumption that adsorption only occurs on a finite number of adsorption sites, and that the adsorbed layer has a thickness of one molecule (monolayer adsorption) (Chen, 2015). The Langmuir adsorption isotherm is given in Equation 6 (Foo & Hameed, 2010):

$$q_e = \frac{Q_{\max} K_L Ce}{1 + K_L Ce} \tag{6}$$

where Q_{max} is the maximum adsorption capacity (mg/g) and K_L is the Langmuir isotherm constant (L/mg).

2.2.3 Freundlich Isotherm

The Freundlich isotherm model is typically used to describe adsorption onto a heterogeneous surface and is illustrated in Equation 7 (Dada *et al*, 2012):

$$q_e = K_f C_e^{\frac{1}{n}} \tag{7}$$

where K_f is the Freundlich isotherm constant (mg/g), n is the adsorption intensity. The term $1/n$ is an indication of how favourable the adsorption. If $1/n$ is greater than one, the adsorption is considered unfavourable. If $1/n$ is greater than zero and less than one ($0 < 1/n < 1$), the adsorption is considered favourable (Al-Ghouti & Da'ana, 2020).

2.2.4 Temkin Isotherm

The Temkin model takes temperature into account and assumes that the heat of adsorption for molecules within the adsorbed layer decreases linearly with increasing interactions between the adsorbate and the adsorbent. It also assumes that the binding energies are uniformly distribute (Chen *et al*, 2022a). The Temkin model is given by Equation 8 (Al-Jubouri *et al*, 2022):

$$q_e = \frac{RT}{b_T} \ln(A_T C_e) \tag{8}$$

where A_T is the Temkin constant representing the maximum binding energy (L/mg), T is the temperature (K), R is the universal gas constant (8.314 J/mol/K), and b_T is the adsorption heat constant (J/mol).

2.2.5 Adsorption Thermodynamics

Thermodynamic studies can help determine the temperature dependence of the adsorption process, and the thermodynamic parameters provide insight into the spontaneity, feasibility, and mechanism of adsorption (Ebelegi *et al*, 2020; Sahmoune, 2019). The thermodynamics parameters are the standard change in Gibbs free energy (ΔG°), the standard change in enthalphy (ΔH°), and the standard change in entropy (ΔS°) (Húmpola *et al*, 2013). Table 3 illustrates the inferred characteristics of the adsorption process, drawn from thermodynamic parameters.

Table 3: Information about adsorption process based on thermodynamic parameters (Doke & Khan, 2013; Molina-Calderón *et al*, 2022).

Condition	Nature of Adsorption Process
$\Delta G^\circ < 0$	Spontaneous and thermodynamically feasible
$\Delta G^\circ > 0$	Non-spontaneous and not thermodynamically feasible
$\Delta H^\circ < 0$	Exothermic
$\Delta H^\circ > 0$	Endothermic
$0 < \lvert\Delta H^\circ$ (kJ/mol)$\rvert < 20$	Physisorption
$20 < \lvert\Delta H^\circ$ (kJ/mol)$\rvert < 80$	Chemisorption and physisorption (ion exchange)
$80 < \lvert\Delta H^\circ$ (kJ/mol)$\rvert < 200$	Chemisorption
$\Delta S^\circ < 0$	Decrease in disorder at the solid-liquid interface
$\Delta S^\circ > 0$	Increase in disorder at the solid-liquid interface

The thermodynamic parameters can be calculated using Equation 9−11 (Lima *et al*, 2020):

$$\Delta G^\circ = -RT \ln(K_e^\circ) \tag{9}$$

$$\Delta G^\circ = \Delta H^\circ - T\Delta S^\circ \tag{10}$$

$$\ln(K_e^\circ) = \frac{\Delta S^\circ}{R} - \frac{\Delta H^\circ}{RT} \tag{11}$$

where K_e° is the thermodynamic equilibrium constant of adsorption (dimensionless). Assuming that the temperature effects on ΔH° and ΔS° is negligible. Equation 11 or the "van't Hoff equation" will produce a linear plot of $\ln(K_e^\circ)$ against $1/T$. The slope and

intercept of the linear plot can be used to determine ΔH° and ΔS° (Salvestrini *et al*, 2022). The Langmuir constant, K_L, is commonly used for K_e°. However, the van't Hoff equation uses K_e° in a logarithm term, therefore K_e° must be dimensionless to ensure unit consistency (González-López *et al*, 2022). Lima *et al* (2019) suggests using the equilibrium constant from best fitting isotherm model, such Liu, Sips or Langmuir, across each temperature and making it dimensionless using Equation 12

$$K_e^\circ = \frac{(1000 \times K_g \times \mathrm{MW} \times C^\circ)}{\gamma} \tag{12}$$

where K_g is the equilibrium constant from the isotherm model (L/mg), MW is the molecular weight of the absorbate, C° is the standard concentration of adsorbate (1 mol·L^{-1}), and γ is the coefficient of activity (dimensionless).

2.2.6 Adsorbent Regeneration

The regeneration of an adsorbent is essential to minimize secondary pollution caused by its disposal and to reduce operational costs by enabling multiple adsorption-desorption cycles (Renu & Sithole, 2024). The two main principles behind adsorbent regeneration are adsorbate desorption and adsorbate decomposition (Dai *et al*, 2019). Desorption refers to the removal of the adsorbed adsorbate from an adsorbent, essentially the reverse of adsorption (El Messaoudi *et al*, 2024). There are various regeneration techniques, including thermal, chemical, electrochemical, ultrasonic, and biological regeneration.(Bayuo *et al*, 2024).

Thermal regeneration involving heating of the adsorbent at elevated temperatures to disrupt the physical/chemical bonds between the absorbent and absorbate. The absorbate is released as a volatile compound potentially causing secondary pollution (Baskar *et al*, 2022). In chemical regeneration, a solvent or chemical reagent such as NaOH, HCl or $CaCl_2$ is employed to desorb the absorbate from the adsorbent (Alsawy *et al*, 2022). Electrochemical regeneration utilises electrochemical reactions and an electric field to induce desorption of the adsorbate (Yasri & Roberts, 2024). Biological regeneration involves the biodegradation of organic adsorbates into smaller toxicants (Bayuo *et al*, 2024). Table 4 shows the advantages and disadvantages of several regeneration methods.

Table 4: Advantages and disadvantages of several regeneration methods (Omorogie *et al*, 2016; Patel, 2021).

Regeneration Method	Advantages	Disadvantages
Biological	Very Efficient for organic pollutants, Eco-friendly	Only applicable for biodegradable pollutants, Very slow, Possible fouling
Thermal	Efficient, Useful for absorbents with various contaminants	Very expensive, Air pollution, Degrades adsorbent's pore-structure
Microwave-assisted	Efficient, Eco-friendly, Short regeneration time	Requires post treatment, Degrade adsorbent's pore structure
Chemical	Fast regeneration Cost-effective	Formation of sludge, Changes adsorbent's chemical structure, Possible toxic by-products
Electrochemical	Very efficient with high conductivity adsorbents Eco-friendly	Efficiency of electrodes reduces with time, Long regeneration times

2.3 Fly ash and Environmental Concerns

2.3.1 Fly ash

Coal ash, is a waste by-product produced during coal burning in thermal power plants and is one of the most produced anthropogenic materials (Yao *et al*, 2015). Coal ash consists of both fly ash and bottom ash, where 70−80 % is fly ash and remainder is bottom ash (Mohammed *et al*, 2021). Bottom Ash is the heavier particles that are collected at the bottom of the furnace (Ramzi *et al*, 2016). Fly ash (FA) refers to fine particles in coal ash that rise with the flue gases and captured by particulate control equipment such as electrostatic or mechanical precipitator (Bhatt *et al*, 2019). In 2005, global fly ash production was estimated be 500 million tonnes, by 2015 it was estimated to be 750 million tonnes. By 2035, coal is projected to account for only 24 % of the world's energy supply down from the 29 % recorded in 2015. However, during the same time period, global energy demand is expected to increase by 30 %. As a result, FA production is likely to rise in the coming years due to the significant increase in global energy demand

(Bhatt *et al*, 2019). The FA production and utilisation for various countries is shown in Figure 5. On a global scale, 53 % of all FA produced is utilised (Ahmed *et al*, 2016).

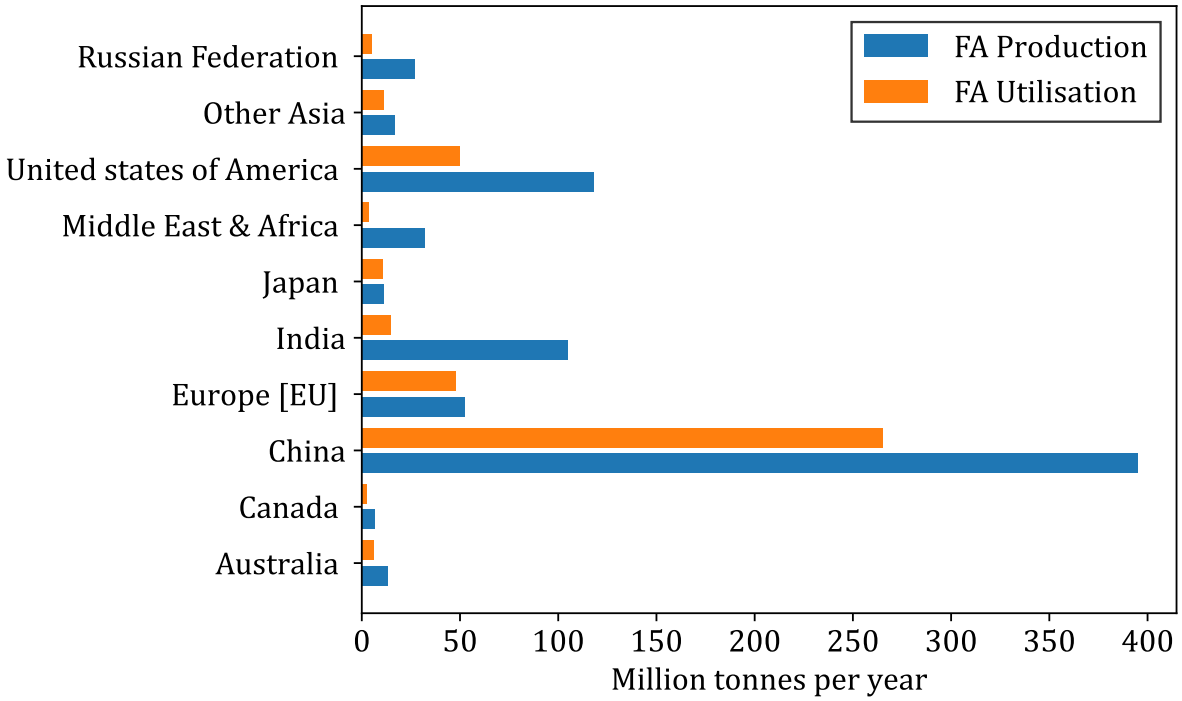

Figure 5: Fly ash production and utilisation for various countries (Ahmed *et al*, 2016).

2.3.2 Physical and Chemical characteristics of Fly Ash

Fly ash is a white-gray to dark-gray fine powder, ranging in size from 8 to 20 μm, and is typically made up of smooth spherical particles (Cui *et al*, 2020). The bulk density of fly ash ranges between 1.12–1.28 g/cm^3, while its specific surface area spans from 1.0 to 9.44 m^2/g (Jayaranjan *et al*, 2014).

The main constituents in fly ash are silicon dioxide (SiO_2), aluminium oxide (Al_2O_3), calcium oxide (CaO), and iron oxide (Fe_2O_3) (Mathapati *et al*, 2022). Some of the trace elements include Na, Mg, Ti, Hg, Zn, Pb, Cd, B, Ni, P, K, Cr and S (Das & Rout, 2023). According to Boboc *et al* (2010), the chemical properties of fly ash varies depending on the type of coal that is burned. Table 5 presents the different fly ash compositions based on the type of coal burned.

Table 5: Different fly ash compositions based on the type of coal (Boboc *et al*, 2010).

Composition (wt %)	Anthracite/bituminous	Sub-bituminous	Lignite
SiO_2	$20-60$	$40-60$	$15-45$
Al_2O_3	$5-35$	$20-30$	$20-25$
Fe_2O_3	$10-40$	$4-10$	$4-15$
CaO	$1-12$	$5-30$	$15-40$
Loss of ignition (LOI)	$0-15$	$0-3$	$0-5$

Due to the diverse composition of fly ash it is classified into two main groups, according to ASTM C618, namely Class C and Class F (Alterary & Marei, 2021).

Class C fly ash originates from sub-bituminous coal or lignite, while Class F fly ash originates from bituminous or anthracite coal (Gene & Lobo, 2014: 25). The ASTM C618 standards to categorise fly ash based on composition are shown in Table 6.

Table 6: ASTM C618 standards for fly ash classes (Suraneni *et al*, 2021).

ASTM C618 Standard	Class F	Class C
$SiO_2 + Al_2O_3 + Fe_2O_3$, minimum %	50	50
CaO %	≤ 18	>18
SO_3, maximum %	5	5
Moisture content, maximum %	3	3
LOI, maximum %	6	6

Depending on the concentration of trace elements, the pH of fly ash can range from 4.50 to 12 (Kelechi *et al*, 2022). But fly ash is typically alkaline, with a surface that becomes negatively charged at high pH levels (Haya & Alkatiri, 2020).

2.3.3 Current applications of fly ashes

There are various methods for FA utilisation, as illustrated in Figure 6. These include applications in construction, soil amelioration, the synthesis of geopolymer and zeolite materials, insulating silica aerogel materials, carbon nanotubes, and valuable metal recovery (Gollakota *et al*, 2019).

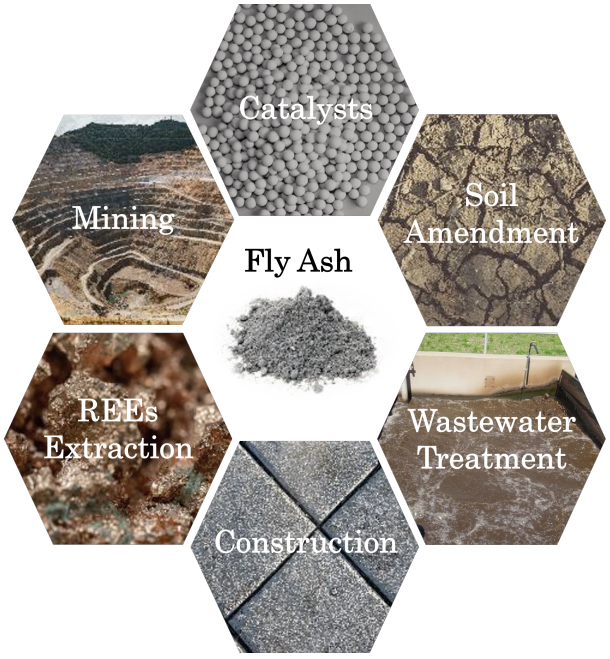

Figure 6: Various applications of fly ash.

Fly ash when applied to soil, can improve several of the soil's properties including bulk density, texture, percolation and water retention. Alkaline fly ash can be used to neutralise acidic soil and as a substitute for lime (Yao *et al*, 2015). There is still a risk of leaching of potential toxic elements (PTEs) within the fly ash, thus the land application of FA needs to be controlled to mitigate PTEs soil contamination (Shaheen *et al*, 2014). The use of FA as a soil amender is limited since it does not contain some essential nutrients for plants such as carbon (C) and nitrogen (N) (Zhou *et al*, 2020).

In the cement and concrete industry, fly ash can serve as a substitute for various raw materials or as a supplement for the cement industry (Alterary & Marei, 2021). The incorporation of FA in concrete production can improve water demand, and reduce bleeding and minimise segregation. However, due to the slow rate of the pozzolanic reaction of fly ash, its contribution to concrete strength only occurs after approximately 28 days. To accelerate this process, activating chemicals such as sodium sulphate can be added or an elevated curing temperatures can be used (De Maeijer *et al*, 2020). Class F FA exhibits pozzolanic properties but lacks the cementitious properties found in Class C FA, which contains a higher CaO content. Therefore, additives like hydrated lime or quicklime, are necessary to enhance the cementitious properties of Class F FA (Kelechi *et al*, 2022).

Geopolymer is produced through the reaction of an aluminosilicate source (i.e. fly ash) with an alkaline solution like sodium hydroxide (NaOH) or sodium silicate (Na_2SiO_3). This process, is known as geopolymerization (Das & Rout, 2021). Geopolymers are likened to amorphous zeolites. Like zeolites, geopolymers consist of a polymeric 3-

D framework of aluminium (Al) and silicon (Si) tetrahedra linked by an oxygen atom (Swanepoel & Strydom, 2002). Geopolymers have many properties that make them a good substitute for Portland cement, including a resistance to acids and chloride penetration, as well as, excellent performance in freeze–thaw cycles (Luhar & Luhar, 2022). However, Zhuang *et al* (2016) notes that fly-ash geopolymer concrete tends to be fragile and susceptible to cracking, limiting its long-term application.

Fly ash can be converted into valuable materials such as adsorbents, coagulants, filters, and catalysts or catalyst supports. These materials have a wide range of applications in wastewater treatment processes, including adsorption, membrane filtration, photocatalysis, and Fenton process (Patel *et al*, 2023). The alumina and iron oxides in FA can be leached out using acidic solutions to produce inexpensive coagulants (Yan *et al*, 2012). FA can act as membrane support or as cheap raw materials to produce ceramic membranes (Sawunyama *et al*, 2024). Most of the wastewater treatment research has focused on Class F FA, mainly in the field of adsorption, and not Class C FA, largely due to the variations of lime content in Class C FA (Mushtaq *et al*, 2019).

Rare earth metals consists of group of 17 elements, namely, scandium, yttrium and 15 lanthanides. In fly ash, the average concentration of rare earth elements (REEs) is around 404 mg per kilogram of fly ash (Huang *et al*, 2020). The most common way to extract REEs is through liquid-liquid extraction (LLE). LLE has some drawbacks, such as extractant loss and the development of a third phase. Solid-liquid extraction (SLE) is a promising eco-friendly alternative to LLE. It uses a sorbent, such as DTPA-associated organosilica, to separate and extract REEs (Dardona *et al*, 2023).

2.3.4 Environmental concerns

The concentration of heavy metals in fly ash is nearly ten times higher than in the original coal (Curpen *et al*, 2023). Some of the heavy metals that may be found include cadmium (Cd), arsenic (As), beryllium (Be), lead (Pb), cobalt (Co) and chromium (Cr). These heavy metals are hazardous to human health and the environment. The fly ash that is not utilised is stored in the dry state in dry specialised landfills or in the wet state in ash ponds (Ghazali *et al*, 2019). Dry disposal of fly ash requires a large area which may not be readily available and will incur high costs (Ghosh & Goel, 2014). Fly ash is made up of fine particles that can become airborne and travel long distance due to wind currents. Smaller fine particles are capable of entering the respiratory system through inhalation and cause severe health issues (Rozhina *et al*, 2021). Ash ponds can reduce the amount area required but if they are inadequately lined, the toxic elements present in the fly ash can leach out and contaminate groundwater aquifiers (Verma & Hussain,

2016). Many potential applications of raw fly ash are significantly hindered by the risk of releasing toxic elements and heavy metals that are present in fly ash. Various methods are available to reduce these risks, including hydrothermal treatment to immobilize heavy metals and acidic treatment to leach them out. These modifications enhance the safety and broaden the potential applications of fly ash (Xu *et al*, 2021; Kang *et al*, 2021).

2.4 Modifications of Fly Ash

Raw fly ash (FA) typically has a low surface area and a crystalline structure, which may result in a low adsorption capacity (Eteba *et al*, 2022). Physical and chemical processes can be employed to enhance its surface area and adsorption capacity (Hussain *et al*, 2022). Some of the physical processes include removal of unburned carbon, gravity separation and grinding. Some chemical processes include acidic treatment, which aides in removing impurities from FA while increases the surface and number of actives sites for adsorption (Kurniasih *et al*, 2025; Sharma *et al*, 2012). Basic treatment which can improve the cation exchange capacity, specific surface area and porous structure of the fly ash (Qi *et al*, 2019). Additionally, impregnating FA with various metal hydroxides, such as iron and aluminium oxide, enhances surface complexation with the adsorbate and increase electrostatic interactions (Banerjee *et al*, 2005). Some authors, such as Xuying *et al* (2024), Truong *et al* (2020), and Nguyen *et al* (2020)have surface modified FA with surfactants such as sodium dodecyl sulfate (SDS) and polyethyleneimine (PEI). Surface modification is a straightforward method for introducing functional groups, enhancing the surface properties of ash and enabling its selectivity for a target adsorbate (Xuying *et al*, 2024).

2.5 Zeolites

FA is rich in silica and alumina, making it an suitable precursor for the production of zeolites (Koshy & Singh, 2016). Zeolites are crystalline aluminosilicate minerals consisting of silicon $(SiO_4)^{4-}$ and aluminium $(AlO_4)^{5-}$ tetrahedra linked by shared oxygen atoms, as illustrated in Figure 7. The replacement of Si (IV) with Al (III) in the zeolite framework introduces a net negative charge (Zdretsov & Gerasimov, 2024). This negative charge is balanced by exchangeable cations, such as Na^+, K^+, Ca^{2+} (Bacariza *et al*, 2017). These charge balancing cations can be readily exchanged with cations in solution. The magnitude of cation exchange that occurs in a mineral is known as its cation exchange capacity (CEC) (Mishra & Clark, 2013: 84).

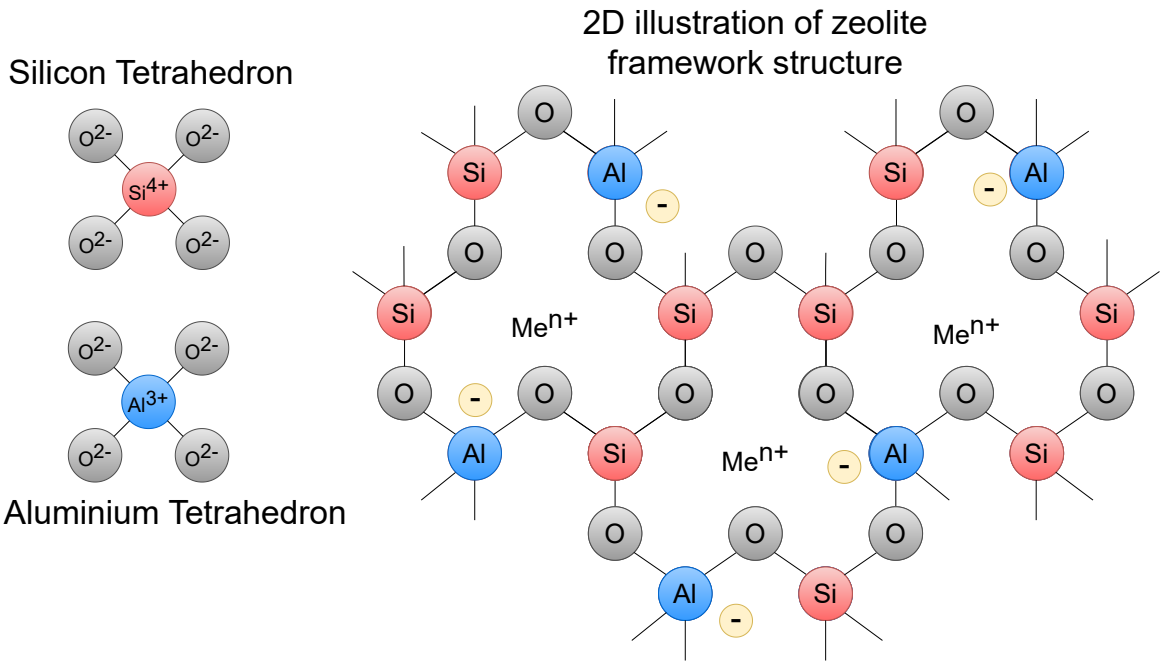

Figure 7: 2D illustration of a zeolite structure consisting of silicon and aluminium tetrahedrons. Note the yellow dot (-) represents a negative charge (adapted from Zdretsov & Gerasimov (2024)).

2.5.1 Zeolite synthesis from Fly Ash

Various methods are used to synthesize zeolites from FA, including, hydrothermal synthesis, alkaline-fusion assisted hydrothermal synthesis and microwave-assisted synthesis (Ren *et al*, 2020). Among these, the hydrothermal and the alkaline fusion methods are the most commonly employed (Buzukashvili *et al*, 2024). Table 7 presents the advantages and disadvantages of the hydrothermal and alkali-fusion synthesis methods.

Table 7: Advantages and disadvantages of hydrothermal and alkali-fusion zeolite synthesis methods.

Method	Advantages	Disadvantages
Hydrothermal Synthesis	Low reaction temperature	Time-consuming
	Low energy requirement	Lower conversion
Alkali-fusion Synthesis	Faster reaction times	High energy input
	Higher purity	Costly

2.5.1.1 Hydrothermal Synthesis

A hydrothermal process refers to the use of a aqueous solution as the reaction medium in an enclosed vessel under a high temperature and is pressurised by the vapour pressure from reaction (Yang & Park, 2019). The hydrothermal synthesis method involves four steps (Ju *et al*, 2021):

- **Dissolution**: Leaching of Si and Al from FA into alkaline solution, mainly from the amorphous phase. NaOH or KOH can be used as the alkaline medium.
- **Condensation**: The soluble Si and Al in solution form an aluminosilicate gel.
- **Nucleation**: The forming of nuclei on the surface of the FA.
- **Crystal Growth**: The growth of zeolite crystal on newly formed nuclei.

Silicate or aluminate compounds can be added to adjust the Si/Al ratio, thereby modifying the resulting zeolite phase. Depending on factors such as hydrothermal temperature, NaOH concentration, reaction time, and Si/Al ratio various types of zeolites can be obtained, including Zeolite A, X, Na-P1, or hydrosodalite (Bukhari *et al*, 2015).

2.5.1.2 Alkaline-Fusion assisted Hydrothermal Synthesis

This synthesis method involves two steps. First, FA is fused with an alkali source, such as NaOH powder, at a high temperature ($550-600$ °C). In the second step, the alkali-fused product undergoes hydrothermal treatment to produce the zeolite material (Ren *et al*, 2020; Szerement *et al*, 2021). Zeolites synthesized using the alkali-fusion method often exhibit higher crystallinity and require shorter reaction times. Unlike the hydrothermal method, alkali-fusion can extract silica and alumina from the inert mullite and quartz phases, enabling a higher conversion of FA into zeolites (Cao *et al*, 2023). This synthesis method favours the production of zeolite A and X (Bukhari *et al*, 2015).

2.6 Silica Nanoparticles

Silica nanoparticles (SiNPs) have a wide range of applications due to its hydrophilic nature, small size, and large surface area (Jeelani *et al*, 2020). These applications include drug delivery, cancer therapy, optical materials, molecular separation, and wastewater treatment as an adsorbent (Yadav & Fulekar, 2019).

The sol-gel method is one of the simplest and most efficient approaches for synthesizing SiNPs (Guo *et al*, 2017). In this method, suspended colloidal particles, known as "sol", are converted into a polymeric chain, referred to as a "gel" (Singh *et al*, 2014). However, conventionally used silica precursors for sol-gel methods such as tetramethyl orthosilicate (TMOS) and tetraethyl orthosilicate (TEOS) are potentially toxic and expensive. An inexpensive and viable non-toxic precursor is sodium silicate (Na_2SiO_3).

FA consists mainly of silica and can serve as an inexpensive and abundant source of silica (Yan *et al*, 2016). The silica in FA can react with an alkali solution, such as NaOH, to form a soluble sodium silicate solution which can be used to make silica nanoparticles by the sol-gel method (Yadav & Fulekar, 2020). Equations 13 and 14 show the reactions steps in the production of silica nanoparticles from fly ash (Owoeye *et al*, 2021):

$$SiO_{2(\text{from FA})} + 2NaOH_{(aq)} \longrightarrow Na_2SiO_{3(aq)} + H_2O_{(l)} \tag{13}$$

$$Na_2SiO_{3(aq)} + 2HCl_{(aq)} \longrightarrow SiO_{(gel)} + 2NaCl + H_2O_{(l)} \tag{14}$$

Table 8 presents a summary on the adsorption of organic pollutants, in particular TC, using modified FA, zeolites and SiNPs.

Table 8: Summary of results on the adsorption of organic pollutants, particularly tetracycline, using modified FA, zeolites and SiNPs.

Absorbent	Adsorbate	Adsorption Mechanism	qm (mg/g)	Reference
Zeolite Na-P1 modified with β-cyclodextrin	TC	chemisorption, hydrogen bonding	38	(Bandura *et al*, 2022)
Fe-doped Zeolite-X	TC	surface complexation, electrostatic interactions	204	(Abadi *et al*, 2019)
MoS_2@Zeolite	TC	electrostatic interaction, $\pi - \pi$ action	216.8	(Liu *et al*, 2021)
CTAB-modified Zeolite	TC	electrostatic interaction, physisorption	85.1	(Mostafapour *et al*, 2022)
Zeolite A modified MCM-41	TC	electrostatic interaction, ion-exchange	419	(Liu *et al*, 2013)
Mesoporous zeolite-hydroxyapatite	TC	physisorption, electrostatic interaction	186	(Khanday & Hameed, 2018)
Zeolite Na-P1 from FA	EE*	physisorption	188	(Bajda *et al*, 2024)
FAU-type zeolite	AZM*	electrostatic interactions, hydrogen bonding	8.5	(de Sousa *et al*, 2018)
Mn-MSNs	TC	electrostatic interaction, cation-π interaction	229	(Qiao *et al*, 2021)
Fe_3O_4/SiO_2/CTAB–SiO_2	TC	electrostatic interaction	220.7	(Zandipak & Sobhanardakani, 2018)
Fe-impregnated mesoporous silicates	TC	chemisorption, surface complexation	41.7	(Vu *et al*, 2010)
H_2SO_4-activated FA	CHD*	chemisorption, ion-exchange	61.3	(Singh *et al*, 2020)
Alkali-modified-FA	CIP*	surface complexation, electrostatic interaction	13.61	(Liu *et al*, 2024)

EE* - 7-alpha-ethinylestradiol
AZM* - Azithromycin
CHD* - Chlorhexidine digluconate
CIP* - Ciprofloxacin

CHAPTER 3 – MATERIALS AND METHOD

3.1 Materials and reagents

Coal fly ash was collected from the Matla Power station located in Kriel, Nkangala, Mpumalanga, South Africa. Tetracycline (99 %), polyethylene glycol (PEG - 6000 MM) and sodium silicate solution (338443-NaO 10.6 %,SiO_2, 26.5 %) were purchased from Sigma-Aldrich, Germany. Hydrochloric acid (HCl) (32 %), sodium hydroxide (NaOH) pellets, acetic acid (99 %), ammonium hydroxide (25 %), potassium dihydrogen phosphate and silver nitrate ($AgNO_3$) were purchased from Glassworld, South Africa. Potassium hydrogen phthalate was purchased from Hopkins and Williams Ltd, South Africa. Sodium acetate trihydrate was purchased from SAARCHEM, South Africa. Deionized (DI) water used in this study was from an Elga Purelab Chorus unit. The filter paper used was a qualitative grade Whatman no. 40 with a pore size of 8 μm. HPLC-grade methanol was purchased from VWR chemicals.

3.2 Adsorbent Synthesis

Several adsorbents were synthesized from FA using different modification techniques. Acid treatment was applied to remove impurities and enhance surface area, while base modification improved cation exchange capacity, surface area, and porosity. Hydrothermal synthesis facilitated the formation of zeolites with enhanced cation exchange capacity and surface area. Additionally, silica nanoparticles were derived from sodium silicate solutions obtained from fly ash.

3.2.1 Pretreatment of Fly Ash (FA)

Before any synthesis/modification, the FA was first washed twice in DI water with a loading of 400 g FA/2 L DI water. The remaining solids (post-washing) were sieved using 75 micron sieve. Particles smaller than 75 μm were used throughout the study.

3.2.2 Acid Modification of Fly Ash

The acid-modification was based on a modification performed by Eteba *et al* (2022). 10 g of FA was mixed with a 50 ml of HCl solution (30 w/w %). The resulting slurry was poured into a glass sealable flask and placed in an oven at 100 °C for 24 h. After 24 h,

the slurry was filtered using vacuum filtration. The resulting filter cake was washed with DI-water several times. After which it was dried in an oven for 24 h at 60 °C.

3.2.3 Base Modification of Fly Ash

The base modification was based on an alkaline hydrothermal synthesis (Wulandari *et al*, 2020). 20 g of fly ash was mixed with a 160 ml of 3.5 M NaOH solution. The resulting slurry was poured into a Teflon-lined autoclave and placed in an oven at 100 °C for 24 h. After 24 h, the slurry was filtered using vacuum filtration. The resulting filter cake was washed with DI-water several times till the filtrate wash-water had a pH lower than 10. After which it was dried in an oven for 24 h at 60 °C.

3.2.4 Preparation of Zeolite Na-P1

The zeolite synthesis consisted of two steps: ageing and hydrothermal treatment (Musyoka *et al*, 2009). In the ageing process, 14 g of fly ash was mixed with a 100 ml of 3.5 M NaOH solution. Note the mass ratio of FA:NaOH was 1:1. The resulting slurry was poured into a sealable polyethylene bottle. The bottle was placed into a silicone-oil bath on a magnetic stirrer and stirred at 800 rpm and 47 °C for 48 h.

In the hydrothermal treatment, approx. 20 ml of DI water was added to the aged-slurry then mixed to obtain homogeneity. This slurry was then put in a Teflon-lined autoclave and placed in an oven at 140 °C for 48 h. After hydrothermal treatment, the resulting zeolite mixture from the autoclave was filtered using vacuum filtration. The obtained zeolites were washed several times till the filtrate wash-water had a pH lower than 10.

3.2.5 Synthesis of Silica Nanoparticles

The silica nanoparticle synthesis was based on the sol-gel method with sodium silicate solutions initially derived from FA and commercial-grade sodium silicate was used.

3.2.5.1 Silica Nanoparticles derived from Fly Ash (FA-SiNPs)

Sodium silicate was initially derived from the fly ash using the Sequential Acid–Alkaline Leaching (SAAL) method adopted from Aphane *et al* (2020). Acid was used to remove large portions of the aluminium present in the fly ash. Then, sodium hydroxide was used to leach silica from the purified FA.

10 g of FA in 100 ml of 10 M HCl was stirred on magnetic stirrer for 4 h at 95 °C and 300 rpm, under reflux conditions. The FA residue after stirring was extracted using a centrifuge for 20 min at 4 °C and 9 000 rpm.

The FA-residue recovered after acid-treatment was placed in 100 ml of 10 M NaOH. The mixture was then placed in silicone bath on a magnetic stirrer for 1 h at 95 °C and 300 rpm. The leachate (sodium silicate) was extracted using filter paper. The sodium silicate solution was added to 20 ml of a 3 w/w % polyethylene glycol (PEG) solution. The PEG solution was first sonicated in a LABOTEC ultrasonic water bath for 30 min at 55 °C. After 30 min, the sodium silicate solution was added slowly to the PEG solution while in a ultrasonic water bath (55 °C, 20 Hz). The PEG-sodium silicate solution was slowly titrated with 5 M HCl to a pH of 4. After titration, the visible gel solution was left to sonicate for 30 min. The gel solution was then covered and left to age overnight. The gel solution was centrifuged for 20 min at 4 °C and 9 000 rpm. The recovered gel was washed several times to remove Na^+ and Cl^- ions. Silver nitrate ($AgNO_3$) was used to test presence of Na^+ and Cl^- ions. If no AgCl precipitate was noted in the supernatant of the wash water, the washing was complete. The final product was calcined at 650 °C for 2 h.

To ensure the purity of the derived silica nanoparticles. 5 g of the derived silica nanoparticles was added to 250 ml of 1 M HCl and stirred on a magnetic stirrer for 3 h at 110 °C and 300 rpm, under reflux conditions. The product was denoted as FA-SiNPs.

3.2.5.2 Iron impregnation of FA-SiNPs (Fe-SiNPs)

The iron impregnation synthesis was adopted from Kiprono *et al* (2023). 5 g of FA-derived silica nanoparticles was added to 25 ml of a 74 mM $FeCl_3 \cdot H_2O$ solution. The pH of the mixture was then adjusted to 7 before being stirred on a shaking table for 1 h at 250 rpm and room temperature. The solution was then centrifuged for 20 min at 4 °C and 9 000 rpm and washed twice and left to dry over night. Finally, the powdered was calcined for 6 h at 500 °C. The product was denoted as Fe-SiNPs.

3.2.5.3 Silica Nanoparticles derived from Sodium Silicate Solution (SSSNPs)

The silica nanoparticles synthesis from sodium silicate solution was a variation of the synthesis from the fly ash. 5 ml of sodium silicate was diluted with 95 ml of DI water and stirred in a silicone oil bath on a magnetic stirrer for 1 h at 95 °C and 300 rpm. Note that the synthesis follows the exact same steps shown in Section 3.2.5.1, from the

addition of the sodium silicate to the PEG solution to the calcination. Note there was no post acid-purification required.

3.3 Characterization Techniques

The characterization techniques were employed to analyse the differences between the modified/derived adsorbents and the parent fly ash. These methods also provided valuable insights into the adsorption mechanism of TC on the adsorbents.

3.3.1 X-ray Diffraction (XRD)

XRD analysis was conducted to determine the crystallinity and mineralogy of the samples. The samples were prepared according to the standardized Panalytical backloading system, which provides a nearly random distribution of the particles. XRD analysis was conducted with a PANalytical X'Pert Pro powder diffractometer in $\Theta - \Theta$ configuration with an X'Celerator detector and variable divergence- and fixed receiving slits with Fe filtered Co-Kα radiation (λ=1.789 Å). The mineralogy was determined by selecting the best–fitting pattern from the ICSD database to the measured diffraction pattern, using X'Pert Highscore plus software. The crystallinity of zeolite Na-P1 was determined using Equation 15

$$\text{Crystallinity } (\%) = \frac{\sum \text{Area of zeolite peaks}}{\sum \text{Area of all peaks in scan}} \tag{15}$$

3.3.2 X-ray Fluorescence (XRF)

The samples were dried & roasted in alumina refractory crucibles, at 100 °C & 1000 °C respectively, to determine loss on ignition (LOI). One gram sample was mixed with 6 g Lithiumteraborate flux and fused at 1030 °C to make a stable fused glass bead. The Thermo Fisher ARL Perform'X Sequential XRF instrument with Uniquant software was used for analyses. The software analyse for all elements in the periodic table between Na and U, but only elements found above the detection limits were reported.

3.3.3 Surface Area Analysis (BET)

The nitrogen sorption isotherm and BET surface area were measured on a Micromeritics TriStar II with a liquid nitrogen temperature of 77.350 K. This was done to determine the

specific surface area and pore size of the synthesized particles. The samples were dried for 24 h prior to the analysis under pure nitrogen flow to remove all water molecules.

3.3.4 Scanning Electron Microscopy (SEM)

The morphology of the synthesized particles was captured on a Zeiss Crossbeam 540 FEG SEM instrument using the Oxford instruments detector and Aztec 3.0 software SP1. A strip with the samples was attached to an aluminum plate before being coated with carbon. The carbon coater used is a SEM auto-coating unit E2500 (Polaron Equipment Ltd).

3.3.5 Zeta Potential

The zeta potential (ζ-potential) was characterised using dynamic light scattering (DLS) on a Zetasizer Nano-ZS instrument (Malvern Instruments, UK). Samples were prepared from a stock solution of 100 ppm of the sample and diluted to 1 ppm. The 1 ppm solutions were then adjusted to various pHs using 0.1 M NaOH and 0.1 M HCl. The samples were left for 24 hours before zeta potential analysis. The zeta potential can aid in determining the surface charge of the sample at various pHs.

3.3.6 Fourier Transform Infrared Spectroscopy (FTIR)

FTIR was conducted on selected adsorbents before and after adsorption on a Shimadzu IRSpirit-TX fourier transform infared spectrophotometer equipped with a quartz attenuated total reflectance assesory (QATR). All FTIR scans were recorded at resolution of 2 cm^{-1} for 45 scans from 4700 cm^{-1} to 350 cm^{-1}. Note that the scans represent an average of the 45 scans. FTIR analysis can assist in determining functional groups on the surface of the sample. This information is vital in determining which functional groups play a role in adsorption.

3.3.7 Cation Exchange Capacity (CEC)

The CEC measurement for FA and AM-FA was adopted from Woolard *et al* (2000) and the CEC measurement for BM-FA and ZNa-P1 was adopted from Musyoka *et al* (2009). Two different methods were employed because the zeolite species, such as BM-FA and ZNa-P1, are saturated with exchangeable sodium, whereas FA and AM-FA are not. Therefore,

in the CEC method for FA and AM-FA, the samples were placed in sodium acetate to introduce exchangeable sodium.
The reagent preparation for both methods is as follows:

- Sodium acetate (1 M): 136 g of sodium acetate trihydrate was diluted with 1000 ml of ultra-pure water. The pH of the solution was altered to 8.2 using acetic acid.
- Ammonium acetate (1 M): 72 ml of acetic acid was added to 1000 ml volumetric flask and diluted to 500 ml with ultra pure water. The dilution was done to reduce the acid-base reaction. Then, 94 ml of ammonium hydroxide added and finally the solution was topped up to 1000 ml with ultra pure water. The pH of the solution was altered to 8.2 by adding ammonium hydroxide.

3.3.7.1 FA and AM-FA CEC Measurement

One gram of ash sample was shaken for 15 min with 33 ml of 1 M sodium acetate then centrifuged for 15 min. The extracted ash sample was again shaken in a 1 M sodium acetate solution for 15 min. This procedure was done a total of three times. The sample was then washed four times in ultra pure water. Finally, the sample was shaken for 15 min with 33 ml of 1 M ammonium acetate solution then centrifuged for 15 min. The supernatant was kept aside for analysis and the extracted sample was again shaken in 1 M ammonium acetate solution for 15 min. This was done a total of three times. The final accumulative volume of supernatants was approximately 100 ml. The concentration of sodium in the final solution was determined using atomic absorption spectroscopy.

3.3.7.2 BM-FA and ZNa-P1 CEC Measurement

Half a gram of zeolites was shaken for 15 min with 25 ml of 1 M ammonium acetate then centrifuged for 15 min. The supernatant was collected and the extracted zeolites was again shaken with 1 M ammonium acetate. This was done a total of four times. The final accumulative volume of supernatants was approximately 100 ml. The concentration of sodium in the final solution was determined using atomic absorption spectroscopy.

3.4 Analytic Analysis

3.4.1 UV-VIS Analysis

The initial and final TC concentrations were determined using a VWR UV-1600PC spectrophotometer at an interval of 1 nm from 500 nm to 300 nm. The sample was diluted

by a factor of 2 in 0.1 M NaOH. The high pH caused deprotonation of the tetracycline molecule and produced a more intense yellow colour that was detectable on the UV-VIS spectrophotometer. The concentration of tetracycline was determined using to a calibration curve developed with the observed peak wavelength at 381 nm. The calibration curve is shown in Figure A.1.

3.5 Adsorption Studies

Firstly, a 200 ppm TC stock solution was prepared. The batch adsorption studies were carried out in 30 ml glass vials and the experimental solutions were prepared by diluting the TC stock with a pH buffer. Fly ash and the derived adsorbents had a strong alkalinity which influenced the pH of the solutions. The pH buffers were used to regulate the pH and avoid pH fluctuations. Kao *et al* (2000) noted that pH fluctuations near the pKa of an adsorbate might impact adsorption more than the presence of a pH buffer.

All experimental samples were agitated on an orbital shaker at a rotation speed of 250 rpm. After adsorption, a 2 ml sample was centrifuged at 10 000 rpm for 1 min to separate the adsorbent from solution and the TC concentration was determined from the supernatant.

3.5.1 Adsorption studies with modified FA and ZNa-P1

Preliminary adsorption tests were conducted with FA, AM-FA, BM-FA and ZNa-P1 to compare and identify the most effective adsorbent for TC removal. Two key process parameters, adsorbent dosage and solution pH, were varied to establish the optimal operating conditions for the adsorption of TC using ZNa-P1. Additionally, adsorption kinetics experiments were performed with ZNa-P1 to determine the equilibrium time, while adsorption isotherms and thermodynamic studies were conducted with the ZNa-P1 to elucidate the underlying adsorption mechanism of TC on ZNa-P1. Please note that for the adsorption isotherm experiments, high initial concentrations ($70 - 120$ ppm) were used to ensure that 100 % removal of TC was not achieved. This approach allowed for better fitting of the adsorption models by capturing both low and high coverage regions of the isotherm. Note that non-linear regression was used to model all isotherm and kinetic data. The non-linear regression was performed on Python using the "curve fit" function that determines the best fitting parameters for a non-linear equation.

Table 9: Summary of the ZNa-P1 adsorption experiments conditions and variables studied.

Adsorption Experiment	Adsorbent(s)	Conditions	Variable Studied
Preliminary Adsorption Test	FA, AM-FA BM-FA, ZNa-P1	Co: 40 ppm, pH: 5, Dosage: 5 g/L, time: 2 h	Comparison of adsorbents
Effect of Dosage	ZNa-P1	Co: 40 ppm, pH: 5, Dosage: 1-12.5 g/L, time: 2 h	Dosage
Effect of pH	ZNa-P1	Co: 60 ppm, pH: 2-9, Dosage: 7.5 g/L, time: 2 h	pH
Adsorption Kinetics	ZNa-P1	Co: 60 ppm, pH: 5, Dosage: 7.5 g/L	Time
Adsorption Isotherms	ZNa-P1	Co: 70-120 ppm, pH: 5, Dosage: 7.5 g/L, time: 4 h	-
Adsorption Thermodynamics	ZNa-P1	T: 30 °C, 40 °C, 50 °C	Effect of temperature

3.5.2 Adsorption studies with silica nanoparticles

A parallel adsorption study was conducted with the silica nanoparticles based adsorbents. Preliminary adsorption tests were conducted with FA-SiNPs, SSSNPs, and Fe-SiNPs to compare and identify the most effective adsorbent for TC removal. The rest of experiments were then carried out with Fe-SiNPs. Similarly, in the adsorption isotherm experiments with Fe-SiNP, higher initial concentrations ($90 - 140$ ppm) were used to ensure that 100 % removal of TC was not achieved.

Table 10: Summary of the Fe-SiNPs adsorption experiments conditions and variables studied.

Adsorption Experiment	Adsorbent(s)	Conditions	Variable Studied
Preliminary Adsorption Test	FA-SiNPs, SSSNPs Fe-SiNPs	Co: 100 ppm, pH: 5, Dosage: 5 g/L, time: 0.5 h	Comparison of adsorbents
Effect of Dosage	Fe-SiNPs	Co: 50 ppm, pH: 5, Dosage: 1-10 g/L, time: 2 h	Dosage
Effect of pH	Fe-SiNPs	Co: 70 ppm, pH: 2-9, Dosage: 5 g/L, time: 2 h	pH
Adsorption Kinetics	Fe-SiNPs	Co: 70 ppm, pH: 5, Dosage: 5 g/L	Time
Adsorption Isotherms	Fe-SiNPs	Co: 90-140 ppm, pH: 5, Dosage: 5 g/L, time: 6 h	-
Adsorption Thermodynamics	Fe-SiNPs	T: 30 °C, 40 °C, 50 °C	Effect of temperature

CHAPTER 4 – RESULTS AND DISCUSSION: MODIFICATION AND ZEOLITES

4.1 XRD Results

XRD analysis was conducted to evaluate the change in crystallinity of FA after modification. The XRD patterns for FA, AM-FA, BM-FA and ZNa-P1 are shown in Figure 8.

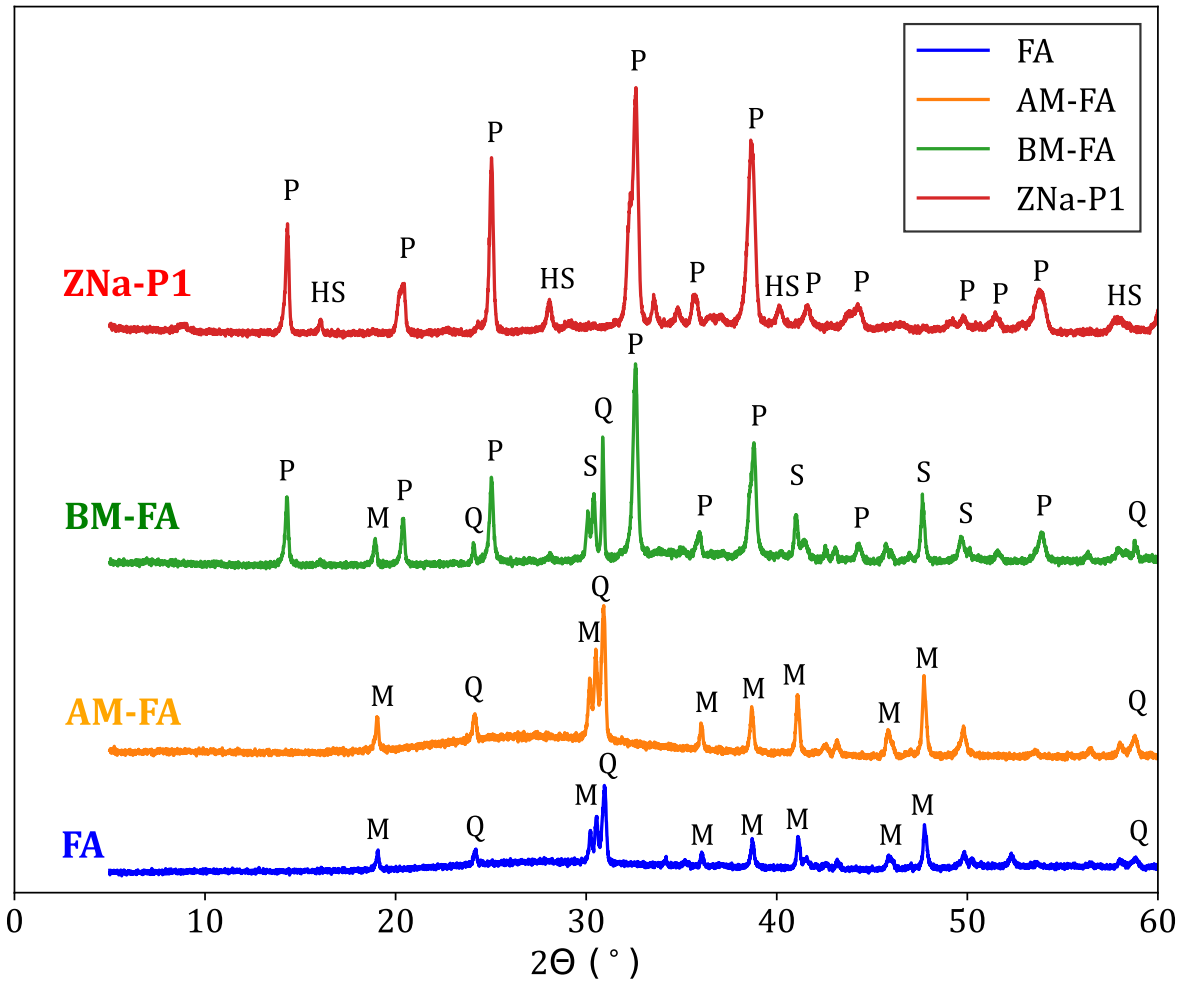

Figure 8: XRD Patterns for FA, AM-FA, BM-FA, and ZNA-P1. The phases indicated in the XRD patterns: mullite (M), quartz (Q), sillimanite (S), hydroxy-sodalite (HS), and zeolite Na-P1 (P).

The XRD pattern for FA indicated that the major crystalline phases were mullite and quartz. There was no significant change noted in XRD pattern of AM-FA after acid-modification. Taufiq *et al* (2018) and Wulandari *et al* (2020) also noted that there was no substantial change after acid modification beyond the reduction of the amorphous phase. The XRD pattern of BM-FA showed the presence of zeolite Na-P1. However, the

occurrence of mullite and quartz peaks indicates only partial digestion of these phases for zeolitization (Mainganye *et al*, 2013). The XRD pattern of ZNa-P1 showed two main phases being zeolite Na-P1 and hydroxy-sodalite. Hydroxy-sodalite, is another zeolite phase which is considered an impurity in the Zeolite Na-P1 synthesis (Musyoka *et al*, 2009). The mullite and quartz peaks completely disappeared, indicating full digestion of these phases for zeolitization and suggests a high conversion of the FA to a zeolite Na-P1 (Mainganye *et al*, 2013). The percentage crystallinity of zeolite Na-P1, as calculated using Equation 15, in BM-FA and ZNa-P1 was 43 % and 86 %, respectively.

4.2 XRF Results

The chemical composition of FA, AM-FA, BM-FA, and ZNa-P1 was analysed using XRF and is shown in Table 11. The fly ash was classified as Class F as per the ASTM C618 standard, since the combined SiO_2, Al_2O_3, Fe_2O_3 content exceeded 70 % and low CaO content ($<$ 18 %) (Elidrissi *et al*, 2023). The results indicate a significant decrease in metal cations, i.e. aluminium, iron, magnesium and calcium, after acid-modification. The observed increase in silicon was attributed to reduction of other elements and the fact that silicon is more resistant to acidic attack (Wulandari *et al*, 2020; de Oliveira *et al*, 2020). After base modification, there was a drop in silicon and aluminium content and an increase in the sodium content. The NaOH could have leached out the silica and aluminium into the solution. The large sodium increase also indicates that zeolitization took place during the base modification (Elidrissi *et al*, 2023). ZNa-P1 has a composition similar to BM-FA. Notably, ZNa-P1 has a higher sodium composition than the BM-FA, indicating more zeolitization occurred in the production of ZNa-P1.

Table 11: Chemical composition of FA, AM-FA, BM-FA, and ZNa-P1.

Oxides (wt%)	SiO_2	Al_2O_3	MgO	Na_2O	P_2O_5	Fe_2O_3	K_2O	CaO	TiO_2	SrO	LOI*
FA	49.88	31.01	1.79	0.36	0.86	3.52	0.84	4.73	1.51	0.53	4.46
AM-FA	57.68	27.62	0.59	0.25	0.47	1.26	0.81	0.97	1.62	0.29	7.95
BM-FA	38.17	28.64	1.70	9.62	0.44	3.25	0.49	4.30	1.39	0.50	11.01
ZNa-P1	40.62	27.76	1.5	14.65	0.24	2.12	0.18	4.42	1.44	0.12	6.33

*Loss on ignition

4.3 SEM and BET Results

Figure 9 shows the SEM images for FA, AM-FA, BM-FA and ZNa-P1. The surface morphology of FA consists of spherical and smooth particles. No significant change in the surface morphology was observed after acid modification. Note that the XRD analysis also showed little change in the mineralogy after acid modification. The surface morphology of BM-FA showed a substantial change after base modification. The particles transformed from smooth spherical shapes to more irregular-shaped crystalline particles. The surface morphology of ZNa-P1 showed more needle-like crystalline shapes which is the typical morphology of zeolite Na-P1 (Mainganye *et al*, 2013). Table 12 gives the specific surface area for FA, AM-FA, BM-FA, and ZNa-P1 determined using BET method. The acid modification increased the specific surface area by approximately 100 %. The base modification showed the largest increase in specific surface area approximately a ten-fold increase. ZNa-P1 adsorbent had a surface area three times as large as FA. After alkali-activation, the particle size of FA decreases due to alkali-etching of the surface of the FA particles, resulting in an increase in surface area (Koshy & Singh, 2016). The large difference in particle sizes between FA and BM-FA/ZNa-P1 is seen Figure 9. The surface area of BM-FA was larger than ZNa-P1. This can be attributed to the smaller particle size of BM-FA compared to ZNa-P1, which appears more rigid and dense.

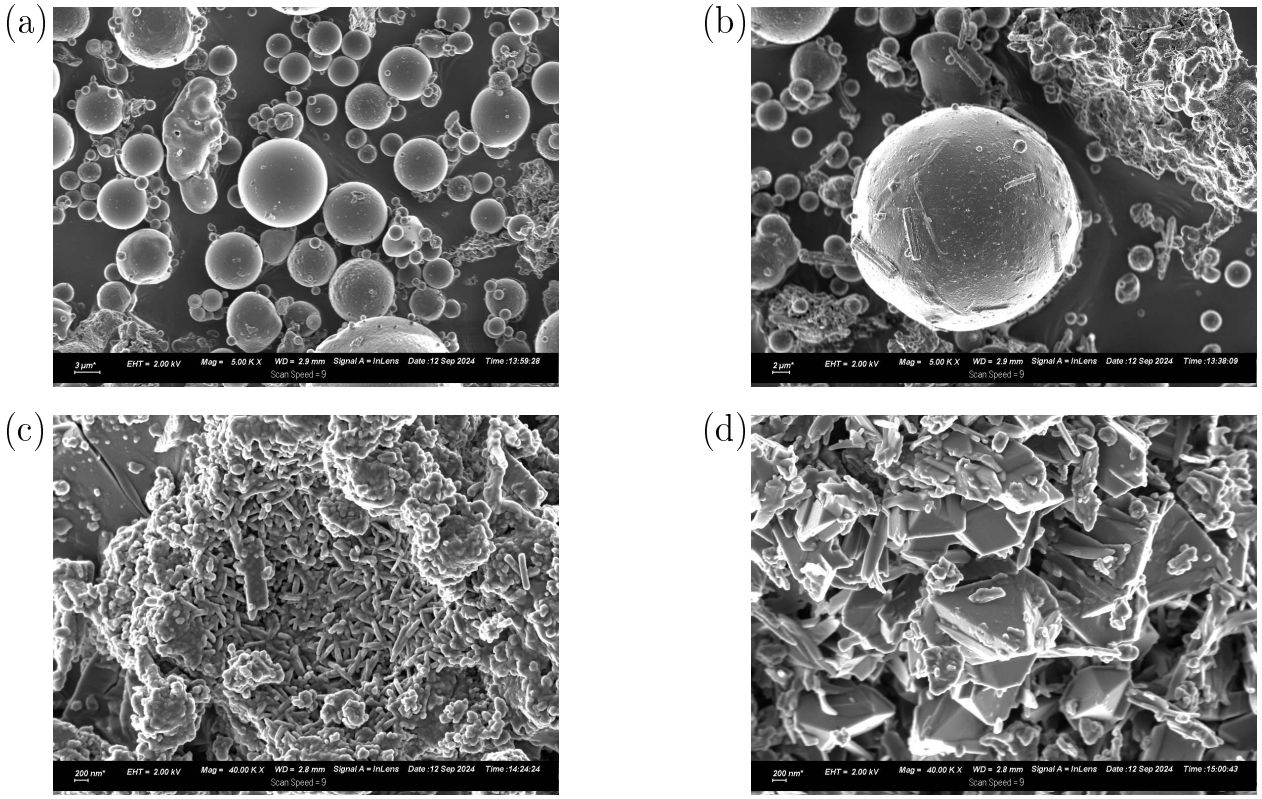

Figure 9: SEM images for (a) FA, (b) AM-FA, (c) BM-FA and (d) ZNa-P1. Note that due to the differences in particle sizes, the magnification for FA and AM-FA is 5000 and BM-FA and ZNa-P1 is 40 000.

Table 12: Specific surface area for FA, AM-FA, BM-FA, and ZNa-P1 determined using the BET method.

Material	FA	AM-FA	BM-FA	ZNa-P1
Specific surface area (m^2/g)	10.94	21.81	110.83	35.75

4.4 CEC Results

Figure 10 shows the cation exchange capacity for FA, AM-FA, BM-FA and ZNa-P1. Both FA and AM-FA had significantly lower CEC values as compared to BM-FA and ZNa-P1. The higher CEC values for BM-FA and ZNa-P1 was attributed to the presence of zeolite Na-P1 in these materials (Zhang *et al*, 2021). As previously stated, the percentage crystallinity of BM-FA and ZNa-P1 was 43 % and 86 %, respectively. Note that the ZNa-P1 had both a higher zeolite crystallinity and higher CEC value, suggesting a correlation between cation exchange capacity and zeolite crystallinity. Zheng *et al* (2019) found a similar conclusion being that the CEC values were directly proportional to the zeolite crystallinity.

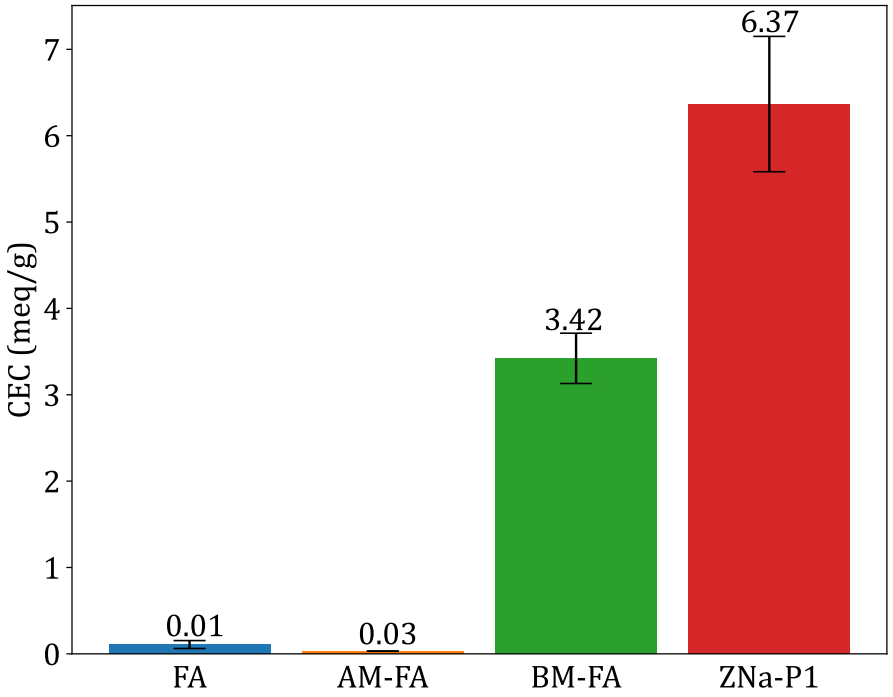

Figure 10: Cation exchange capacity for FA, AM-FA, BM-FA and ZNa-P1.

4.5 Comparison of AM-FA, BM-FA and ZNa-P1 for Tetracycline adsorption

The preliminary adsorption test was conducted under the same set of conditions for FA, AM-FA, BM-FA, and ZNa-P1. The percentage removals of TC for FA, AM-FA, BM-FA, and ZNa-P1 are shown in Figure 11. The percentage removal of FA was 35 %, after acid modification the percentage removal reduced to 11 %. Though the surface of AM-FA increased, the CEC value decreased. Both BM-FA and ZNa-P1 had a significant increase in TC removal, 76 % and 90 %, respectively. Both BM-FA and ZNa-P1 had high surface areas and high CEC values. It should be noted that ZNa-P1 had a lower surface area than BM-FA but a higher CEC value. The higher percentage removal of ZNa-P1 could be attributed to the high CEC value due to the purer zeolite phase (Na-P1) present in ZNa-P1. Therefore, the adsorption of TC is directly proportional to the CEC of a material and not the surface area. CEC refers to the ability of a material to adsorb exchangeable cations. A higher CEC signifies that the material can more effectively adsorb cations through electrostatic forces (Munthali *et al*, 2015). Note that the rest of the adsorption studies in Chapter 4 were conducted with ZNa-P1.

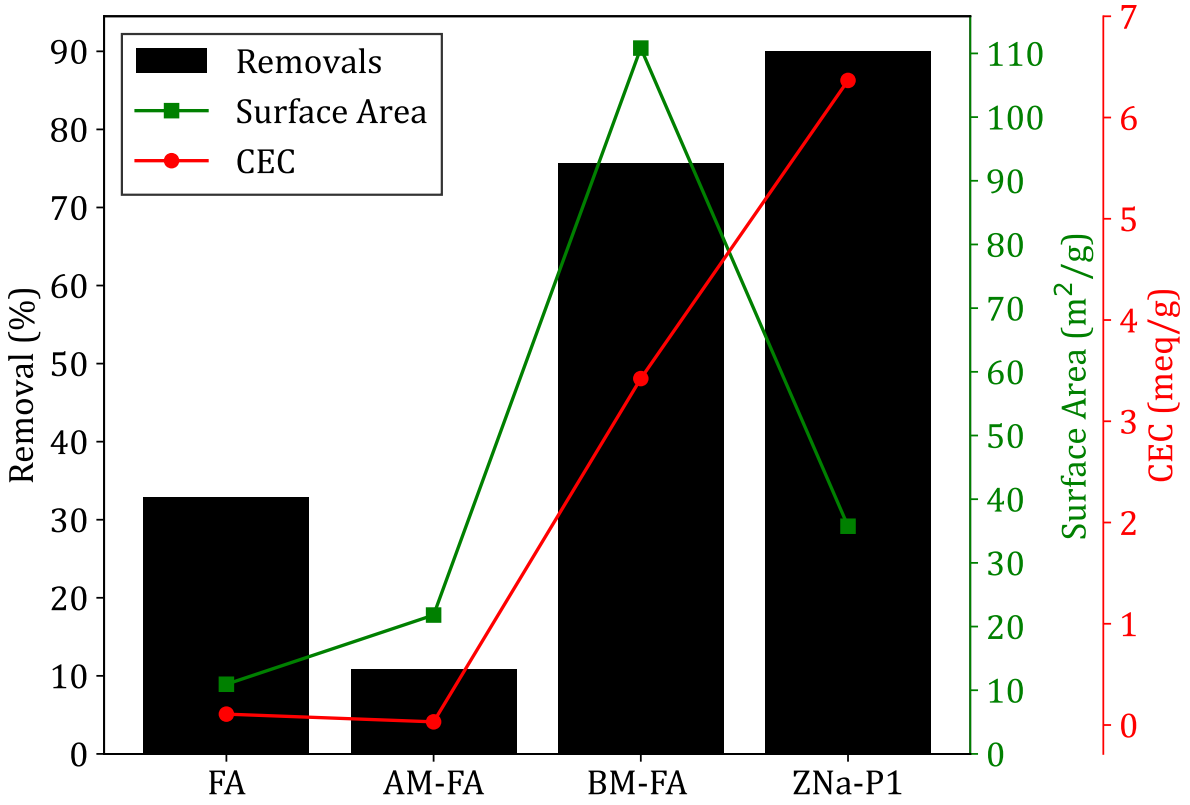

Figure 11: The percentage removal, Surface Area (right axis) and CEC (far-right axis) of FA, AM-FA, BM-FA and ZNA-P1 (conditions for removal experiments - pH: 5, Dosage: 5 g/L, contact time: 2 h, C_O: 40 ppm).

4.6 Tetracycline Adsorption with ZNa-P1

4.6.1 The effect of Dosage

The effect of adsorbent dosage on the removal of TC is shown in Figure 12 (a). The results indicate that an increase in the adsorbent dosage, increased the removal of TC. This could be attributed to the increase in active sites for adsorption at higher dosages. The optimal dosage was 7.5 g/L, as there was no substantial increase in the percentage removal of TC after a dosage of 7.5 g/L.

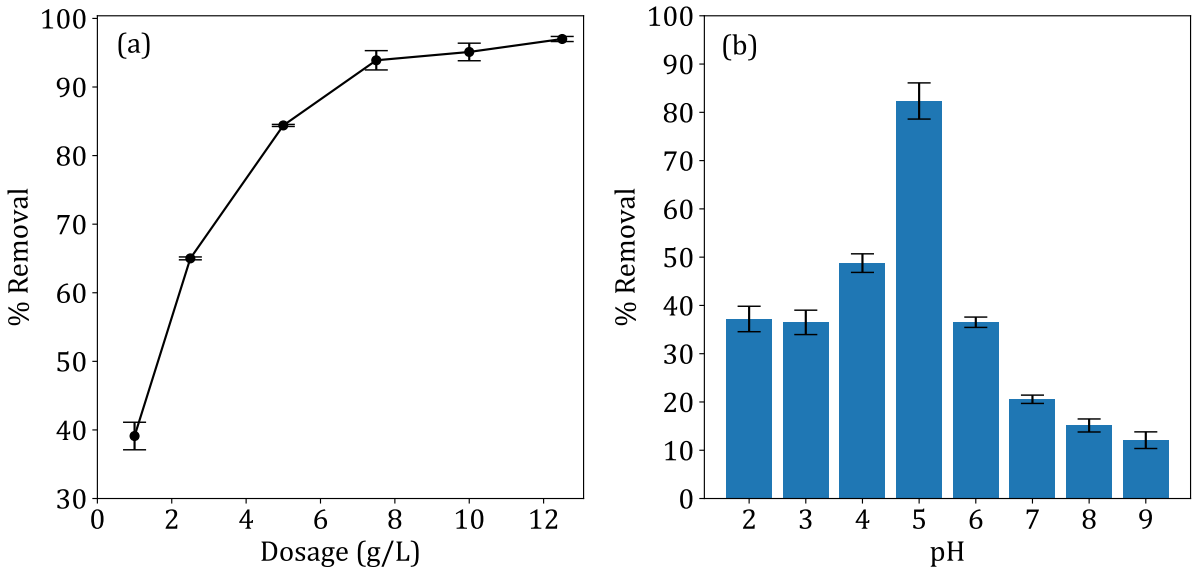

Figure 12: (a) The effect of ZNa-P1 dosage and (b) the effect of pH on TC removal.

4.6.2 The effect of pH

The effect of pH on the removal of tetracycline is shown in Figure 12 (b). Due to the amphoteric nature of tetracycline it can exists as a cationic, anionic, or neutral species, based on the pH (Turku *et al*, 2007). Figure 13 presents the zeta potential of ZNa-P1 as a function of pH. The highest percentage removal was noted at a pH of 5, therefore pH 5 was determined to be the optimal pH. As seen in Figure 1 (b), at a pH of 5, tetracycline is neutral and ZNa-P1 surface is negatively charged. According to Jia *et al* (2008), though tetracycline may not have a net charge (neutral) its adsorption behaves as though it was positively charged. This suggest there is an electrostatic attraction at a pH of 5. At a pH$<$ 5, tetracycline adsorption decreased. At a pH$<$ 5, tetracycline becomes cationic whereas ZNa-P1 surface becomes neutral and thus the electrostatic attraction between TC and ZNa-P1 no longer exists. At pH$>$ 5, tetracycline adsorption decreased. At pH$>$ 5, tetracycline becomes anionic and ZNa-P1 surface possesses a negative charge

causing electrostatic repulsion between ZNa-P1 and TC reducing adsorption. Note that as the pH increases, the negative charge of on the surface ZNa-P1 increases, increasing electrostatic repulsion and TC-adsorption decreases.

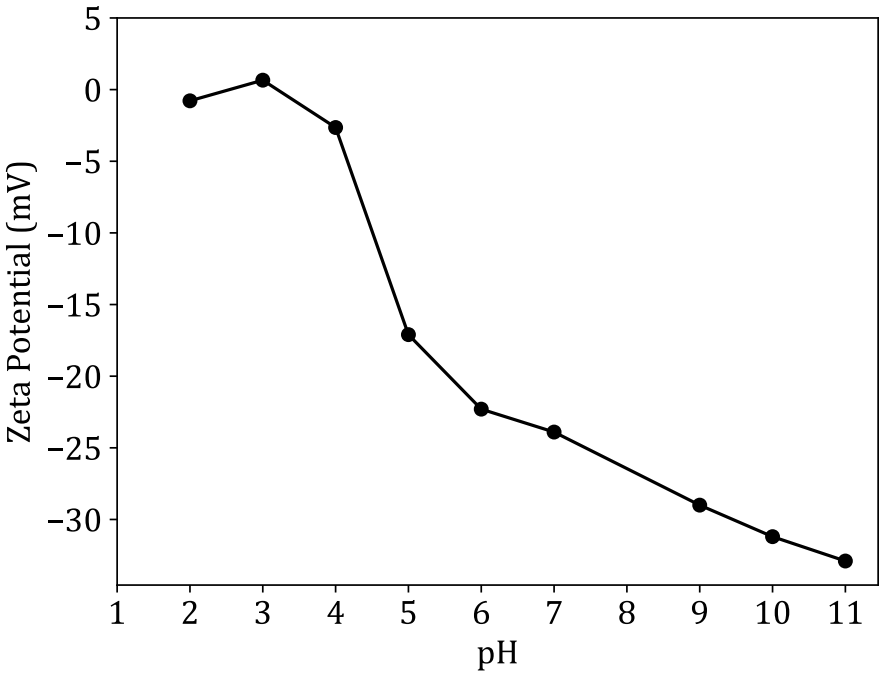

Figure 13: Zeta potential of ZNa-P1 as a function of pH as determined using a Zetasizer.

4.6.3 Adsorption Kinetics

The adsorption kinetics were modelled using non-linear regression. The non-linear regression was conducted on Python using the function "curve-fit". The function uses a non-linear equation and determines the best fit parameters based on guess values. The models used to describe the adsorption kinetics were the pseudo first order model (PFO), pseudo second order model (PSO), Elovich model and the Langmuir kinetic model, given in Equations 2, 3, 4, and 5, respectively. Figure 14 shows the adsorption kinetics of TC on ZNa-P1, fitted with pseudo first order, pseudo second order, Elovich, and Langmuir kinetic models. Table 13 presents a summary of model parameters and statistical parameters for each fitted model. The pseudo-second-order model exhibited the lowest squared error and highest R^2 value, indicating that the adsorption kinetics of TC were best described by this model. According to Molina-Calderón *et al* (2022), the pseudo-second-order model is useful for explaining adsorption where the rate-controlling steps involve chemisorption mechanisms (such as complexation) or ion exchange. However, Bandura *et al* (2022) cautions that the adsorption mechanism cannot be definitively determined by the PFO or PSO models. The best fit of the PSO model in this case suggests

that chemisorption or ion exchange could be the dominant mechanism for tetracycline adsorption onto ZNa-P1.

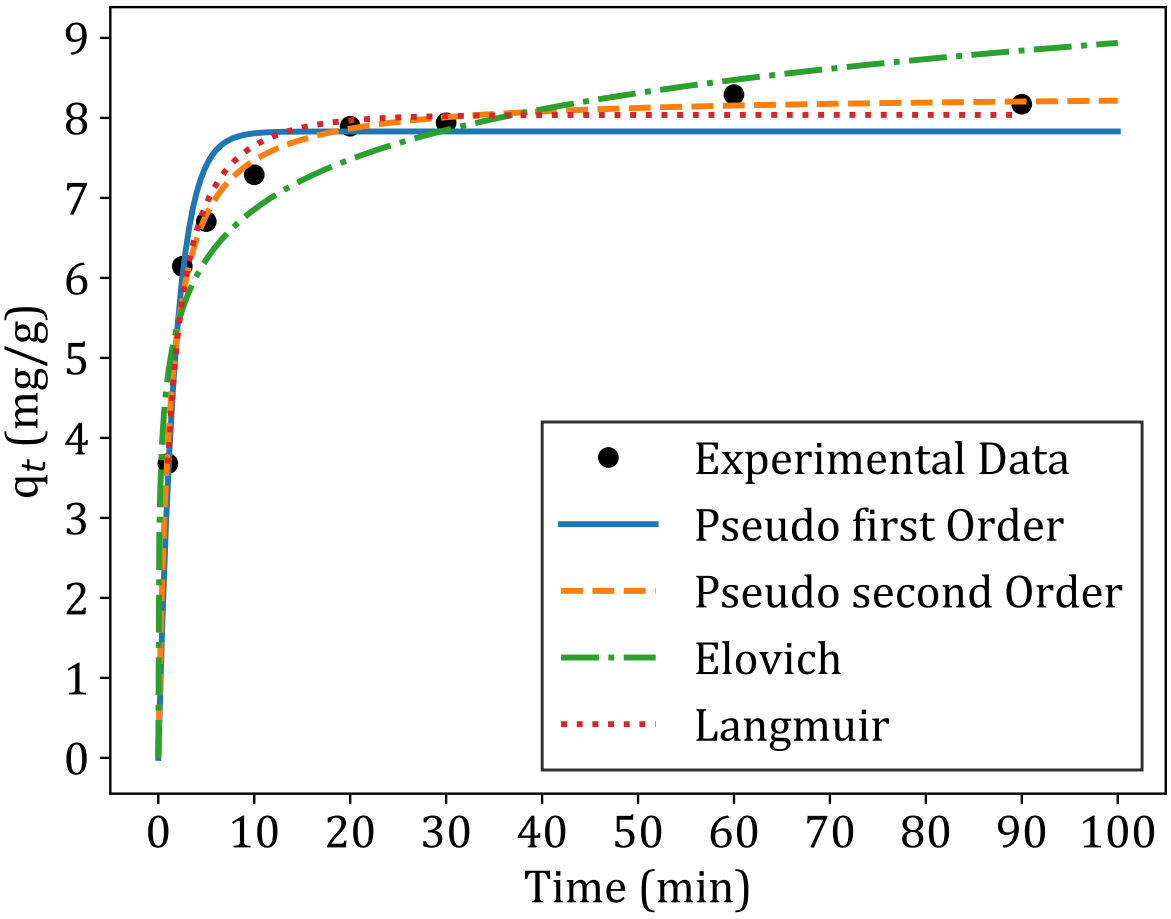

Figure 14: Adsorption kinetics of TC on ZNa-P1 fitted with adsorption kinetic models (conditions for kinetic experiments - pH: 5, Dosage: 7.5 g/L, C_O: 60 ppm).

Table 13: Adsorption kinetic model parameters and statistical parameters for the adsorption of TC on ZNa-P1.

Kinetic Model	Kinetic Parameters			Statistical Parameters	
Pseudo first order (PFO)	q_e (mg/g)	k_1 (1/min)		Squared Error	R^2
	7.83	0.58		1.17	0.93
Pseudo second order (PSO)	q_e (mg/g)	k_2 (g/mg/min)		Squared Error	R^2
	8.31	0.11		0.29	0.98
Elovich	α (mg/g/min)	β (g/mg)		Squared Error	R^2
	177.43	1.11		2.58	0.85
Langmuir kinetic	k_a (L/g/min)	k_d (mg/L/min)	q_{max} (mg/g)	Squared Error	R^2
	0.09	0.00	8.04	0.45	0.97

4.6.4 Adsorption Isotherms

The adsorption isotherms were modelled using non-linear regression. The same non-linear regression procedure was utilised in Python. The models used to describe the adsorption isotherms were the Langmuir isotherm model, Freundlich isotherm model, and the Temkin isotherm model, given in Equations 6, 7, 8, respectively. Figure 15 shows the adsorption isotherms of TC on ZNa-P1 at 30 °C, 40 °C and 50 °C fitted with Langmuir, Freundlich, and Temkin isotherm models. Table 14 presents a summary of the adsorption isotherm model parameters and statistical parameters for each isotherm model. The Langmuir isotherm model showed the lowest squared error and highest R^2 value at all temperatures, except for 40 °C, indicating that the adsorption isotherms of tetracycline were best described by this model. The Langmuir model best fit suggests that tetracycline adsorption onto ZNa-P1 occurred as a monolayer on a homogeneous surface (Aliyu *et al*, 2022). Table 15 presents the maximum adsorption capacities (q_m) of various adsorbents for tetracycline removal. Notably, the β-cyclodextrin-modified Zeolite Na-P1 exhibited a lower adsorption capacity, implying that the organic modification did not significantly enhance tetracycline adsorption.

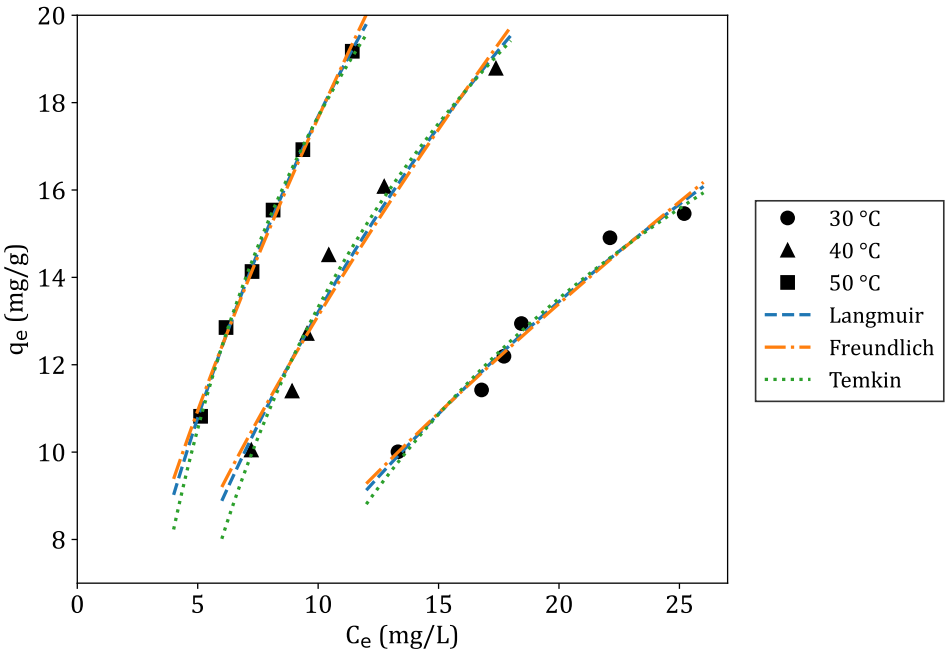

Figure 15: Adsorption isotherms of tetracycline at 30 °C, 40 °C and 50 °C fitted with the adsorption isotherm models (conditions for isotherm experiments - pH: 5, Dosage: 7.5 g/L, contact time: 4 h).

Table 14: Adsorption isotherm model parameters and statistical parameters for the adsorption of TC on ZNa-P1 at 30 °C, 40 °C, and 50 °C.

Isotherm Model	Temperature		
	30 °C	**40 °C**	**50 °C**
Langmuir isotherm model			
Isotherm Constants			
q_m (mg/g)	46.34	48.79	49.14
K_L (L/mg)	0.020	0.037	0.056
Statistical Parameters			
Squared Error	0.58	1.70	0.09
R^2	0.973	0.967	0.998
Freundlich isotherm model			
Isotherm Constants			
K_f (mg/g)	1.55	2.65	3.61
n	1.39	1.44	1.45
Statistical Parameters			
Squared Error	0.64	2.23	0.22
R^2	0.971	0.957	0.995
Temkin isotherm model			
Isotherm Constants			
B_T (J/mol)	0.22	0.36	0.56
A_T (L/mg)	9.22	10.38	10.31
Statistical Parameters			
Squared Error	0.61	1.26	0.10
R^2	0.972	0.976	0.998

Table 15: Comparison of maximum adsorption capacities of adsorbents for TC removal

Absorbent	q_m (mg/g)	pH	Temperature (°C)	Reference
Modified rubber waste (MRW)	76.33	3	25	(Aliyu *et al*, 2022)
Zeolite Na-P1 modified with β-cyclodextrin	38	-	-	(Bandura *et al*, 2022)
Rice husk ash (RHA)	8.370	5	40	(Chen *et al*, 2016)
Activated carbon derived from Palm leave waste	132.94	5.86	25	(Islam *et al*, 2024)
Shrimp shell waste (SSW)	381.75	7	25	(Chang *et al*, 2020)
Na-montmorillonite	49.8	5.5	-	(Figueroa *et al*, 2004)
Polyvinyl chloride (PVC) Microplastics	21	7	-	(Zahmatkesh Anbarani *et al*, 2023)
Pumice stone	20.1	3	20	(Guler & Sarioglu, 2014)
ZNa-P1	46.34	5	30	This study

4.6.5 Adsorption Thermodynamics

The Gibbs free energy (ΔG°) was calculated using Equation 9. The entropy change (ΔS°) and enthalpy change (ΔH°), was calculated using Equation 11. The dimensionless constant, K_{eq}, was determined from the Langmuir constant, K_L, using Equation 12. Similarly to Tran *et al* (2021), both $C^\circ_{\text{absorbate}}$ and $\gamma_{\text{absorbate}}$ were assumed to be unity. Table 16 presents a summary of the thermodynamic parameters for the adsorption of tetracycline on ZNa-P1. The negative value of ΔG° signified that the adsorption process occurred spontaneously. The positive ΔS° indicated increased randomness at solid/solution interface during adsorption and that the adsorbent had an affinity for the adsorbate (Liu & Lee, 2014). The value of ΔH° was positive indicating that the adsorption process was endothermic and more favourable at higher temperatures. According to Molina-Calderón *et al* (2022), if the value of ΔH° is between 20 and 80 kJ/mol it indicates that adsorption is a combination of physisorption and chemisorption, typically associated with an ion-exchange mechanism. The ΔH° value was 41.26 kJ/mol suggesting that a ion-exchange mechanism for the adsorption of TC on ZNa-P1.

Table 16: Thermodynamics parameters for tetracycline adsorption on ZNa-P1.

Temperature (°C)	K_D	ΔG° (kJ/mol)	ΔH° (kJ/mol)	ΔS° (kJ/mol)	R^2
30	9085.12	−22.97	41.26	0.21	0.993
40	16 490.54	−25.28			
50	24 983.65	−27.21			

4.6.6 Adsorption Mechanism

Figure 16 gives the FTIR spectra of ZNa-P1 before and after adsorption of TC. The bands at $610 - 580$ cm^{-1} is associated with the double ring vibration of zeolite Na-P1. The bands at $770 - 660$ cm^{-1} corresponds to the symmetric stretching vibration of TO_4 (where T is Si or Al) (Amri *et al*, 2024). The band at $1100 - 900$ cm^{-1} corresponds to the asymmetric stretching vibration of TO_4 (Liu *et al*, 2018b). The band at 1680—1620 cm^{-1} is attributed to the bending vibration of OH groups, while the broad band at 3700—3000 cm^{-1} is associated with the stretching vibration of OH groups (Bandura *et al*, 2022).

After the adsorption of TC, shifts were noted in the peaks corresponding to the symmetric and asymmetric vibrations of TO_4 at $770 - 660$ cm^{-1} and $1100 - 900$ cm^{-1}, respectively. This indicated interactions between TC and ZNa-P1, confirming the adsorption of TC

onto ZNa-P1. Additionally, a shift and an increase in the intensity of the stretching OH band, originally observed at 3700—3000 cm^{-1}, was noted after adsorption. This suggested the presence of hydrogen bonding or other interactions between the hydroxyl groups in ZNa-P1 and the functional groups in TC (Zhao *et al*, 2024). The effect of pH revealed the presence of electrostatic attraction between TC and ZNa-P1, while adsorption thermodynamics indicated a potential ion-exchange mechanism.

Ultimately, the adsorption mechanism of tetracycline on ZNa-P1 involved electrostatic attraction, hydrogen bonding, and ion exchange. Liu *et al* (2013) used zeolite A to adsorb tetracycline and noted a similar adsorption mechanism being an ion-exchange process and electrostatic attraction.

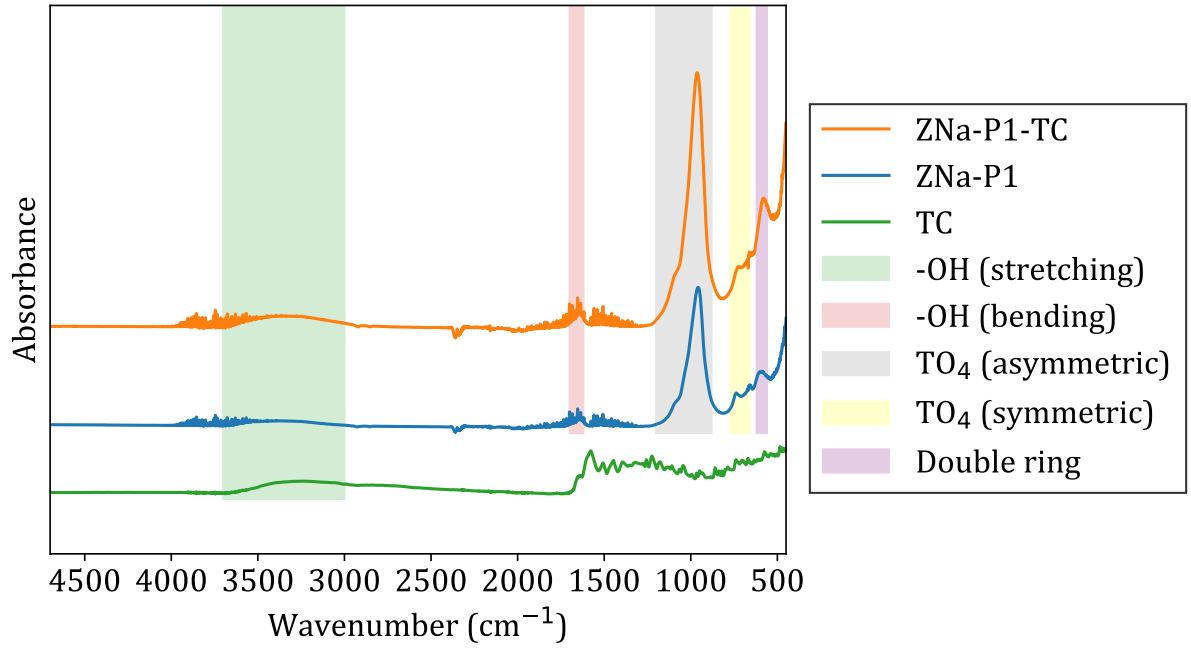

Figure 16: FTIR spectra of ZNa-P1 before and after adsorption of TC. Note that the FTIR spectra before adsorption is denoted as ZNa-P1 and the FTIR spectra after adsorption is denoted as ZNa-P1-TC.

CHAPTER 5 – RESULTS AND DISCUSSION: SILICA NANOPARTICLES

5.1 XRD Results

The XRD analysis, in this chapter focuses on the crystallinity of the silica nanoparticles. The XRD patterns for FA-SiNPs, SSSNPS, and Fe-SiNPs are shown in Figure 17. None of the materials exhibit sharp peaks but only a single broad peak centred at $2\theta = 25°$ This indicates the amorphous nature of the materials (Nallathambi *et al*, 2011). There was also no change in crystallinity noted in Fe-SiNPs after the iron modification.

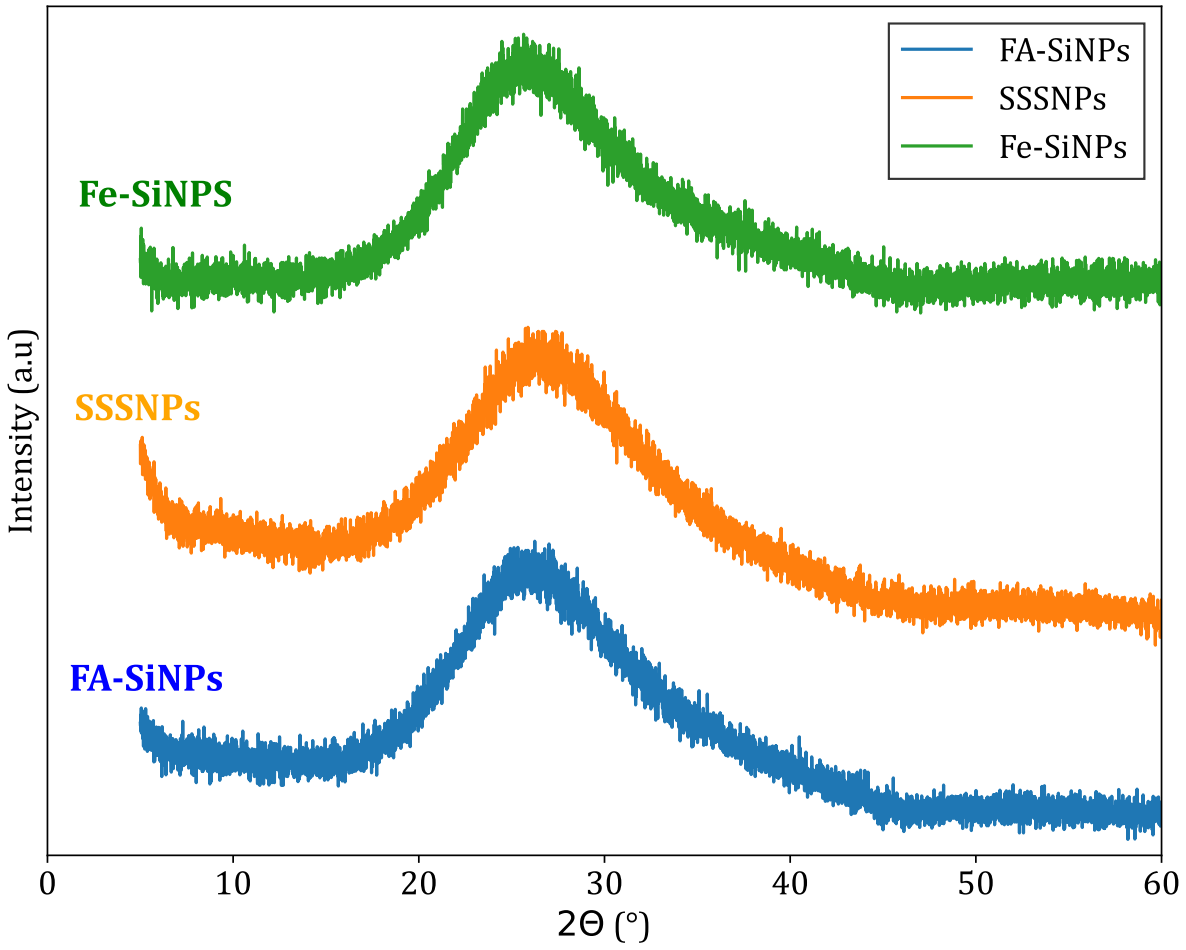

Figure 17: XRD Patterns for FA-SiNPs, SSSNPS, and Fe-SiNPs.

5.2 XRF Results

The chemical composition of FA-SiNPs, SSSNPs, and Fe-SiNPs is shown in Table 17. Both FA-SiNPs and SSSNPs had a high silicon content (> 90 %), with FA-SiNPs con-

taining small amounts of impurities, primarily aluminium. Fe-SiNPs showed a 2 % iron content, confirming the iron modification.

Table 17: Chemical composition of FA-SiNPs, SSSNPs, and Fe-SiNPs.

Oxides (wt %)	SiO_2	Al_2O_3	Fe_2O_3	Na_2O	K_2O	P_2O_5	MgO	TiO_2	CaO	CuO	LOI*
FA-SiNPs	94.45	0.14	0.01	0.05	0.00	0.00	0.03	0.07	0.01	0.00	5.23
SSSNPs	91.83	0	0.02	0.02	0	0.02	0.02	0.01	0.01	0	8.06
Fe-SiNPs	91.38	0.55	1.91	0.56	0.10	0.09	0.08	0.07	0.03	0.02	5.19

5.3 SEM and BET Results

Figure 18 displays the SEM images of FA-SiNPs, SSSNPs, and Fe-SiNPs. The surface morphology of all adsorbents is characterized by spherical particles with sizes of $\leq$ 200 nm. Notably, the morphology remained unchanged following iron modification.

Table 18 summarizes the specific surface areas of FA-SiNPs, SSSNPs, and Fe-SiNPs as determined by BET analysis. Among these, SSSNPs exhibited the highest specific surface area of 305 m^2/g, while FA-SiNPs had a specific surface area of 140 m^2/g, which is approximately half that of SSSNPs. As depicted in Figure 18, FA-SiNPs formed large agglomerates of nanoparticles, in contrast to SSSNPs. This agglomeration reduces the available interfacial area, thereby decreasing the surface area (Gosens *et al*, 2010). The formation of large agglomerates in FA-SiNPs synthesis could be attributed to the presence of impurities, primarily aluminium and iron. These impurities act as coagulating agents, promoting excessive coagulation of colloidal silica, which leads to the development of large agglomerates. A greater emphasis should be placed on pre-acidic treatment during the synthesis process to obtain a high surface area FA-SiNPs.

The specific surface area of Fe-SiNPs was lower than that of the parent FA-SiNPs, likely due to the loading of iron oxide onto the surface of FA-SiNPs (Javed *et al*, 2023).

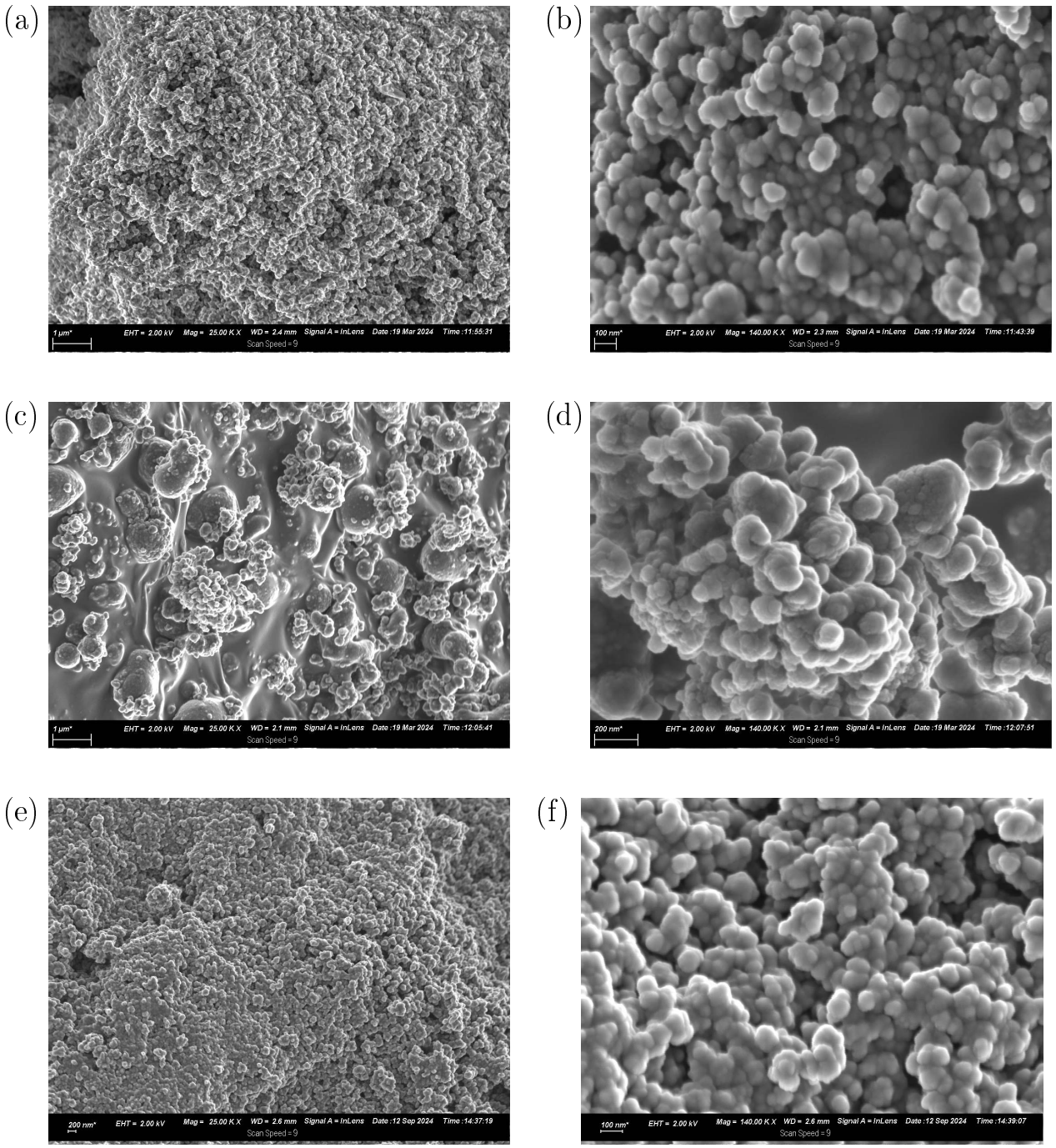

Figure 18: SEM images for (a & b) FA-SiNPs, (c & d) SSSNPs, and (e & f) Fe-SiNPs. Note that the magnification for (a), (c), (e) is 25 000 and for (b), (d), (f) is 140 000.

Table 18: Specific surface area for FA-SiNPs, SSSNPs, and Fe-SiNPs using BET method.

Material	FA-SiNPs	SSSNPs	Fe-SiNPs
Specific surface area (m^2/g)	140.6	305	97.8

5.4 Comparison of FA-SiNPs, SSSNPs, and Fe-SiNPs for Tetracycline Adsorption

The preliminary adsorption test was conducted under the same set of conditions for FA-SiNPs, SSSNPs, and Fe-SiNPs. The percentage removals of TC for FA-SiNPs, SSSNPs, and Fe-SiNPs are shown in Figure 19. FA-SiNPs and SSSNPs demonstrated relatively low percentage removals, at 30 % and 20 %, respectively. The slightly higher percentage removal observed for FA-SiNPs was attributed to the presence of small impurities, such as aluminium. Fe-SiNPs had the highest percentage removal at 59 %. The high percentage removal was attributed the presence of iron in Fe-SiNPs. Zhang *et al* (2015a) observes that the adsorption characteristics of TC can be improved by the presence of iron in the adsorbent, owing to surface complexation between TC, a chelating agent, and iron. Note that all further adsorption studies carried out in chapter 5 were conducted with Fe-SiNPs.

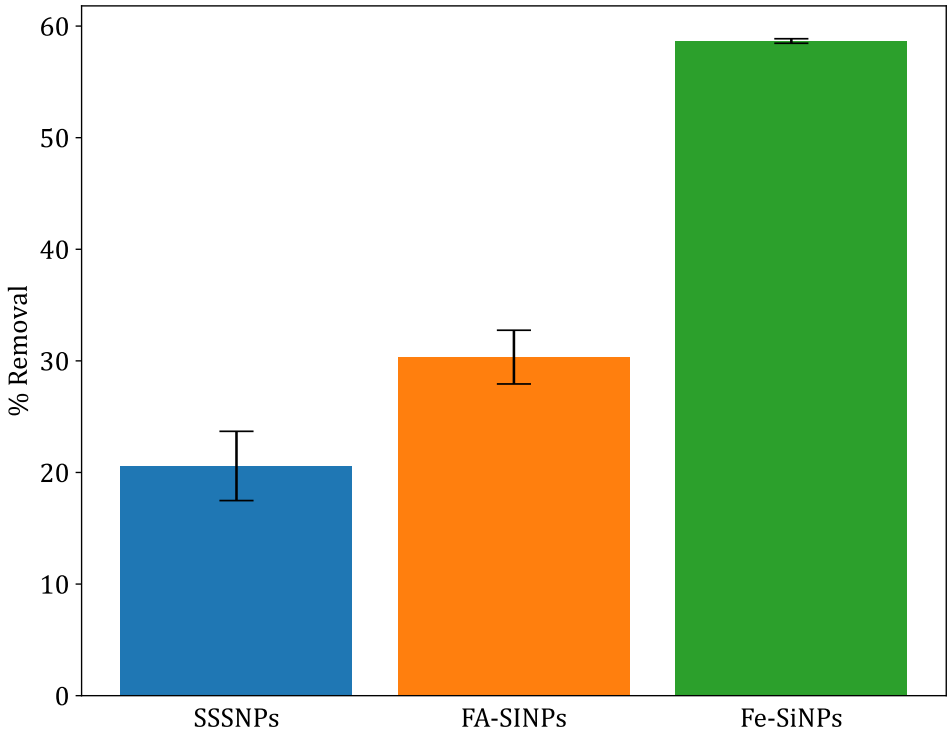

Figure 19: The percentage removal of FA-SiNPs, SSSNPs, and Fe-SiNPs (conditions for removal experiments - pH: 5, Dosage: 5 g/L, contact time: 30 min, C_O: 100 ppm).

5.5 Tetracycline Adsorption with Fe-SiNPs

5.5.1 The effect of Dosage

Figure 20 (a) shows the effect of the adsorbent dosage of Fe-SiNPs on the removal of TC. As discussed in section 4.6.1, an increase in the adsorbent dosage of Fe-SiNPs, increased the removal of TC. The optimal dosage was 5 g/L, as there was no substantial increase in the percentage removal of TC after a dosage of 5 g/L.

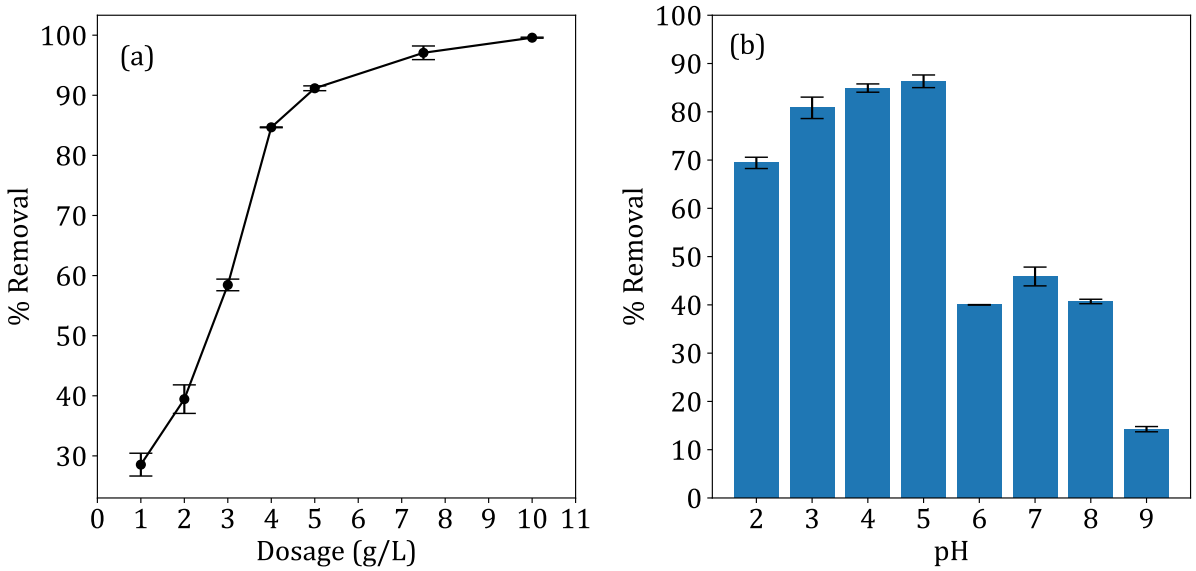

Figure 20: (a) The effect of Fe-SiNPs dosage and (b) the effect of pH on TC removal.

5.5.2 The effect of pH

Figure 20 (b) shows the effect of pH on the removal of TC on Fe-SiNPs. Figure 21 presents the zeta potential of Fe-SiNPs as a function of pH. The highest percentage removal was noted at pHs 4 and 5, therefore the optimal pH was $4-5$. At pHs of $4-5$, TC is neutral while Fe-SiNPs is negatively charged. As previously discussed in section 4.6.2, at pHs of $4-5$, TC can be absorbed as a cationic species. This suggests there is an electrostatic attraction at pHs 4 and 5. At a pH<4, tetracycline adsorption decreased. At a pH<4, tetracycline becomes cationic whereas Fe-SiNPs surface becomes less negative and thus the electrostatic attraction between TC and Fe-SiNPs decreases. At pH>5, tetracycline adsorption decreased. At pH>5, tetracycline becomes anionic and Fe-SiNPs surface possesses a negative charge causing electrostatic repulsion between Fe-SiNPs and TC reducing adsorption.

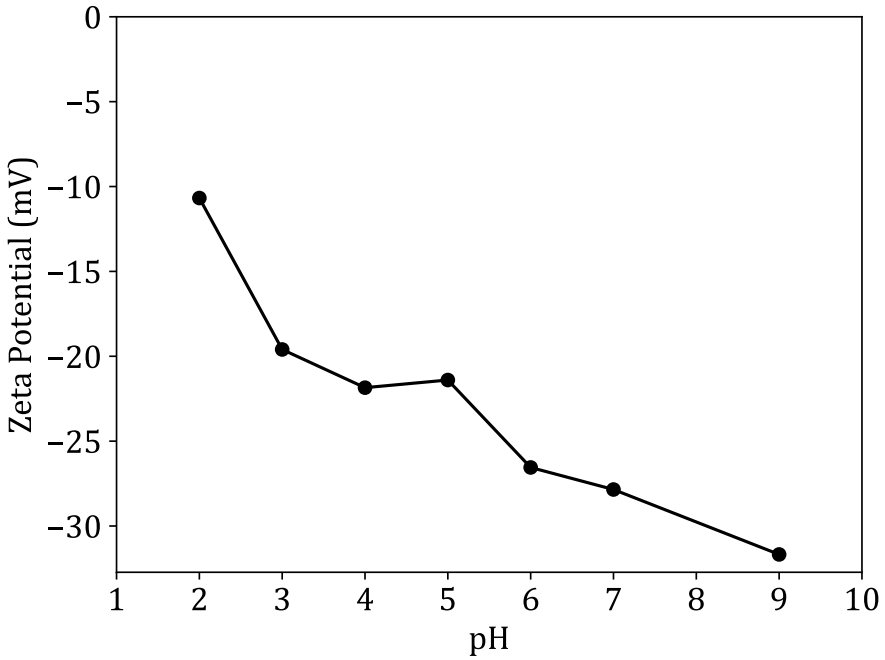

Figure 21: Zeta potential of Fe-SiNPs as a function of pH determined using a Zetasizer.

5.5.3 Adsorption Kinetics

Figure 22 shows the adsorption kinetics of TC on Fe-SiNPs, fitted with pseudo first order, pseudo second order, Elovich, and Langmuir kinetic models. Table 19 presents a summary of model parameters and statistical parameters for each fitted model. The Elovich model exhibited the lowest squared error and highest R^2 value, indicating that the adsorption kinetics of TC were best described by this model. Though the fitting of the Elovich model has no physical meaning. According to Molina-Calderón *et al* (2022), the Elovich model is widely employed to model the chemisorption of organic pollutants on modified adsorbents. Suggesting that chemisorption is a potential adsorption mechanism for TC on Fe-SiNPs.

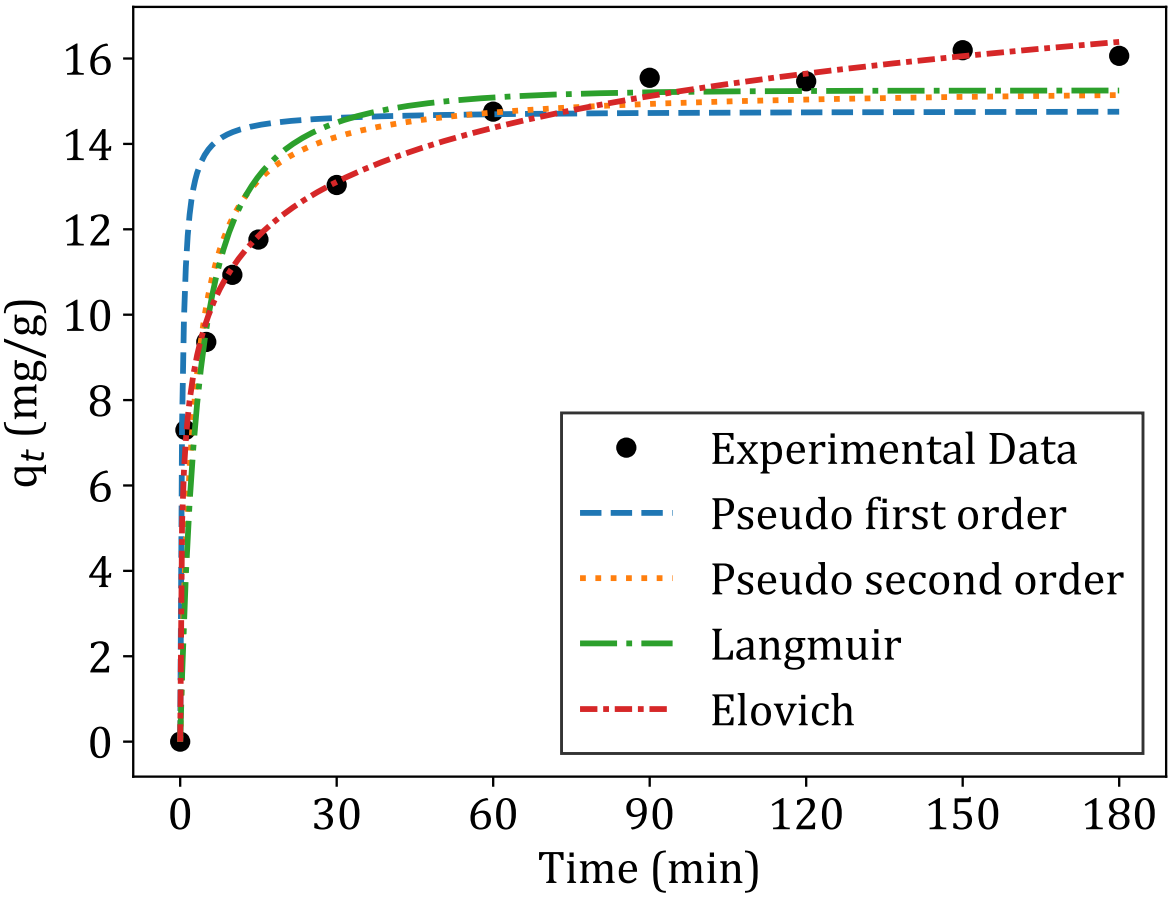

Figure 22: Adsorption kinetics of TC on Fe-SiNPs fitted with adsorption kinetic models (conditions for kinetic experiments - pH: 5, Dosage: 5 g/L, C_O: 70 ppm).

Table 19: Adsorption kinetic model parameters and statistical parameters for the adsorption of TC on Fe-SiNPs.

Kinetic Model	Kinetic Parameters			Statistical Parameters	
Pseudo first order (PFO)	q_e (mg/g)	k_1 (1/min)		Squared Error	R^2
	14.78	0.19		37.51	0.84
Pseudo second order (PSO)	q_e (mg/g)	k_2 (g/mg/min)		Squared Error	R^2
	15.36	0.03		16.91	0.93
Elovich	α (mg/g/min)	β (g/mg)		Squared Error	R^2
	78.69	0.55		0.89	0.996
Langmuir kinetic	k_a (L/g/min)	k_d (mg/L/min)	q_{max} (mg/g)	Squared Error	R^2
	0.053	0.00	15.25	20.91	0.91

5.5.4 Adsorption Isotherms

Figure 23 shows the adsorption isotherms of TC on Fe-SiNPs at 30 °C, 40 °C and 50 °C fitted with Langmuir, Freundlich, and Temkin isotherm models. Table 20 presents a summary of the adsorption isotherm model parameters and statistical parameters for each isotherm model. The Langmuir isotherm model showed the lowest squared error and highest R^2 value at all temperatures, except for 40 °C, indicating that the adsorption isotherms of tetracycline were best described by this model. The Langmuir model's best fit suggests that tetracycline adsorption onto Fe-SiNPs occurred as a monolayer on a homogeneous surface (Aliyu *et al*, 2022). Table 21 presents the maximum adsorption capacities (q_m) of similar adsorbents to Fe-SiNPs for tetracycline removal.

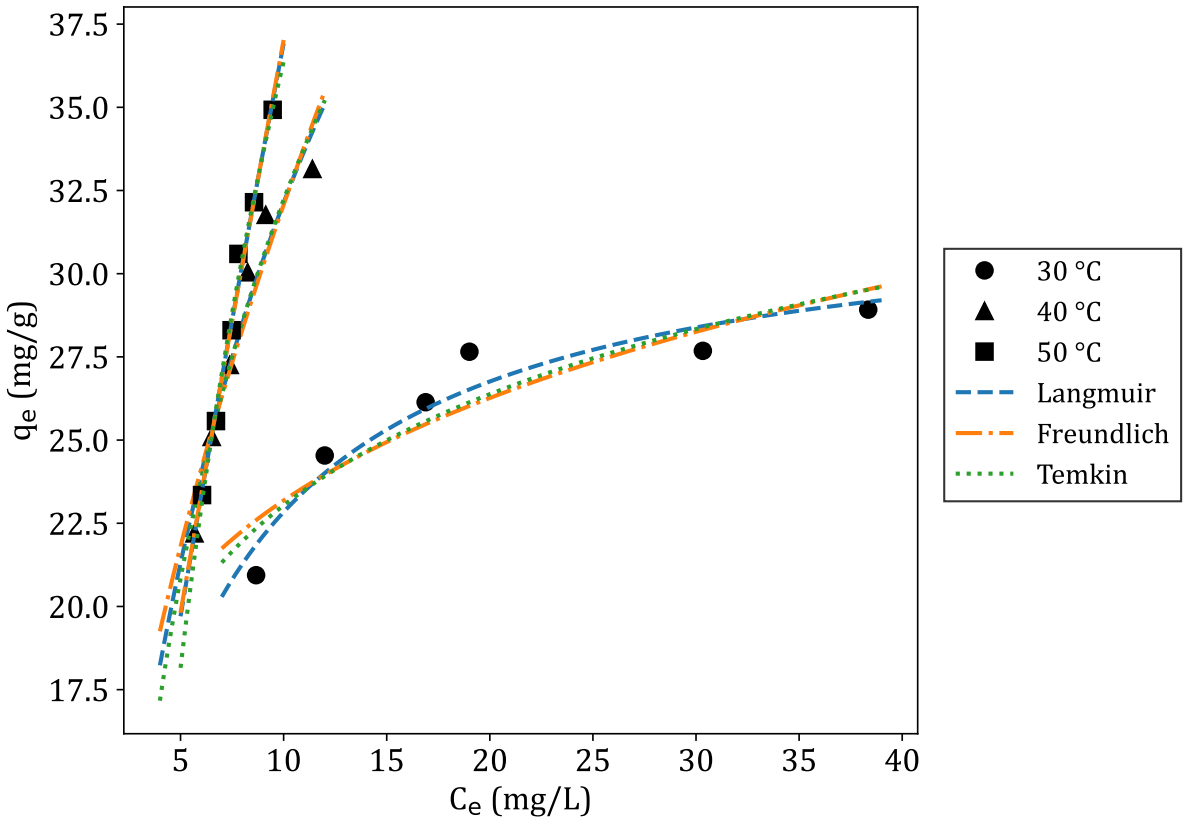

Figure 23: Adsorption isotherms of TC on Fe-SiNPs at 30 °C, 40 °C and 50 °C fitted with the adsorption isotherm models (conditions for isotherm experiments - pH: 5, Dosage: 5 g/L, contact time: 6 h).

Table 20: Adsorption isotherm model parameters and statistical parameters for the adsorption of TC on Fe-SiNPs at 30 °C, 40 °C, and 50 °C.

Isotherm Model	Temperature		
	30 °C	**40 °C**	**50 °C**
Langmuir isotherm model			
Isotherm Constants			
q_m (mg/g)	32.31	65.36	291.70
K_L (L/mg)	0.241	0.097	0.014
Statistical Parameters			
Squared Error	3.04	4.51	1.14
R^2	0.927	0.948	0.988
Freundlich isotherm model			
Isotherm Constants			
K_f (mg/g)	15.32	8.90	4.64
n	5.56	1.80	1.11
Statistical Parameters			
Squared Error	6.93	6.42	1.21
R^2	0.834	0.926	0.987
Temkin isotherm model			
Isotherm Constants			
B_T (J/mol)	11.88	0.71	0.40
A_T (L/mg)	4.82	16.43	26.28
Statistical Parameters			
Squared Error	5.87	4.04	1.72
R^2	0.86	0.954	0.980

Table 21: The maximum adsorption capacity of tetracycline for adsorbents similar to Fe-SiNPs.

Absorbent	q_m (mg/g)	Temperature (°C)	Reference
Fe-MSNs	56.98	25	(Qiao *et al*, 2021)
Fe_3O_4/SiO_2/CTAB–SiO_2	220.7	25	(Zandipak & Sobhanardakani, 2018)
Ni-Fe with silica template	90.9	30	(Wang *et al*, 2022)
Fe-impregnated mesoporous silicates	41.7	25	(Vu *et al*, 2010)
Amino-Fe(III) functionalized mesoporous silica	23.95	25	(Zhang *et al*, 2015b)
Silica magnetic nanoparticles	61.73	25	(Farhadian *et al*, 2017)
Amino-Fe(III) functionalized SBA15	43.07	25	(Zhang *et al*, 2015a)
Fe-SiNPs	65.36	40	This study

5.5.5 Adsorption thermodynamics

Table 22 presents a summary of the thermodynamic parameters for the adsorption of tetracycline on Fe-SiNPs. The negative value of ΔG° signified that the adsorption process occurred spontaneously. The negative ΔS° indicated decreased randomness at solid/solution interface during adsorption (Liu & Lee, 2014). The value of ΔH° was negative, indicating that the adsorption process was exothermic. According to Molina-Calderón *et al* (2022), if the value of ΔH° is above 80 kJ/mol it indicates that adsorption is chemisorption (surface complexation).

Table 22: Thermodynamics parameters for tetracycline adsorption on Fe-SiNPs.

Temperature (°C)	K_D	$\Delta G°$ (kJ/mol)	$\Delta H°$ (kJ/mol)	$\Delta S°$ (kJ/mol)	R^2
30	107 175.80	−29.19			
40	42 979.88	−27.78	−114.05	−0.278	0.953
50	6 439.32	−23.56			

5.5.6 Adsorption Mechanism

Figure 24 gives the FTIR spectra of Fe-SiNPs before and after adsorption of TC. The band at $460-430$ cm^{-1} corresponds to the bending vibration of a Fe-O bond from Fe_2O_3 (Hanh *et al*, 2023). The band at $1050-990$ cm^{-1} and $810-790$ cm^{-1} are attributed to the antisymmetric and symmetric stretching vibrations of Si–O–Si, respectively (Hanh

et al, 2023; Imoisili *et al*, 2022). These Si-O-Si bands confirm the presence of silicon dioxide in the sample (Hanh *et al*, 2023).

The broad band at $3700 - 3000$ cm^{-1} is associated with the stretching vibration of OH groups (Bandura *et al*, 2022). The band $1640-1590$ cm^{-1} is associated with the stretching vibration of C=O groups (Zhang *et al*, 2015a). Notably, shifts were observed in the C=O ($1640 - 1590$ cm^{-1}) and OH ($3700 - 3000$) cm^{-1}) bands after TC adsorption. According to Zhang *et al* (2015a), the shift in the C=O band after adsorption ($1640 - 1590$ cm^{-1}) indicates complexation between TC and Fe(III). Similarly, Bello (2013) reported that broadening of the OH group after adsorption signifies hydrogen bonding between the absorbate and adsorbent.

The adsorption thermodynamic studies and the effect of pH suggested that the interaction between TC and Fe-SiNPs involved chemisorption and electrostatic attraction. Consequently, the adsorption mechanism can be attributed to surface complexation (chemisorption), electrostatic attraction, and hydrogen bonding.

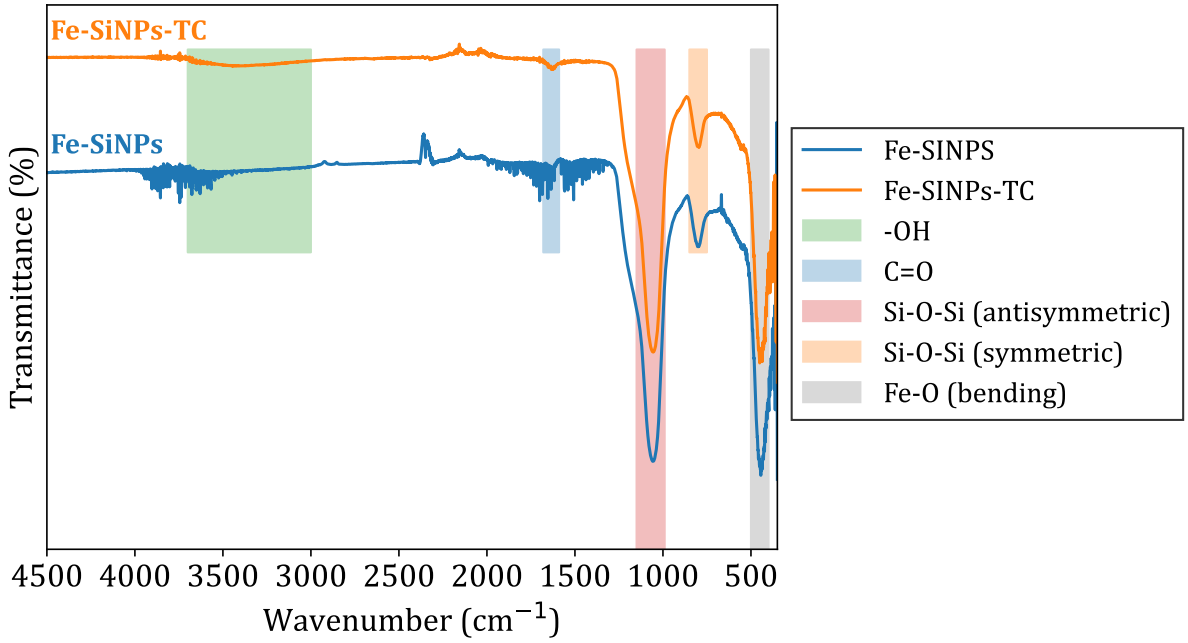

Figure 24: FTIR spectra of Fe-SiNPs before and after adsorption of TC. Note that the FTIR spectra before adsorption is denoted as Fe-SiNPs and the FTIR spectra after adsorption is denoted as Fe-SiNPs-TC.

CHAPTER 6 – CONCLUSIONS AND RECOMMENDATIONS

The best-performing adsorbent, when comparing FA, AM-FA, BM-FA, and ZNa-P1, was ZNa-P1, achieving the highest tetracycline removal. This high removal efficiency was attributed to its high zeolite purity, which resulted in a high cation exchange capacity (CEC) and increased surface area. TC removal was found to be directly proportional to the CEC rather than the surface area. The optimal dosage and pH for TC adsorption using ZNa-P1 were 7.5 g/L and pH 5, respectively. The adsorption kinetics of TC on ZNa-P1 followed the pseudo-second-order model, as indicated by the smallest squared error and highest R^2 value. The adsorption isotherms of TC on ZNa-P1 were best described by the Langmuir model, suggesting monolayer adsorption on a homogeneous surface. The adsorption thermodynamics of TC on ZNa-P1 indicated that the adsorption process was endothermic and occurred spontaneously. Overall, the adsorption mechanism of TC on ZNa-P1 involved ion exchange, hydrogen bonding and electrostatic attraction.

The best-performing adsorbent, when comparing FA-SiNPs, SSSNPs, and Fe-SiNPs, was Fe-SiNPs, achieving the highest tetracycline removal. The high percentage removal was attributed to the presence of iron in Fe-SiNPs, which increased complexation between TC and Fe-SiNPs. The optimal dosage and pHs for TC adsorption using Fe-SiNPs were 5 g/L and pH 4−5, respectively. The adsorption kinetics of TC on Fe-SiNPs followed the Elovich model, as indicated by the smallest squared error and highest R^2 value. The adsorption isotherms of TC on Fe-SiNPs were best described by the Langmuir model, suggesting monolayer adsorption on a homogeneous surface. The adsorption thermodynamics of TC on Fe-SiNPs indicated that the adsorption process was endothermic and occurred spontaneously. Overall, the adsorption mechanism of TC on Fe-SiNPs was concluded to be chemisorption (surface complexation), electrostatic attraction, and hydrogen bonding.

Future research should explore the use of ZNa-P1 and Fe-SiNPs in desorption and column adsorption studies to better simulate real-world applications. Investigating their adsorption-desorption cycles would provide valuable insights into their reusability. The development of zeolite and silica nanoparticle beads could also support column adsorption studies by improving material stability and flow dynamics, making them more suitable for continuous and industrial-scale processes. Additionally, A full-cost analysis should be conducted to determine whether these adsorbents are truly low-cost.

Additionally, future studies should evaluate the performance of ZNa-P1 and Fe-SiNPs in the removal of other contaminants other than tetracycline. Targeting pollutants such as heavy metals, dyes, and other pharmaceuticals could indicate their versatility as effective adsorbents.

REFERENCES

Abadi, MHJ, Nouri, SMM, Zhiani, R, Heydarzadeh, HD and Motavalizadehkakhky, A (2019), "Removal of tetracycline from aqueous solution using Fe-doped zeolite", *International Journal of Industrial Chemistry*, 10 (4): 291–300.

Abas, SNA, Ismail, MHS, Kamal, ML and Izhar, S (2013), "Adsorption process of heavy metals by low-cost adsorbent: A review", *World Applied Sciences Journal*, 28 (11): 1518–1530.

Abbasnia, A, Zarei, A, Yeganeh, M, Sobhi, HR, Gholami, M and Esrafili, A (2022), "Removal of tetracycline antibiotics by adsorption and photocatalytic-degradation processes in aqueous solutions using metal organic frameworks (MOFs): A systematic review", *Inorganic Chemistry Communications*, 145: 109959.

Ahmad, F, Zhu, D and Sun, J (2021), "Environmental fate of tetracycline antibiotics: degradation pathway mechanisms, challenges, and perspectives", *Environmental Sciences Europe*, 33 (1): 64.

Ahmed, S, Saurikhia, A, Haleem, A and Gangopadhyay, S (2016), "Geographical spread of fly ash generation and residual potential for its utilization in India", *International Journal of Innovative Research and Review*, 4 (1): 8–19.

Aigbe, UO, Ukhurebor, KE, Onyancha, RB, Osibote, OA, Darmokoesoemo, H and Kusuma, HS (2021), "Fly ash-based adsorbent for adsorption of heavy metals and dyes from aqueous solution: a review", *Journal of Materials Research and Technology*, 14: 2751–2774.

Aliyu, M, Abdullah, AH and Tahir, MIbM (2022), "Adsorption tetracycline from aqueous solution using a novel polymeric adsorbent derived from the rubber waste", *Journal of the Taiwan Institute of Chemical Engineers*, 136: 104333.

Alsawy, T, Rashad, E, El-Qelish, M and Mohammed, RH (2022), "A comprehensive review on the chemical regeneration of biochar adsorbent for sustainable wastewater treatment", *NPJ Clean Water*, 5 (1): 29.

Alterary, SS and Marei, NH (2021), "Fly ash properties, characterization, and applications: A review", *Journal of King Saud University - Science*, 33 (6): 101536.

Amangelsin, Y, Semenova, Y, Dadar, M, Aljofan, M and Bjørklund, G (2023), "The impact of tetracycline pollution on the aquatic environment and removal strategies", *Antibiotics*, 12 (3): 440.

Amarasiri, M, Sano, D and Suzuki, S (2020), "Understanding human health risks caused by antibiotic resistant bacteria (ARB) and antibiotic resistance genes (ARG) in water environments: Current knowledge and questions to be answered", *Critical Reviews in Environmental Science and Technology*, 50 (19): 2016–2059.

Amri, I, Assadi, AA, Mellah, B and Hamdi, N (2024), "Optimized removal of chloroform and DMDS using synthetic zeolite (Na-P1) and activated carbon composite", *Modeling Earth Systems and Environment*, 10 (2): 2309–2328.

Aphane, ME, Doucet, FJ, Kruger, RA, Petrik, L and Merwe, EM van der (2020), "Preparation of Sodium Silicate Solutions and Silica Nanoparticles from South African Coal Fly Ash", *Waste and Biomass Valorization*, 11 (8): 4403–4417.

Bacariza, MC, Bértolo, R, Graça, I, Lopes, JM and Henriques, C (2017), "The effect of the compensating cation on the catalytic performances of Ni/USY zeolites towards CO_2 methanation", *Journal of CO_2 Utilization*, 21: 280–291.

Bajda, T, Grela, A, Pamuła, J, Kuc, J, Klimek, A, Matusik, J, Franus, W, Alagarsamy, SKK, Danek, T and Gara, P (2024), "Using zeolite materials to remove pharmaceuticals from water", *Materials*, 17 (15): 3848.

Balakrishnan, A, Chinthala, M, Polagani, RK and Vo, DVN (2023), "Removal of tetracycline from wastewater using g-C_3N_4 based photocatalysts: a review", *Environmental Research*, 216: 114660.

Bandura, L, Bialoszewska, M, Leiviska, T and Franus, M (2022), "The Role of Zeolite Structure in Its β-cyclodextrin Modification and Tetracycline Adsorption from Aqueous Solution: Characteristics and Sorption Mechanism", *Materials*, 15 (18).

Banerjee, S, Joshi, M and Jayaram, R (2005), "Removal of Cr (VI) and Hg (II) from aqueous solutions using fly ash and impregnated fly ash", *Separation science and technology*, 39 (7): 1611–1629.

Baskar, AV, Bolan, N, Hoang, SA, Sooriyakumar, P, Kumar, M, Singh, L, Jasemizad, T, Padhye, LP, Singh, G, Vinu, A, Sarkar, B, Kirkham, M, Rinklebe, J, Wang, S, Wang, H,

Balasubramanian, R and Siddique, KH (2022), "Recovery, regeneration and sustainable management of spent adsorbents from wastewater treatment streams: A review", *Science of The Total Environment*, 822: 153555, ISSN: 0048-9697.

Bayuo, J, Rwiza, MJ, Choi, JW, Mtei, KM, Hosseini-Bandegharaei, A and Sillanpää, M (2024), "Adsorption and desorption processes of toxic heavy metals, regeneration and reusability of spent adsorbents: Economic and environmental sustainability approach", *Advances in Colloid and Interface Science*, 329: 103196, ISSN: 0001-8686.

Bello, OS (2013), "Adsorptive removal of malachite green with activated carbon prepared from oil palm fruit fibre by KOH activation and CO_2 gasification", *South African Journal of Chemistry*, 66: 32–41.

Bhatt, A, Priyadarshini, S, Mohanakrishnan, AA, Abri, A, Sattler, M and Techapaphawit, S (2019), "Physical, chemical, and geotechnical properties of coal fly ash: A global review", *Case Studies in Construction Materials*, 11: e00263.

Boboc, V, Rotaru, A and Boboc, A (2010), "A material for substructure and road works: Mechanical characteristics of pozzolana fly ash from thermal power plant of iasi, Romania", *WSEAS Transactions on Environment and Development*, 6: 437–446.

Bukhari, SS, Behin, J, Kazemian, H and Rohani, S (2015), "Conversion of coal fly ash to zeolite utilizing microwave and ultrasound energies: A review", *Fuel*, 140: 250–266.

Buzukashvili, S, Sommerville, R, Rowson, NA and Waters, KE (2024), "An overview of zeolites synthesised from coal fly ash and their potential for extracting heavy metals from industrial wastewater", *Canadian Metallurgical Quarterly*, 63 (1): 130–152.

Cao, C, Xuan, W, Yan, S and Wang, Q (2023), "Zeolites synthesized from industrial and agricultural solid waste and their applications: A review", *Journal of Environmental Chemical Engineering*, 11 (5): 110898.

Cedeño-Muñoz, JS, Aransiola, SA, Reddy, KV, Ranjit, P, Victor-Ekwebelem, MO, Oyedele, OJ, Pérez-Almeida, IB, Maddela, NR and Rodríguez-Díaz, JM (2024), "Antibiotic resistant bacteria and antibiotic resistance genes as contaminants of emerging concern: occurrences, impacts, mitigations and future guidelines", *Science of The Total Environment*, 952: 175906.

Chang, D, Mao, Y, Qiu, W, Wu, Y and Cai, B (2023), "The source and distribution of tetracycline antibiotics in China: A review", *Toxics*, 11 (3): 214.

Chang, J, Shen, Z, Hu, X, Schulman, E, Cui, C, Guo, Q and Tian, H (2020), "Adsorption of Tetracycline by Shrimp Shell Waste from Aqueous Solutions: Adsorption Isotherm, Kinetics Modeling, and Mechanism", *ACS Omega*, 5 (7): 3467–3477.

Chen, X, Hossain, MF, Duan, C, Lu, J, Tsang, YF, Islam, MS and Zhou, Y (2022a), "Isotherm models for adsorption of heavy metals from water-a review", *Chemosphere*, 307: 135545.

Chen, X, Yang, Y, Ke, Y, Chen, C and Xie, S (2022b), "A comprehensive review on biodegradation of tetracyclines: Current research progress and prospect", *Science of The Total Environment*, 814: 152852.

Chen, X (2015), "Modeling of experimental adsorption isotherm data", *Information (Switzerland)*, 6 (1): 14–22.

Chen, Y, Wang, F, Duan, L, Yang, H and Gao, J (2016), "Tetracycline adsorption onto rice husk ash, an agricultural waste: Its kinetic and thermodynamic studies", *Journal of Molecular Liquids*, 222: 487–494.

Cheng, D, Ngo, HH, Guo, W, Chang, SW, Nguyen, DD, Liu, Y, Wei, Q and Wei, D (2020), "A critical review on antibiotics and hormones in swine wastewater: Water pollution problems and control approaches", *Journal of Hazardous Materials*, 387: 121682.

Conde-Cid, M, Núñez-Delgado, A, Fernández-Sanjurjo, MJ, Álvarez-Rodríguez, E, Fernández-Calviño, D and Arias-Estévez, M (2020), "Tetracycline and sulfonamide antibiotics in soils: presence, fate and environmental risks", *Processes*, 8 (11): 1479.

Crini, G, Lichtfouse, E, Wilson, LD and Morin-Crini, N (2019), "Conventional and non-conventional adsorbents for wastewater treatment", *Environmental Chemistry Letters*, 17: 195–213.

Cui, Y, Liu, J, Wang, L, Liu, R and Pang, B (2020), "Effect of Fly Ash with Different Particle Size Distributions on the Properties and Microstructure of Concrete", *Journal of Materials Engineering and Performance*, 29 (10): 6631–6639.

Curpen, S, Teutsch, N, Kovler, K and Spatari, S (2023), "Evaluating life cycle environmental impacts of coal fly ash utilization in embankment versus sand and landfilling", *Journal of Cleaner Production*, 385: 135402.

Dada, AO, Olalekan, AP, Olatunya, AM and Dada, OO (2012), "Langmuir, Freundlich, Temkin and Dubinin-Radushkevich Isotherms Studies of Equilibrium Sorption of Zn^{2+} Unto Phosphoric Acid Modified Rice Husk", *IOSR Journal of Applied Chemistry (IOSR-JAC)*, 3 (1).

Daghrir, R and Drogui, P (2013), "Tetracycline antibiotics in the environment: a review", *Environmental chemistry letters*, 11: 209–227.

Dai, Y, Zhang, N, Xing, C, Cui, Q and Sun, Q (2019), "The adsorption, regeneration and engineering applications of biochar for removal organic pollutants: A review", *Chemosphere*, 223: 12–27, ISSN: 0045-6535.

Dardona, M, Mohanty, SK, Allen, MJ and Dittrich, TM (2023), "From ash to oxides: Recovery of rare-earth elements as a step towards valorization of coal fly ash waste", *Separation and Purification Technology*, 314: 123532.

Das, D and Rout, PK (2021), "Synthesis, Characterization and Properties of Fly Ash Based Geopolymer Materials", *Journal of Materials Engineering and Performance*, 30 (5): 3213–3231.

Das, D and Rout, PK (2023), "A review of coal fly ash utilization to save the environment", *Water, Air, & Soil Pollution*, 234 (2): 128.

De Maeijer, PK, Craeye, B, Snellings, R, Kazemi-Kamyab, H, Loots, M, Janssens, K and Nuyts, G (2020), "Effect of ultra-fine fly ash on concrete performance and durability", *Construction and Building Materials*, 263: 120493.

de Oliveira, FF, Moura, KO, Costa, LS, Vidal, CB, Loiola, AR and do Nascimento, RF (2020), "Reactive Adsorption of Parabens on Synthesized Micro- and Mesoporous Silica from Coal Fly Ash: pH Effect on the Modification Process", *ACS Omega*, 5 (7): 3346–3357.

de Sousa, DNR, Insa, S, Mozeto, AA, Petrovic, M, Chaves, TF and Fadini, PS (2018), "Equilibrium and kinetic studies of the adsorption of antibiotics from aqueous solutions onto powdered zeolites", *Chemosphere*, 205: 137–146.

Deletic, A and Wang, H (2019), "Water pollution control for sustainable development", *Engineering*, 5 (5): 839–840.

Ding, D, Wang, B, Zhang, X, Zhang, J, Zhang, H, Liu, X, Gao, Z and Yu, Z (2023), "The spread of antibiotic resistance to humans and potential protection strategies", *Ecotoxicology and Environmental Safety*, 254: 114734.

Doke, KM and Khan, EM (2013), "Adsorption thermodynamics to clean up wastewater; critical review", *Reviews in Environmental Science and Bio/Technology*, 12 (1): 25–44.

Ebelegi, AN, Ayawei, N and Wankasi, D (2020), "Interpretation of adsorption thermodynamics and kinetics", *Open Journal of Physical Chemistry*, 10 (3): 166–182.

El Messaoudi, N, El Khomri, M, El Mouden, A, Bouich, A, Jada, A, Lacherai, A, Iqbal, HM, Mulla, SI, Kumar, V and Américo-Pinheiro, JHP (2024), "Regeneration and reusability of non-conventional low-cost adsorbents to remove dyes from wastewaters in multiple consecutive adsorption–desorption cycles: a review", *Biomass conversion and biorefinery*, 14 (11): 11739–11756.

Elidrissi, ZC, Idrissi, DEM, Kouzi, Y, Achiou, B, Tahiri, S, Ouammou, M and Younssi, SA (2023), "Effective conversion of fly ash waste into Na-P1 zeolite and its application on the adsorption of Cr (VI)", *Inorganic Chemistry Communications*, 156: 111192.

Eteba, A, Bassyouni, M and Saleh, M (2022), "Utilization of chemically modified coal fly ash as cost-effective adsorbent for removal of hazardous organic wastes", *International Journal of Environmental Science and Technology*,

Fahimi, A, Zanoletti, A, Federici, S, Assi, A, Bilo, F, Depero, LE and Bontempi, E (2020), "New eco-materials derived from waste for emerging pollutants adsorption: The case of diclofenac", *Materials*, 13 (18): 3964.

Fang, C, Wang, S, Xu, H and Huang, Q (2022), "Degradation of tetracycline by atmospheric-pressure non-thermal plasma: Enhanced performance, degradation mechanism, and toxicity evaluation", *Science of The Total Environment*, 812: 152455.

Farhadian, N, Rezaeian, MS, Aseyednezhad, S, Haffar, F and Fard, SM (2017), "Removal of tetracycline antibiotic from aqueous environments using core-shell silica magnetic nanoparticles", *Desalination and Water Treatment*, 87: 348–357.

Figueroa, RA, Leonard, A and MacKay, AA (2004), "Modeling tetracycline antibiotic sorption to clays", *Environmental science & technology*, 38 (2): 476–483.

Foo, KY and Hameed, BH (2010), "Insights into the modeling of adsorption isotherm systems", *Chemical Engineering Journal*, 156 (1): 2–10.

Gene, DD and Lobo, CL (2014), *User's Guide to ASTM Specification C94/C94M on Ready-Mixed Concrete*, 2nd ed., ASTM International, ISBN: 978-0-8031-7054-4.

Ghazali, N, Muthusamy, K and Ahmad, SW (2019), "Utilization of Fly Ash in Construction", *IOP Conference Series: Materials Science and Engineering*, 601 (1): 012023.

Ghosh, P and Goel, S (2014), "Physical and chemical characterization of pond ash", *International Journal of Environmental Research and Development*, 4 (2): 129–134.

Al-Ghouti, MA and Da'ana, DA (2020), "Guidelines for the use and interpretation of adsorption isotherm models: A review", *Journal of Hazardous Materials*, 393: 122383.

Gollakota, AR, Volli, V and Shu, CM (2019), "Progressive utilisation prospects of coal fly ash: A review", *Science of The Total Environment*, 672: 951–989.

González-López, ME, Laureano-Anzaldo, CM, Pérez-Fonseca, AA, Arellano, M and Robledo-Ortíz, JR (2022), "A critical overview of adsorption models linearization: methodological and statistical inconsistencies", *Separation & Purification Reviews*, 51 (3): 358–372.

Gosens, I, Post, JA, Fonteyne, LJ de la, Jansen, EH, Geus, JW, Cassee, FR and Jong, WH de (2010), "Impact of agglomeration state of nano-and submicron sized gold particles on pulmonary inflammation", *Particle and fibre toxicology*, 7: 1–11.

Guler, UA and Sarioglu, M (2014), "Removal of tetracycline from wastewater using pumice stone: equilibrium, kinetic and thermodynamic studies", *Journal of Environmental Health Science and Engineering*, 12: 1–11.

Guo, Q, Huang, D, Kou, X, Cao, W, Li, L, Ge, L and Li, J (2017), "Synthesis of disperse amorphous SiO_2 nanoparticles via sol–gel process", *Ceramics International*, 43 (1, Part A): 192–196.

Halling-Sørensen, B, Sengeløv, G and Tjørnelund, J (2002), "Toxicity of tetracyclines and tetracycline degradation products to environmentally relevant bacteria, including selected

tetracycline-resistant bacteria", *Archives of environmental contamination and toxicology*, 42: 263–271.

Hanh, PTH, Phoungthong, K, Chantrapromma, S, Choto, P, Thanomsilp, C, Siriwat, P, Wisittipanit, N and Suwunwong, T (2023), "Adsorption of Tetracycline by Magnetic Mesoporous Silica Derived from Bottom Ash—Biomass Power Plant", *Sustainability*, 15 (6): 4727.

Haya, A and Alkatiri, H (2020), "Study of Blending Fly Ash with Potentially Acid Forming Material to Prevent Acid Mine Drainage", *Journal of Physics: Conference Series.* 1569 (4): 042075.

He, C, Zhou, J, Yang, C, Song, Z, He, J, Huang, Z, Deng, Y, Wang, J, Xiong, Y and Dang, Z (2023), "Accumulation, transportation, and distribution of tetracycline and cadmium in rice", *Journal of Environmental Sciences*, 126: 58–69.

Huang, Z, Fan, M and Tian, H (2020), "Rare earth elements of fly ash from Wyoming's Powder River Basin coal", *Journal of Rare Earths*, 38 (2): 219–226.

Húmpola, P, Odetti, HS, Fertitta, AE and Vicente, JL (2013), "Thermodynamic analysis of adsorption models of phenol in liquid phase on different activated carbons", *Journal of the Chilean Chemical Society*, 58 (1): 1541–1544.

Hussain, Z, Chang, N, Sun, J, Xiang, S, Ayaz, T, Zhang, H and Wang, H (2022), "Modification of coal fly ash and its use as low-cost adsorbent for the removal of directive, acid and reactive dyes", *Journal of Hazardous Materials*, 422: 126778.

Imoisili, PE, Nwanna, EC and Jen, TC (2022), "Facile preparation and characterization of silica nanoparticles from South Africa fly ash using a sol–gel hydrothermal method", *Processes*, 10 (11): 2440.

Islam, GM and Gilbride, KA (2019), "The effect of tetracycline on the structure of the bacterial community in a wastewater treatment system and its effects on nitrogen removal", *Journal of Hazardous Materials*, 371: 130–137.

Islam, MA, Chowdhury, MA, Mozumder, MSI and Uddin, MT (2021), "Langmuir Adsorption Kinetics in Liquid Media: Interface Reaction Model", *ACS Omega*, 6 (22): 14481–14492.

Islam, MA, Nazal, MK, Akinpelu, AA, Sajid, M, Alhussain, NA, Billah, REK and Bahsis, L (2024), "Novel activated carbon derived from a sustainable and low-cost palm leaves biomass waste for tetracycline removal: Adsorbent preparation, adsorption mechanisms and real application", *Diamond and Related Materials*, 147: 111375.

Javed, K, Mahmood, S, Ammar, M, Abbas, N, Shah, M, Ahmed, T and Mustafa, G (2023), "Rice husk ash adsorbent modified by iron oxide with excellent adsorption capacity for arsenic removal from water", *International Journal of Environmental Science and Technology*, 20 (3): 2819–2828.

Jayaranjan, MLD, Hullebusch, E van and Annachhatre, A (2014), "Reuse Options for Coal Fired Power Plant Bottom Ash and Fly Ash", *Reviews in Environmental Science and Bio/Technology*, 13.

Jeelani, PG, Mulay, P, Venkat, R and Ramalingam, C (2020), "Multifaceted application of silica nanoparticles. A review", *Silicon*, 12 (6): 1337–1354.

Jia, DA, Zhou, DM, Wang, YJ, Zhu, HW and Chen, JL (2008), "Adsorption and cosorption of Cu(II) and tetracycline on two soils with different characteristics", *Geoderma*, 146 (1-2): 224–230.

Ju, T, Meng, Y, Han, S, Lin, L and Jiang, J (2021), "On the state of the art of crystalline structure reconstruction of coal fly ash: A focus on zeolites", *Chemosphere*, 283: 131010.

Al-Jubouri, SM, Al-Jendeel, HA, Rashid, SA and Al-Batty, S (2022), "Antibiotics adsorption from contaminated water by composites of ZSM-5 zeolite nanocrystals coated carbon", *Journal of Water Process Engineering*, 47: 102745.

Kafle, A, Timilsina, A, Gautam, A, Adhikari, K, Bhattarai, A and Aryal, N (2022), "Phytoremediation: Mechanisms, plant selection and enhancement by natural and synthetic agents", *Environmental Advances*, 8: 100203.

Kang, D, Yoo, Y and Park, J (2021), "Stabilization of heavy metals in municipal solid waste incineration fly ash via CO_2 uptake procedure by using various weak acids", *Journal of Industrial and Engineering Chemistry*, 94: 472–481.

Kao, PC, Tzeng, JH and Huang, TL (2000), "Removal of chlorophenols from aqueous solution by fly ash", *Journal of Hazardous Materials*, 76 (2-3): 237–249.

Kasumba, J, Appala, K, Agga, GE, Loughrin, JH and Conte, ED (2020), "Anaerobic digestion of livestock and poultry manures spiked with tetracycline antibiotics", *Journal of Environmental Science and Health, Part B*, 55 (2): 135–147.

Kelechi, SE, Adamu, M, Uche, OAU, Okokpujie, IP, Ibrahim, YE and Obianyo, II (2022), "A comprehensive review on coal fly ash and its application in the construction industry", *Cogent Engineering*, 9 (1): 2114201.

Khan, SA, Uddin, I, Moeez, S and Ahmad, A (2014), "Fungus-mediated preferential bioleaching of waste material such as fly-ash as a means of producing extracellular, protein capped, fluorescent and water soluble silica nanoparticles", *PLoS One*, 9 (9): e107597.

Khanday, WA and Hameed, BH (2018), "Zeolite-hydroxyapatite-activated oil palm ash composite for antibiotic tetracycline adsorption", *Fuel*, 215: 499–505.

Kim, HY, Jeon, J, Hollender, J, Yu, S and Kim, SD (2014), "Aqueous and dietary bioaccumulation of antibiotic tetracycline in D. magna and its multigenerational transfer", *Journal of Hazardous Materials*, 279: 428–435.

Kiprono, P, Kiptoo, J, Nyawade, E and Ngumba, E (2023), "Iron functionalized silica particles as an ingenious sorbent for removal of fluoride from water", *Scientific Reports*, 13 (1): 8018.

Koshy, N and Singh, DN (2016), "Fly ash zeolites for water treatment applications", *Journal of Environmental Chemical Engineering*, 4 (2): 1460–1472.

Kurniasih, M, Aprilita, NH, Roto, R and Mudasir, M (2025), "Modification of coal fly ash for high capacity adsorption of methylene blue", *Case Studies in Chemical and Environmental Engineering*, 11: 101101.

Le, HT, Maguire, RO and Xia, K (2018), "Method of dairy manure application and time before rainfall affect antibiotics in surface runoff", *Journal of Environmental Quality*, 47 (6): 1310–1317.

Leichtweis, J, Vieira, Y, Welter, N, Silvestri, S, Dotto, GL and Carissimi, E (2022), "A review of the occurrence, disposal, determination, toxicity and remediation technologies of the tetracycline antibiotic", *Process Safety and Environmental Protection*, 160: 25–40.

Liao, Q, Rong, H, Zhao, M, Luo, H, Chu, Z and Wang, R (2021), "Interaction between tetracycline and microorganisms during wastewater treatment: A review", *Science of the Total Environment*, 757: 143981.

Lima, EC, Gomes, AA and Tran, HN (2020), "Comparison of the nonlinear and linear forms of the van't Hoff equation for calculation of adsorption thermodynamic parameters (ΔS° and ΔH°)", *Journal of Molecular Liquids*, 311: 113315.

Lima, EC, Hosseini-Bandegharaei, A, Moreno-Piraján, JC and Anastopoulos, I (2019), "A critical review of the estimation of the thermodynamic parameters on adsorption equilibria. Wrong use of equilibrium constant in the Van't Hoof equation for calculation of thermodynamic parameters of adsorption", *Journal of Molecular Liquids*, 273: 425–434.

Lima, EC, Adebayo, MA and Machado, FM (2015), *Kinetic and Equilibrium Models of Adsorption*, Springer International Publishing, ISBN: 978-3-319-18875-1.

Lin, Y, Yu, J, Wang, M and Wu, L (2023), "Toxicity of single and combined 4-epianhydrotetracycline and cadmium at environmentally relevant concentrations on the zebrafish embryos (Danio rerio)", *Environmental Pollution*, 316: 120543.

Litynska, M, Kyrii, S, Nosovska, O and Ryzhenko, N (2021), "Problem of antibiotics in natural water: A review", *Water And Water Purification Technologies. Scientific And Technical News*, 31 (3): 26–34.

Liu, J, Lin, H, Dong, Y, He, Y, Liu, W and Shi, Y (2021), "The effective adsorption of tetracycline onto MoS_2@Zeolite-5: Adsorption behavior and interfacial mechanism", *Journal of Environmental Chemical Engineering*, 9 (5): 105912.

Liu, L, Wu, W, Zhang, J, Lv, P, Xu, L and Yan, Y (2018a), "Progress of research on the toxicology of antibiotic pollution in aquatic organisms", *Acta Ecologica Sinica*, 38 (1): 36–41.

Liu, M, Hou, La, Yu, S, Xi, B, Zhao, Y and Xia, X (2013), "MCM-41 impregnated with A zeolite precursor: Synthesis, characterization and tetracycline antibiotics removal from aqueous solution", *Chemical engineering journal*, 223: 678–687.

Liu, T, Liu, W, Li, X, Wang, H, Lan, Y, Zhang, S, Wang, Y and Liu, H (2024), "Effect of environmental factors on adsorption of ciprofloxacin from wastewater by microwave alkali modified fly ash", *Scientific Reports*, 14 (1): 19831.

Liu, X and Lee, DJ (2014), "Thermodynamic parameters for adsorption equilibrium of heavy metals and dyes from wastewaters", *Bioresource technology*, 160: 24–31.

Liu, Y, Yan, C, Zhao, J, Zhang, Z, Wang, H, Zhou, S and Wu, L (2018b), "Synthesis of zeolite P1 from fly ash under solvent-free conditions for ammonium removal from water", *Journal of Cleaner Production*, 202: 11–22.

Lohrentz, L, Bhaumik, M and Brink, HG (2023), "High-capacity adsorption of hexavalent chromium by a polyaniline-Ni (0) nanocomposite adsorbent: Expanding the Langmuir-Hinshelwood kinetic model", *Journal of Molecular Liquids*, 389: 122931.

Luhar, I and Luhar, S (2022), "A Comprehensive Review on Fly Ash-Based Geopolymer", *Journal of Composites Science*, 6 (8).

Lundström, SV, Östman, M, Bengtsson-Palme, J, Rutgersson, C, Thoudal, M, Sircar, T, Blanck, H, Eriksson, KM, Tysklind, M, Flach, CF and Larsson, DG (2016), "Minimal selective concentrations of tetracycline in complex aquatic bacterial biofilms", *Science of The Total Environment*, 553: 587–595.

Mainganye, D, Ojumu, TV and Petrik, L (2013), "Synthesis of zeolites Na-P1 from South African coal fly ash: effect of impeller design and agitation", *Materials*, 6 (5): 2074–2089.

Mancuso, G, Midiri, A, Gerace, E and Biondo, C (2021), "Bacterial antibiotic resistance: the most critical pathogens", *Pathogens*, 10 (10): 1310.

Mathapati, M, Amate, K, Prasad, CD, Jayavardhana, M and Raju, TH (2022), "A review on fly ash utilization", *Materials Today: Proceedings*, 50: 1535–1540.

Mishra, A and Clark, JH (2013), *Green Materials for Sustainable Water Remediation and Treatment*, Royal Society of Chemistry (RSC), ISBN: 978-1-84973-621-3.

Mohammed, SA, Koting, S, Katman, HYB, Babalghaith, AM, Abdul Patah, MF, Ibrahim, MR and Karim, MR (2021), "A Review of the Utilization of Coal Bottom Ash (CBA) in the Construction Industry", *Sustainability*, 13 (14): 8031.

Molina-Calderón, L, Basualto-Flores, C, Paredes-García, V and Venegas-Yazigi, D (2022), "Advances of magnetic nanohydrometallurgy using superparamagnetic nanomaterials as rare earth ions adsorbents: A grand opportunity for sustainable rare earth recovery", *Separation and Purification Technology*, 299: 121708.

Mostafapour, FK, Yilmaz, M, Mahvi, AH, Younesi, A, Ganji, F and Balarak, D (2022), "Adsorptive removal of tetracycline from aqueous solution by surfactant-modified zeolite: equilibrium, kinetics and thermodynamics", *Desalination and Water Treatment*, 247 (8803540): 216–228.

Muliwa, AM, Oyewo, OA and Maity, A (2023), "Recent progress on the removal of aqueous mercury by carbon-based adsorbents: a review", *Inorganic Chemistry Communications*, 111207.

Munthali, M, Johan, E, Aono, H and Matsue, N (2015), "Cs^{+} and Sr^{2+} adsorption selectivity of zeolites in relation to radioactive decontamination", *Journal of Asian ceramic societies*, 3 (3): 245–250.

Mushtaq, F, Zahid, M, Bhatti, IA, Nasir, S and Hussain, T (2019), "Possible applications of coal fly ash in wastewater treatment", 240: 27–46.

Musyoka, N, Petrik, L, Balfour, G, Misheer, N, Gitari, W and Mabovu, B (2009), "Removal of toxic elements from brine using zeolite Na-P1 made from a South African coal fly ash", *Int. Mine Water*, 5: 680–687.

Nallathambi, G, Ramachandran, T, Rajendran, V and Palanivelu, R (2011), "Effect of silica nanoparticles and BTCA on physical properties of cotton fabrics", *Materials Research*, 14: 552–559.

Nawaz, I (2013), "Disposal and utilization of fly ash to protect the environment", *International journal of innovative research in science, engineering and technology*, 2 (10): 5259–5266.

Nguyen, T, Tran, T, Dao, V, Quoc Trung, V, Nguyen, T and Thai, H (2020), "Using Modified Fly Ash for Removal of Heavy Metal Ions from Aqueous Solution", *Journal of Chemistry*, 2020: 1–11.

Omorogie, MO, Babalola, JO and Unuabonah, EI (2016), "Regeneration strategies for spent solid matrices used in adsorption of organic pollutants from surface water: A critical review", *Desalination and water treatment*, 57 (2): 518–544.

Owoeye, SS, Abegunde, SM and Oji, B (2021), "Effects of process variable on synthesis and characterization of amorphous silica nanoparticles using sodium silicate solutions as precursor by sol–gel method", *Nano-Structures & Nano-Objects*, 25: 100625.

Ozumchelouei, EJ, Hamidian, AH, Zhang, Y and Yang, M (2020), "Physicochemical properties of antibiotics: A review with an emphasis on detection in the aquatic environment", *Water Environment Research*, 92 (2): 177–188.

Pal, A, Mahamallik, P, Saha, S and Majumdar, A (2017), "Degradation of tetracycline antibiotics by advanced oxidation processes: application of MnO_2 nanomaterials", *Natural Resources & Engineering*, 2 (1): 32–42.

Patel, H (2021), "Review on solvent desorption study from exhausted adsorbent", *Journal of Saudi Chemical Society*, 25 (8): 101302, ISSN: 1319-6103.

Patel, MG, Marakana, PG, Dey, A, Saini, B and Chokshi, H (2023), "Coal fly ash derived adsorbent for enhancing waste water treatment", *Materials Today: Proceedings*, 77: 163–167.

Peng, H, Ye, B, Luo, M and Zheng, X (2024), "Mg–Fe Layered Double Hydroxides/Polyacrylonitrile Nanofibers for Solar-Light Induced Peroxymonosulfate Elimination of Tetracycline Hydrochloride", *Water*, 16 (10): 1345.

Pulicharla, R, Hegde, K, Brar, SK and Surampalli, RY (2017), "Tetracyclines metal complexation: Significance and fate of mutual existence in the environment", *Environmental Pollution*, 221: 1–14.

Qi, L, Teng, F, Deng, X, Zhang, Y and Zhong, X (2019), "Experimental study on adsorption of Hg(II) with microwave-assisted alkali-modified fly ash", *Powder Technology*, 351: 153–158.

Qiao, H, Wang, X, Liao, P, Zhang, C and Liu, C (2021), "Enhanced sequestration of tetracycline by Mn(II) encapsulated mesoporous silica nanoparticles: Synergistic sorption and mechanism", *Chemosphere*, 284: 131334.

Ramzi, NIR, Shahidan, S, Maarof, MZ and Ali, N (2016), "Physical and chemical properties of coal bottom ash (CBA) from Tanjung Bin Power Plant", 160 (1): 012056.

Rathi, BS and Kumar, PS (2021), "Application of adsorption process for effective removal of emerging contaminants from water and wastewater", *Environmental Pollution*, 280.

Raykova, MR, McGuire, K, Peveler, WJ, Corrigan, DK, Henriquez, FL and Ward, AC (2023), "Towards direct detection of tetracycline residues in milk with a gold nanostructured electrode", *PLoS One*, 18 (6): e0287824.

Ren, P, Wang, L, Ma, T, Zhao, Y, Guo, B, Luo, C, Li, S and Ji, P (2024), "A thorough investigation into the adsorption behavior of sophorolipid-modified fly ash towards compound pollution of lead and tetracycline", *Science of The Total Environment*, 947: 174679.

Ren, X, Qu, R, Liu, S, Zhao, H, Wu, W, Song, H, Zheng, C, Wu, X and Gao, X (2020), "Synthesis of zeolites from coal fly ash for the removal of harmful gaseous pollutants: A review", *Aerosol and Air Quality Research*, 20 (5): 1127–1144.

Renu and Sithole, T (2024), "A review on regeneration of adsorbent and recovery of metals: Adsorbent disposal and regeneration mechanism", *South African Journal of Chemical Engineering*, 50: 39–50, ISSN: 1026-9185.

Rizwan, K, Babar, ZB, Munir, S, Arshad, A and Rauf, A (2022), "Recent advancements in engineered biopolymeric-nanohybrids: A greener approach for adsorptive-remediation of noxious metals from aqueous matrices", *Environmental Research*, 215: 114398.

Rozhina, E, Ishmukhametov, I, Nigamatzyanova, L, Akhatova, F, Batasheva, S, Taskaev, S, Montes, C, Lvov, Y and Fakhrullin, R (2021), "Comparative Toxicity of Fly Ash: An In Vitro Study", *Molecules*, 26 (7).

Sahmoune, MN (2019), "Evaluation of thermodynamic parameters for adsorption of heavy metals by green adsorbents", *Environmental Chemistry Letters*, 17 (2): 697–704.

Salvestrini, S, Ambrosone, L and Kopinke, FD (2022), "Some mistakes and misinterpretations in the analysis of thermodynamic adsorption data", *Journal of Molecular Liquids*, 352: 118762.

Samal, K, Mahapatra, S and Ali, MH (2022), "Pharmaceutical wastewater as Emerging Contaminants (EC): Treatment technologies, impact on environment and human health", *Energy Nexus*, 6: 100076.

Saravanan, A, Kumar, PS, Jeevanantham, S, Anubha, M and Jayashree, S (2022), "Degradation of toxic agrochemicals and pharmaceutical pollutants: Effective and alternative approaches toward photocatalysis", *Environmental Pollution*, 298: 118844.

Sawunyama, L, Olatunde, OC, Oyewo, OA, Bopape, MF and Onwudiwe, DC (2024), "Application of coal fly ash based ceramic membranes in wastewater treatment: A sustainable alternative to commercial materials", *Heliyon*, 10 (2): e24344.

Serwecińska, L (2020), "Antimicrobials and antibiotic-resistant bacteria: a risk to the environment and to public health", *Water*, 12 (12): 3313.

Shaheen, SM, Hooda, PS and Tsadilas, CD (2014), "Opportunities and challenges in the use of coal fly ash for soil improvements – A review", *Journal of Environmental Management*, 145: 249–267.

Shaikh, AA (2020), *Heterogeneous Catalysis: Essentials for Chemical Engineers*, De Gruyter, Berlin, Boston, ISBN: 9783110624861.

Shao, S and Wu, X (2020), "Microbial degradation of tetracycline in the aquatic environment: a review", *Critical reviews in biotechnology*, 40 (7): 1010–1018.

Sharma, A, Srivastava, K, Devra, V and Rani, A (2012), "Modification in properties of fly ash through mechanical and chemical activation", *American Chemical Science Journal*, 2 (4): 177–187.

Shi, X, Zhang, W and Li, B (2021), "Characteristics of adsorption kinetics and isotherms of Cu(II) by sediment under different hydrodynamic of the Ganjiang river, China", *Water Supply*, 22 (2): 1337–1346.

Singh, A, Sonal, S, Kumar, R and Mishra, BK (2020), "Adsorption of chlorhexidine digluconate on acid modified fly ash: Kinetics, isotherms and influencing factors", *Environmental Engineering Research*, 25 (2): 205–211.

Singh, LP, Bhattacharyya, SK, Kumar, R, Mishra, G, Sharma, U, Singh, G and Ahalawat, S (2014), "Sol-Gel processing of silica nanoparticles and their applications", *Advances in Colloid and Interface Science*, 214: 17–37.

Somashekara, D and Mulky, L (2023), "Sequestration of Contaminants from Wastewater: A Review of Adsorption Processes", *ChemBioEng Reviews*, 10 (4): 491–509.

Sophia, CA and Lima, EC (2018), "Removal of emerging contaminants from the environment by adsorption", *Ecotoxicology and Environmental Safety*, 150: 1–17.

Sun, Y, Dai, Y, Wang, X and Shan, D (2022), "Rapid adsorption of tetracycline from aqueous solution on fly ash", *Desalination and Water Treatment*, 248: 226–236.

Suraneni, P, Burris, L, Shearer, C and Hooton, D (2021), "ASTM C618 Fly Ash Specification: Comparison with Other Specifications, Shortcomings, and Solutions", *ACI Materials Journal*, 118.

Swanepoel, JC and Strydom, CA (2002), "Utilisation of fly ash in a geopolymeric material", *Applied Geochemistry*, 17 (8): 1143–1148.

Szerement, J, Szatanik-Kloc, A, Jarosz, R, Bajda, T and Mierzwa-Hersztek, M (2021), "Contemporary applications of natural and synthetic zeolites from fly ash in agriculture and environmental protection", *Journal of Cleaner Production*, 311: 127461.

Tan, KL and Hameed, BH (2017), "Insight into the adsorption kinetics models for the removal of contaminants from aqueous solutions", *Journal of the Taiwan Institute of Chemical Engineers*, 74: 25–48.

Taufiq, A, Hidayat, P and Hidayat, A (2018), "Modified coal fly ash as low cost adsorbent for removal reactive dyes from batik industry", paper presented at*MATEC Web of Conferences*, vol. 154, EDP Sciences: p. 01037.

Tkaczyk, A, Bownik, A, Dudka, J, Kowal, K and Ślaska, B (2021), "Daphnia magna model in the toxicity assessment of pharmaceuticals: A review", *Science of The Total Environment*, 763: 143038.

Tran, HN, Lima, EC, Juang, RS, Bollinger, JC and Chao, HP (2021), "Thermodynamic parameters of liquid–phase adsorption process calculated from different equilibrium constants related to adsorption isotherms: A comparison study", *Journal of Environmental Chemical Engineering*, 9 (6): 106674.

Truong, HB, Ike, IA, Ok, YS and Hur, J (2020), "Polyethyleneimine modification of activated fly ash and biochar for enhanced removal of natural organic matter from water via adsorption", *Chemosphere*, 243: 125454.

Turku, I, Sainio, T and Paatero, E (2007), "Thermodynamics of tetracycline adsorption on silica", *Environmental Chemistry Letters*, 5 (4): 225–228.

Umar, M (2022), "From conventional disinfection to antibiotic resistance control—status of the use of chlorine and UV irradiation during wastewater treatment", *International Journal of Environmental Research and Public Health*, 19 (3): 1636.

Van Den Broek, LAM and Boeriu, CG (2020), *Chitin and Chitosan - Properties and Applications*, John Wiley & Sons, ISBN: 978-1-119-45043-6.

Varadharajan, V, Senthilkumar, DS, Senthilkumar, K, Sundramurthy, VP, Manikandan, R, Senthilarasan, H, Ganesan, H, Kesavamoorthy, I and Ramasamy, A (2022), "Process modeling and toxicological evaluation of adsorption of tetracycline onto the magnetized cotton dust biochar", *Journal of Water Process Engineering*, 49: 103046.

Vasu, G, Deivasigamani, P, Sivamani, S and Sivakumar, P (2023), "A Review on Cassava Residues as Adsorbents for Removal of Organic and Inorganic Contaminants in Water and Wastewater", *Journal of Chemistry*, 2023: 1–27.

Verma, SMC and Hussain, A (2016), "Heavy metal contamination of groundwater due to fly ash disposal of coal-fired thermal power plant, Parichha, Jhansi, India", *Cogent Engineering*, 3 (1): 1179243.

Vu, BK, Shin, EW, Snisarenko, O, Jeong, WS and Lee, HS (2010), "Removal of the antibiotic tetracycline by Fe-impregnated SBA-15", *Korean Journal of Chemical Engineering*, 27 (1): 116–120.

Wang, C and Jian, JJ (2015), "Degradation and detoxicity of tetracycline by an enhanced sonolysis", *Journal of Water and Environment Technology*, 13 (4): 325–334.

Wang, J and Guo, X (2020a), "Adsorption isotherm models: Classification, physical meaning, application and solving method", *Chemosphere*, 258: 127279.

Wang, J and Guo, X (2020b), "Adsorption kinetic models: Physical meanings, applications, and solving methods", *Journal of Hazardous materials*, 390: 122156.

Wang, X, Cheng, B, Zhang, L, Yu, J and Normatov, I (2022), "Adsorption performance of tetracycline on NiFe layered double hydroxide hollow microspheres synthesized with silica as the template", *Journal of Colloid and Interface Science*, 627: 793–803.

Woolard, C, Petrus, K and Horst, M van der (2000), "The use of a modified fly ash as an adsorbent for lead", *Water SA*, 26 (4): 531–536.

Worch, E (2021), *Adsorption Technology in Water Treatment - Fundamentals, Processes, and Modeling*, 2nd ed., De Gruyter, ISBN: 978-3-11-071542-2.

Wulandari, W, Saefumillah, A and Yunarti, R (2020), "Modification of fly ash using acids and alkali by hydrothermal method and its application as adsorbents material for phosphate adsorption in aquatic system", *IOP Conference Series: Materials Science and Engineering*, 902: 12034.

Xu, D, Ji, P, Wang, L, Zhao, X, Hu, X, Huang, X, Zhao, H and Liu, F (2021), "Effect of modified fly ash on environmental safety of two soils contaminated with cadmium and lead", *Ecotoxicology and Environmental Safety*, 215: 112175.

Xuying, G, Zilong, Z, Xinle, G, Yanrong, D, Honglei, F and Xiaoyue, Z (2024), "Study on the adsorption performance of modified high silica fly ash for methylene blue", *RSC Advances*, 14: 21342–21354.

Yadav, VK and Fulekar, MH (2020), "Advances in Methods for Recovery of Ferrous, Alumina, and Silica Nanoparticles from Fly Ash Waste", *Ceramics*, 3 (3): 384–420, ISSN: 2571-6131.

Yadav, VK and Fulekar, M (2019), "Green synthesis and characterization of amorphous silica nanoparticles from fly ash", *Materials Today: Proceedings*, 18: 4351–4359.

Yan, F, Jiang, J, Tian, S, Liu, Z, Shi, J, Li, K, Chen, X and Xu, Y (2016), "A green and facile synthesis of ordered mesoporous nanosilica using coal fly ash", *ACS Sustainable Chemistry & Engineering*, 4 (9): 4654–4661.

Yan, L, Song, X, Miao, J, Ma, Y, Zhao, T and Yin, M (2024), "Removal of tetracycline from water by adsorption with biochar: A review", *Journal of Water Process Engineering*, 60: 105215.

Yan, L, Wang, Y, Ma, H, Han, Z, Zhang, Q and Chen, Y (2012), "Feasibility of fly ash-based composite coagulant for coal washing wastewater treatment", *Journal of Hazardous Materials*, 203-204: 221–228.

Yang, G and Park, SJ (2019), "Conventional and microwave hydrothermal synthesis and application of functional materials: A review", *Materials*, 12 (7): 1177.

Yao, ZT, Ji, XS, Sarker, P, Tang, J, Ge, L, Xia, M and Xi, Y (2015), "A comprehensive review on the applications of coal fly ash", *Earth-science reviews*, 141: 105–121.

Yasri, N and Roberts, EP (2024), "Electrochemical Regeneration of Adsorbents: An Electrochemist's Perspective", *Current Opinion in Electrochemistry*, 101504.

Zahmatkesh Anbarani, M, Najafpoor, A, Barikbin, B and Bonyadi, Z (2023), "Adsorption of tetracycline on polyvinyl chloride microplastics in aqueous environments", *Scientific Reports*, 13 (1): 17989.

Zandipak, R and Sobhanardakani, S (2018), "Novel mesoporous Fe_3O_4/SiO_2/CTAB–SiO_2 as an effective adsorbent for the removal of amoxicillin and tetracycline from water", *Clean Technologies and Environmental Policy*, 20 (4): 871–885.

Zdretsov, IM and Gerasimov, AM (2024), "Green and low-cost synthesis of zeolites from kaolin: a promising technology or a delusion?", *Reaction Chemistry & Engineering*, 9 (8): 1994–2027.

Zhang, Y, Zhou, L, Chen, L, Guo, Y, Guo, F, Wu, J and Dai, B (2021), "Synthesis of zeolite Na-P1 from coal fly ash produced by gasification and its application as adsorbent for removal of Cr(VI) from water", *Frontiers of Chemical Science and Engineering*, 15 (3): 518–527.

Zhang, Z, Lan, H, Liu, H and Qu, J (2015a), "Removal of tetracycline antibiotics from aqueous solution by amino-Fe (III) functionalized SBA15", *Colloids and Surfaces A: Physicochemical and Engineering Aspects*, 471: 133–138.

Zhang, Z, Liu, H, Wu, L, Lan, H and Qu, J (2015b), "Preparation of amino-Fe(III) functionalized mesoporous silica for synergistic adsorption of tetracycline and copper", *Chemosphere*, 138: 625–632.

Zhao, L, Li, Q, Wang, H, Zhou, Z, Li, N, Pan, H, Liu, Y and Liu, X (2024), "Enhanced Adsorptive Removal of Tetracycline by Phosphomolybdic Acid-Modified Low-Temperature Sludge Biochar", *Langmuir*, 40 (1): 751–760.

Zhao, Y, Tong, F, Gu, X, Gu, C, Wang, X and Zhang, Y (2014), "Insights into tetracycline adsorption onto goethite: Experiments and modeling", *Science of The Total Environment*, 470-471: 19–25.

Zheng, Z, Ma, X, Zhang, Z and Li, Y (2019), "In-situ transition of amorphous gels to Na-P1 zeolite in geopolymer: Mechanical and adsorption properties", *Construction and Building Materials*, 202: 851–860.

Zhou, W, Lu, X, Qi, C and Yang, M (2020), "Utilisation of ultrasonic treatment to improve the soil amelioration property of coal fly ash", *Journal of Environmental Management*, 276: 111311.

Zhuang, XY, Chen, L, Komarneni, S, Zhou, CH, Tong, DS, Yang, HM, Yu, WH and Wang, H (2016), "Fly ash-based geopolymer: clean production, properties and applications", *Journal of Cleaner Production*, 125: 253–267.

Ziembowicz, S and Kida, M (2022), "Limitations and future directions of application of the Fenton-like process in micropollutants degradation in water and wastewater treatment: A critical review", *Chemosphere*, 296: 134041.

Appendix A - Calibration Curve

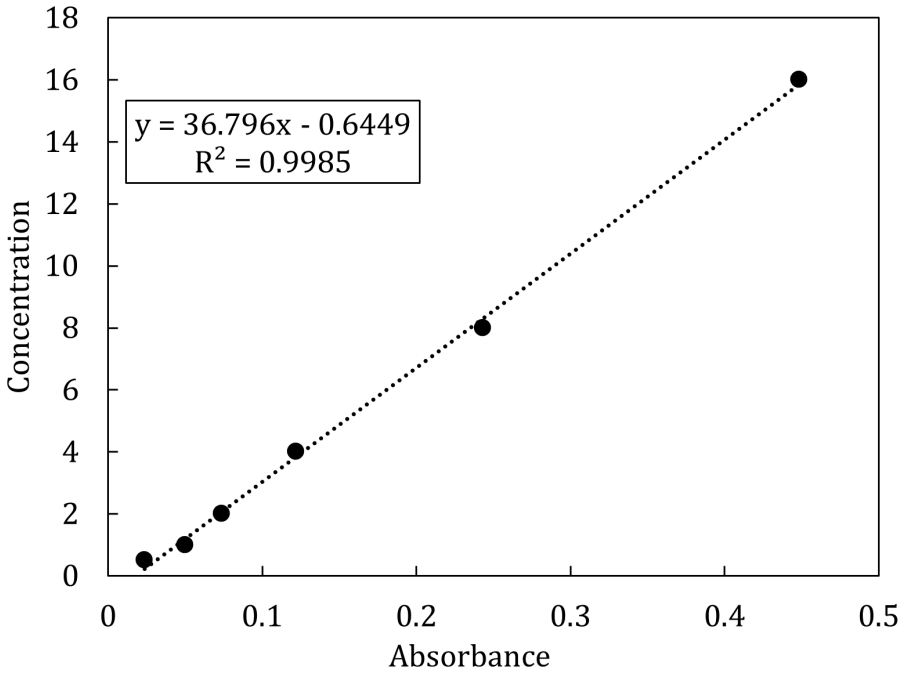

Figure A.1: Calibration curve for tetracycline at 381 nm.